Mathematisches Forschungsinstitut Oberwolfach

Report No. 55/2015

DOI: 10.4171/OWR/2015/55

Geometric Partial Differential Equations: Surface and Bulk Processes

Organised by
Klaus Deckelnick, Magdeburg
Charles M. Elliott, Coventry
Ralf Kornhuber, Berlin
James A. Sethian, Berkeley

29 November – 5 December 2015

Abstract. The workshop brought together experts representing a wide range of topics in geometric partial differential equations ranging from analyis over numerical simulation to real-life applications. The main themes of the conference were the analysis of curvature energies, new developments in pdes on surfaces and the treatment of coupled bulk/surface problems.

Mathematics Subject Classification (2010): 35-XX, 49-XX, 65-XX.

Introduction by the Organisers

Geometric partial differential equations are a flourishing research area at the interface between differential geometry and pde theory. These equations arise from a variety of problems, and describe a host of phenomena. One traditional and important source are minimization problems involving geometric objects like curves or surfaces. More recently, pdes *on* stationary or evolving surfaces - possibly coupled to equations that hold in the domain bounded by the surface - have emerged as a very active research field.

While the the study of geometric partial differential equations leads to interesting and challenging problems both from the analytical and the numerical point of view, they also frequently arise in the modeling of physical interfaces or membranes. For this reason, understanding the mathematical theory behind these equations and constructing efficient algorithms to approximate solutions is of great importance in application areas such as materials science, biology, image processing and astrophysics.

The workshop brought together about 50 experts from Europe and America covering a wide variety of aspects bridging analysis, numerical analysis, scientific computation and real-life applications. The scientific programme consisted of 26 plenary talks with the following topics emerging as the main directions of current research:

Curvature energies: Pozzi considered the minimisation of the anisotropic Willmore energy via a natural formulation of the corresponding gradient flow, while Bartels suggested and analysed a numerical approach for the minimisation of a bilayer bending energy involving an isometry constraint. Röger introduced a 'mesoscale' model for lipid bilayer membranes and considered a corresponding macroscopic limit. The talk by Lipowsky was concerned with the stability of certain membrane shapes in a spontaneous curvature model. In their two talks Gräser and Schmeiser discussed mathematical modelling of different aspects of the mutual interaction of cell membranes, membrane proteins and the cytoskeleton, while a hyperboli-parabolic model for the polymerization of the filaments in the cytoskeleton was presented by Stevens. Simulations of the wrinkling behavior of thin elastic sheets were presented by Sander who used a Cosserat shell model and geodesic finite elements.

PDEs on surfaces and evolving domains: Several talks were concerned with refinements and extensions of methods that have been developed recently. Olshanskii presented new ideas for mesh adaption on the basis of octree background meshes while Reusken introduced a higher order trace finite element method. Giesselmann's talk focussed on hyperbolic conservation laws on surfaces with particular emphasis on the approximation of geometry. Lubich derived an error analysis for an advection–diffusion equation on an evolving hypersurface whose velocity is given through its coupling to a regularized mean curvature type evolution law. Optimal control problems for PDEs on surfaces and their numerical analysis were the subject of Hinze's talk. Ranner presented an abstract framework for the analysis of finite element discretization for PDEs in evolving domains.

Coupled surface/bulk problems and applications: Several presentations showed how sophisticated numerical methods for surface PDEs can be incorporated into the simulation of complicated coupled surface/bulk problems. Garzon used the level set method in order to treat a fluid/interface problem arising in electrohydrodynamics, while Stricker considered the motion of liquid droplets driven by Marangoni flow. Optimal control of multiphase fluids and droplets described by a phase-field model was presented by Hintermüller. An algorithm for solving coupled surface/bulk reaction diffusion equations arising in a model for cell migration and chemotaxis was presented by Mackenzie. Nürnberg simulated the dynamics of fluidic biomembranes in a bulk fluid through the coupling of bulk and surface Navier–Stokes equations which has in the latter the first variation of the Willmore energy as a forcing term. The accurate discretization of parabolic problems on moving domains with moving interfaces motivated by fluid-structure-interaction problems was discussed by Richter.

While the abovementioned talks were primarily concerned with computational aspects, there were several presentations that focussed an modeling and analytical issues: Garcke suggested a mathematical model for tumour growth including chemotaxis and active transport and which couples the Cahn–Hilliard equation to Darcy flow. Sprekels analized optimal boundary control problems for Cahn-Hilliard systems with dynamic boundary conditions. Stinner presented a model for multiphase flow taking into account the impact of surfactants on the separating interfaces involving certain coupling conditions at triple junctions. Venkataraman analysed various parameter limits for a receptor-ligand dynamics model giving rise to surface free boundary problems.

In addition two talks presented interesting new ideas relevant for the efficient simulation of geometric PDEs: Fritz presented a systematic approach to the generation of good surface meshes using reparametrizations based on the harmonic map heat flow. Chopp suggested a locally adaptive time stepping strategy that can be applied in order to speed up the calculation of solutions to the Cahn–Hilliard problem.

The organizers had deliberately invited experts covering all aspects of geometric pdes including analysis, numerical analysis, scientific computing, modeling and applications. This led to lively discussions and exchange of ideas during and after the talks which was continued throughout the afternoon breaks. On Tuesday and Wednesday evening two well attended 'Young Researcher sessions' took place with three presentations in each session. In a more informal 'movie night' on Thursday evening a host of participants took the opportunity to show impressive videos of numerical simulations related to the subject of the conference.

Acknowledgement: The MFO and the workshop organizers would like to thank the National Science Foundation for supporting the participation of junior researchers in the workshop by the grant DMS-1049268, "US Junior Oberwolfach Fellows". Moreover, the MFO and the workshop organizers would like to thank the Simons Foundation for supporting Robert Strehl in the "Simons Visiting Professors" program at the MFO.

Workshop: Geometric Partial Differential Equations: Surface and Bulk Processes

Table of Contents

Abstracts

Numerical methods for large bilayer bending problems

Sören Bartels
(joint work with Andrea Bonito, Ricardo H. Nochetto)

Bilayer bending problems describe the elastic deformation of two thin connected films with different responses to changes in the enviroment, e.g., changes in temperature. If the upper layer contracts and the lower one expands when the temperature is increased, then the bilayer starts to bend, cf. Fig. 1. Bending deformations of bilayers are characterized by small elastic energies and large deformations. Classical applications include bimetal strips in thermostats while modern applications range from the fabrication of nanotubes to the development of microcapsules.

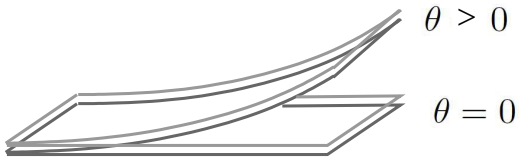

Figure 1. Bending of a bilayer sheet due to a mismatch of material responses to, e.g., temperature.

A rigorous derivation of a dimensionally reduced model from three-dimensional hyperelasticity has been carried out in [7] following [5], leading to a fourth order problem with isometry constraint. In its simplest form it consists in the minimization problem:

$$\begin{aligned} &\text{Minimize} \quad E(y) = \frac{1}{2}\int_\omega |II - Z|^2 dx - \int_\omega f \cdot y \, dx \\ &\text{subject to } I = I_2, \quad y|_{\partial_D\omega} = [\mathrm{id}, 0], \quad \nabla y|_{\partial_D\omega} = [I_2, 0]^T. \end{aligned}$$

The minimization is over the set of deformations $y : \omega \to \mathbb{R}^3$, where $\omega \subset \mathbb{R}^2$ is the flat reference configuration of the bilayer strip, satisfying $y \in H^2(\omega; \mathbb{R}^3)$. The mappings $I, II : \omega \to \mathbb{R}^{2\times 2}$ are the first and second fundamental form of the surface $\Gamma = y(\omega)$ parametrized by y, respectively. Note that we have $II = -(\nabla y)^T \nabla \nu$ with the unit normal $\nu = \partial_1 y \times \partial_2 y$. The matrix Z acts as a spontaneous curvature and encodes the material properties, in particular, the amount of mismatch of the two involved materials, e.g., $Z = \alpha I_2$ with the identity matrix $I_2 \in \mathbb{R}^{2\times 2}$. The isometry condition $I = I_2$ implies that the surface has vanishing Gaussian curvature K. This has the important implication that

$$|h|^2 = |D^2 y|^2 = |\Delta y|^2 = H^2$$

with Frobenius norms and the mean curvature H. Following [1, 2], the discretization of the problem proposed in [3] is based on rectangular Kirchhoff finite elements, see [4], which have been developed for the approximation of linear fourth

order problems. These introduce H^1 conforming finite element spaces for the approximation of the deformation and the deformation gradient. A discrete gradient operator that approximates the exact gradient operator establishes a connection between the spaces, cf. Fig 2 for a conceptual description of this nonconforming finite element method.

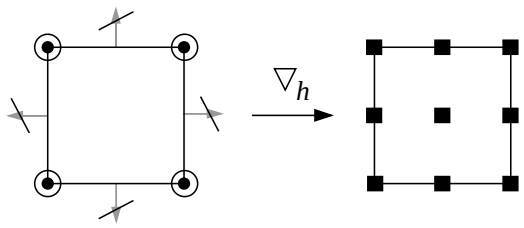

FIGURE 2. Finite element spaces for the deformation and the deformation gradient together with a discrete gradient operator.

The degrees of freedom in the method are the deformations and deformation gradients at the vertices of elements contained in the set $\mathcal{N}_h$. This particular feature allows us to impose the isometry constraint at the vertices. We thus arrive at the following finite-dimensional minimization problem, where constant terms have been neglected in the energy functional:

$$\begin{aligned}
&\text{Minimize} \quad E_h(y_h) = \frac{1}{2}\int_\omega |\nabla\nabla_h y_h|^2 dx + \int_\omega \left[(\nabla y_h)^T \nabla \nu_h\right] : Z dx - \frac{1}{2}\int_\omega f\cdot y\, dx\\
&\text{subject to} \quad (\nabla y_h(z))^T(\nabla y_h(z)) = I_2 \quad \text{for all } z\in\mathcal{N}_h\\
&\text{and} \quad y_h(z) = [z,0], \quad \nabla y_h(z) = [I_2,0]^T \quad \text{for all } z\in\mathcal{N}_h\cap\partial_D\omega.
\end{aligned}$$

Convergence of discrete minimizers to solutions of the continuous minimization problem is established within the framework of Γ-convergence. This avoids the unjustified use of regularity or uniqueness properties. Crucial for this are the density of smooth isometries among H^2 isometries, cf. [6], and interpolation properties of the involved finite element spaces. An iterative scheme for the practical minimization of the nonlinear, constrained problem is developed in two steps. First, a discrete gradient flow with linearized isometry condition leads to a sequence of minimization problems with linear constraints. This scheme is energy decreasing and the violation of the constraint is controlled by the step size, i.e., we have for all $k \geq 0$ that

$$\begin{aligned}
E_h(y_h^{k+1}) + \tau\sum_{j=0}^{k} \|(y_h^{j+1}-y_h^j)/\tau\|_h^2 &\leq E_h(y_h^0),\\
\|(\nabla y_h^{k+1})^T\nabla y_h^{k+1} - I_2\|_{L_h^1(\omega)} &\leq c\tau,
\end{aligned}$$

where $\tau > 0$ is the step size. Second, the minimization problems in the pseudo-time steps are computed with fixed-point iterations. Its convergence is established under a mild, h-independent condition on τ. Some snapshots of a discrete evolution are

depicted in Figure 3. The results confirm the tendency of bilayers towards forming cylinders, cf. [8].

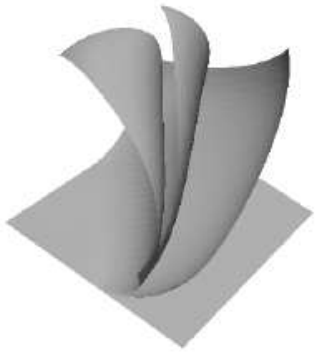

FIGURE 3. Discrete evolution of a bilayer plate clamped around one corner due to a temperature induced stress towards an equilibrium configuration.

REFERENCES

[1] S. Bartels, *Approximation of large bending isometries with discrete Kirchhoff triangles. SIAM J. Numer. Anal. 51*, 1 (2013), 516–525.

[2] S. Bartels, *Numerical methods for nonlinear partial differential equations*, vol. 47 of *Springer Series in Computational Mathematics*. Springer, 2015.

[3] S. Bartels, A. Bonito, R. Nochetto, *Bilayer plates: model reduction, Γ-convergent finite element approximation and discrete gradient flow. Comm. Pure Appl. Math.* (2015), to appear.

[4] D. Braess, *Finite elements*, third ed. Cambridge University Press, Cambridge, 2007.

[5] G. Friesecke, R. D. James, and S. Müller, *A theorem on geometric rigidity and the derivation of nonlinear plate theory from three-dimensional elasticity. Comm. Pure Appl. Math. 55*, 11 (2002), 1461–1506.

[6] P. Hornung, *Approximation of flat $W^{2,2}$ isometric immersions by smooth ones. Arch. Ration. Mech. Anal. 199*, 3 (2011), 1015–1067.

[7] B. Schmidt, *Plate theory for stressed heterogeneous multilayers of finite bending. J. Math. Pures Appl.* (9) 88, 1 (2007), 107–122.

[8] B. Schmidt, *Minimal energy configurations of strained multi-layers. Calc. Var. Partial Differential Equations 30*, 4 (2007), 477–497.

An octree trace finite element method for PDEs posed on surfaces

MAXIM OLSHANSKII

(joint work with Arnold Reusken, Alexei Chernyshenko)

Let Ω be an open domain in $\mathbb{R}^3$ and Γ be a connected C^2 compact hyper-surface contained in Ω. In the talk we focused on the following elliptic problem defined on the stationary surface:

$$-\varepsilon\Delta_\Gamma u + \mathbf{w}\cdot\nabla_\Gamma u + (c + \operatorname{div}_\Gamma \mathbf{w})\, u = f \quad \text{on } \Gamma, \tag{1}$$

with $f \in L^2(\Gamma)$ and $c = c(\mathbf{x}) \in L^\infty(\Gamma)$.

The trace finite element method (FEM) for PDEs posed on manifolds was devised in [1]. In a number of more recent publications the methodology was extended to coupled surface-bulk problems, parabolic equations posed on evolving surfaces, transport dominated problems and other interesting cases. Most of these developments, following the original contribution, use a background tetrahedra mesh, which is unfitted to the surface. The point was made in the talk that if mesh adaptation and/or dynamic mesh reconstruction are important to simulate phenomena taking place on the surface or in the bulk, then the trace FEM approach greatly benefits in its efficiency from using *octree cubic* background meshes. The talk reported on some recent results in this direction from [2] and discussed open problems. In the remainder of the extended abstract we briefly draft the method and suggest a few interesting topics for further research.

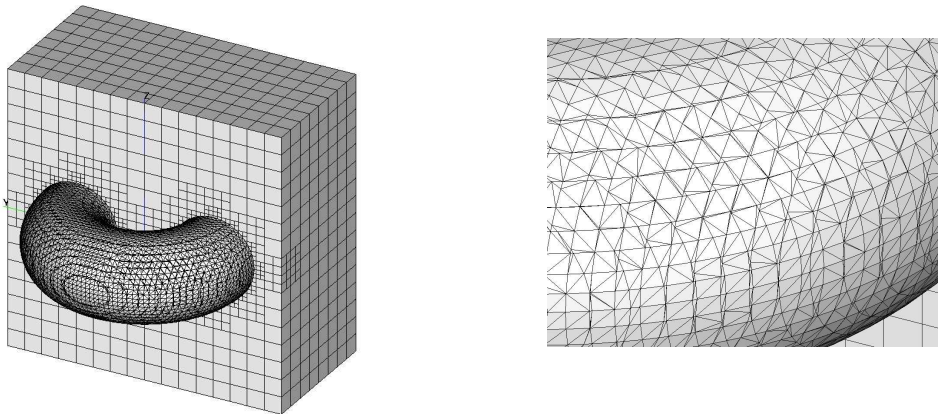

FIGURE 1. Left: A cutaway of a bulk domain shows the background octree mesh three times refined towards the surface and the resulting trace mesh on Γ_h. Right: The zoom-in of the resulting surface triangulation.

Consider an octree cubic mesh $\mathcal{T}_h$ covering the bulk domain Ω. For a given discrete level-set function ϕ_h, denote by Γ_h a reconstruction of its zero level produced by a variant of the well-known marching cubes method (cubical marching squares method were used in our implementation). The resulting Γ_h is a $C^{0,1}$ surface without boundary. Under reasonable assumptions on how well ϕ_h approximates the level-set function of Γ, the recovered Γ_h provides the second order accurate surface reconstruction. Figure 1 illustrates the background octree mesh and the recovered Γ_h when Γ is a torus.

The surface Γ_h can be partitioned in planar triangular segments and so numerical integration over Γ_h is straightforward. This brings us to the following finite element method for (1). Consider the volumetric finite element space of all piecewise trilinear continuous functions with respect to the bulk octree mesh $\mathcal{T}_h$:

$$V_h := \{v_h \in C(\Omega) \mid v|_S \text{ is trilinear on any } \ S \in \mathcal{T}_h\}.$$

The trace FEM for (1) reads: Find $u_h \in V_h$ s.t.

$$(2) \qquad \varepsilon \int_{\Gamma_h} \nabla_{\Gamma_h} u_h \cdot \nabla_{\Gamma_h} v_h \; - (\mathbf{w}_h \cdot \nabla_{\Gamma_h} v_h) u_h + c_h \, u_h v_h \, \mathrm{d}\mathbf{s}_h = \int_{\Gamma_h} f_h v_h \, \mathrm{d}\mathbf{s}_h$$

for all $v_h \in V_h$. Here $\mathbf{w}_h$, c_h and f_h are some approximations of the data on Γ_h.

Under suitable assumptions, method (2) is well-posed and the solution is proved to converge with optimal order (second order in surface L^2-norm, first order in surface H^1-norm, and independent of how Γ_h cuts the mesh) to the corresponding solution of (1). It is natural and technologically convenient to represent solution u_h on Γ_h using nodal functions of the background octree mesh. Clearly only nodal functions for cells intersected by Γ_h are involved in this representation and so in computations. Due to possible small intersections of Γ_h and $S \in \mathcal{T}_h$ the resulting algebraic system can be poorly conditioned. One can deal with this issue either on algebraic level or by introducing suitable consistent stabilization to the formulation (2), see [2] for the review.

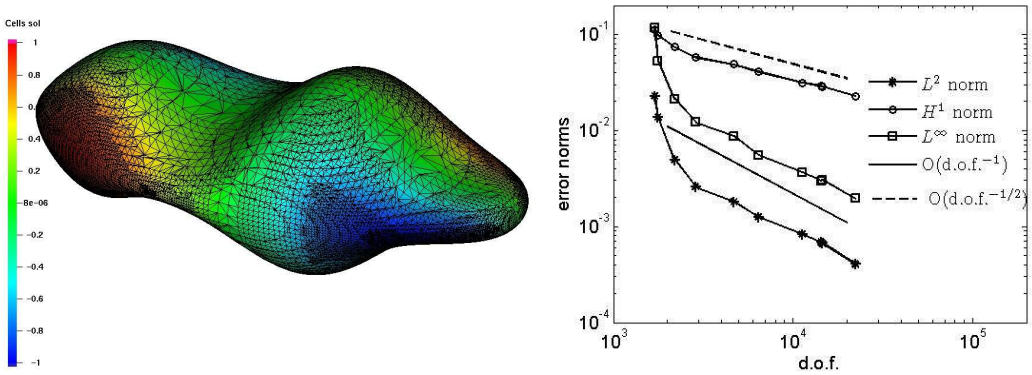

FIGURE 2. Left: Triangulation after 7 steps of adaptation based on the error indicators colored by solution levels. Right: Adaptive trace FEM convergence.

The cartesian structure and embedded hierarchy of octree grids makes mesh adaptation, reconstruction and data access fast and easy, which is not always the case for tetrahedral meshes. Various physics based or numerical indicators, based, for example, on the surface geometry, solution structure or FEM residuals, can drive the mesh adaptation. One can show the estimate

$$\|\nabla_\Gamma (u - u_h^\ell)\|_{L_2(\Gamma)} \leq C \, (\sum_{T \in \Gamma_h} \eta_R(T)^2 + \eta_E(T)^2 + \eta_G(T)^2)^{1/2},$$

with indicators

$$\eta_R(T)^2 = h_{S_T}^2 \| f_h + \varepsilon \Delta_{\Gamma_h} u_h - (c_h + \mathrm{div}_{\Gamma_h} \mathbf{w}_h) u_h - \mathbf{w}_h \cdot \nabla_{\Gamma_h} u_h \|^2_{L^2(T)},$$
$$\eta_E(T)^2 = \sum_{e \in \partial T} h_{S_T} \left(\| [\![\varepsilon \nabla_{\Gamma_h} u_h]\!] \|^2_{L^2(e)} + \| \mathbf{w}_h \cdot [\![\mathbf{m}_h]\!] \|^2_{L^2(e)} \right),$$
$$\eta_G(T)^2 = h_{S_T}^4 \| \mathbf{H}_h \|^2_{L^\infty(T)} \left(\| f^e \|^2_{L^2(T)} + \| u_h \|^2_{H^1(T)} \right).$$

Here T is a surface triangle with edges e, h_{S_T} is the corresponding background cubic cell size, $\mathbf{H}_h$ is a reconstructed Hessian of ϕ_h. This estimate can serve for the adaptivity purpose, where the decision about refinement of $S \in \mathcal{T}$ is based on the values of indicators for all $T \subset S$. An illustration of adaptive trace FEM applied to solve the Laplace-Beltrami equation on a surface and its (optimal) convergence based on the above indicators is given in Figure 2. Further details and examples can be found in [2].

Analysis and numerical results suggest that the combination of cartesian adaptive meshes and the unfitted (trace) finite elements provide simple, efficient, and reliable tool for numerical treatment of PDEs posed on surfaces. Below we include a non-exhaustive list of topics, which in our opinion deserve further studies:

- Currently the trace method is extended to the case of evolving surfaces within a *space-time* finite element framework [3], which requires the reconstruction of a surface in the interior of a space-time prismatic element. The challenge is to build at least second order in time trace FEM for evolving surfaces, which avoids this reconstruction procedure.
- Properties of trace *Discontinuous Galerkin* FE are of interest, especially in conjunction with octree grids.
- Stability of trace finite elements for fluid flow problems on manifolds are also of interest. For example, one may ask: whether traces of bulk inf-sup stable FE pairs satisfy a corresponding surface inf-sup condition?
- The development of higher order surface finite element methods using background octree meshes will likely need some new tools for higher order surface reconstruction and numerical integration among other ingredients.

References

[1] M.A. Olshanskii, A. Reusken, J. Grande, *A finite element method for elliptic equations on surfaces*, SIAM J.Num.Anal. **47** (2009), 3339–3358.

[2] A. Chernyshenko, M.A. Olshanskii, *An adaptive octree finite element method for PDEs posed on surfaces*, Comp.Meth.Appl.Mech.Eng. **291** (2015), 146–172.

[3] M.A. Olshanskii, A. Reusken, *Error analysis of a space-time finite element method for solving PDEs on evolving surfaces*, SIAM J.Numer.Anal. **52** (2014), 2092–2120.

Diffuse interface approach to PDEs on clusters and networks with applications to surfactants in multi-phase flow.

Björn Stinner
(joint work with Oliver Dunbar)

The impact of surface active agents (surfactants) on the rheological properties of multi-phase flows is exploited in diverse industrial applications and in natural, living systems. Classically the flows are described by problems with moving interfaces (sharp interface model) we consider a phase field approach to the multi-phase fluids (diffuse interface model) and then study how the bulk and interfacial equations for the surfactant(s) have to be set up. Our goal is to ensure thermodynamic consistency and also to obtain a good structure that facilitates the transfer of parameters and functional dependencies from the sharp interface model. We extend previous work on two-phase flow [5, 6] to multiple phases $M \geq 3$. Consequently, a focus of our investigation is on the triple junctions (points in 2D, lines in 3D) formed by three phases and how surfactant mass fluxes between the interfaces through the triple junction can be realised in the diffuse interface setting.

Starting with the related sharp interface setting we have domains $\Omega^{(i)}$, $i \in \{1, \dots, M\}$, separated by interfaces $\Gamma^{(i,j)}$ which form triple junctions $T^{(i,j,k)}$. For bulk and interface surfactant mass densities $c^{(i)}$ and $c^{(i,j)}$, respectively, we postulate a free energy of the form

$$\sum_i \int_{\Omega^{(i)}} G_i(c^{(i)}) + \sum_{i<j} \int_{\Gamma^{(i,j)}} \gamma_{i,j}(c^{(i,j)}). \tag{1}$$

The densities G_i and $\gamma_{i,j}$ need to be chosen such that experimental relations are satisfied. Here, we have equilibrium isotherms at the interface in mind and equations of state for the surfactant dependence of the surface tension which is $\sigma_{i,j}(c^{(i,j)}) = \gamma_{i,j}(c^{(i,j)}) - \gamma'_{i,j}(c^{(i,j)})c^{(i,j)}$. Diffusive fluxes associated with the bulk and interface surfactant then can be chosen to ensure thermodynamic consistency. For instance, $\boldsymbol{J}_c^{(i)} = -M_c^{(i)}(c^{(i)})\nabla G_i'(c^{(i)})$ and $\boldsymbol{J}_c^{(i,j)} = -M_c^{(i,j)}(c^{(i,j)})\nabla_{\Gamma^{(i,j)}}\gamma'_{i,j}(c^{(i,j)})$ with non-negative mobilities M_c. Further closing conditions concern the adsorption / desorption at the interfaces $\Gamma^{(i,j)}$,

$$\boldsymbol{J}_c^{(i)} \cdot \boldsymbol{\nu}^{(i,j)} = \alpha^{(i,j)}\big(G_i'(c^{(i)}) - \gamma'_{i,j}(c^{(i,j)})\big) \tag{2}$$

with non-negative $\alpha^{(i,j)}$ which may depend on the surfactant, and the flux from an interface into the triple junction $T^{(i,j,k)}$,

$$\begin{aligned} \boldsymbol{J}_c^{(i,j)} \cdot \boldsymbol{\mu}^{(i,j,k)} =& \beta_{(i,j)\leftrightarrow(i,k)}\big(\gamma'_{i,j}(c^{(i,j)}) - \gamma'_{i,k}(c^{(i,k)})\big) \\ &+ \beta_{(i,j)\leftrightarrow(j,k)}\big(\gamma'_{i,j}(c^{(i,j)}) - \gamma'_{j,k}(c^{(j,k)})\big) \end{aligned} \tag{3}$$

where the $\boldsymbol{\mu}^{(i,j,k)}$ are the external co-normals of the interfaces $\Gamma^{(i,j)}$ in the triple junctions $T^{(i,j,k)}$ pointing into the $\Omega^{(k)}$ and the β are non-negative coefficients. By suitable symmetry assumptions on the β no mass is deposited in the triple junctions.

With regards to the diffuse interface setting let us first consider the multi-phase flow where we generalise the approach by [1] to more than two phases. We have phase field variables $\phi^{(i)}$ which represent the presence of fluid i. These fulfil $\sum_i \phi^{(i)} = 1$, and $\phi^{(i)}$ is close to one in $\Omega^{(i)}$ and zero in the other domains while the interfaces $\Gamma^{(i,j)}$ are replaced by thin layers with a thickness that scales with a small parameter $\varepsilon > 0$. The free energy density for the the phase field setting is of the form

$$e = \rho\frac{|\boldsymbol{v}|^2}{2} + \varepsilon a(c,\phi,\nabla\phi) + \frac{1}{\varepsilon}w(c,\phi) + f(c,\phi)$$

with a gradient potential $a(c,\phi,\nabla\phi) = \sum_{i<j}\gamma_{i,j}(c^{(i,j)})a_{i,j}(\phi,\nabla\phi)$, a multi-well potential $w(c,\phi) = \sum_{i<j}\gamma_{i,j}(c^{(i,j)})w_{i,j}(\phi)$, and a bulk potential given by $f(c,\phi) = \sum_i \xi_i(\phi^{(i)})G_i(c^{(i)})$ where $\xi_i(\phi^{(i)})$ approximates the characteristic function $\chi_\Omega^{(i)}$. The choice of the $a_{i,j}$ and the $w_{i,j}$ is crucial to ensure that the Γ limit indeed is the sharp interface free energy (1) when $\varepsilon \to 0$ and to avoid so-called third phase contributions, see [7, 2, 8, 3, 4]. The thermodynamically consistent model then reads

$$\begin{aligned}
\nabla\cdot\boldsymbol{v} &= 0,\\
\partial_t^\bullet(\rho\boldsymbol{v}) &= \nabla\cdot\Big(-p\boldsymbol{I} + 2\eta D(\boldsymbol{v}) + \boldsymbol{v}\otimes\bar{\boldsymbol{J}}\Big)\\
&\quad + \sum_{i<j}\delta_{i,j}\nabla\sigma_{i,j} + \sum_l\big(\mu^{(l)} - \xi_l'(G_l - c^{(l)}G_l')\big)\nabla\phi^{(l)},\\
\partial_t^\bullet\phi^{(i)} &= \nabla\cdot\Big(\sum_l L^{(i,l)}\nabla\mu^{(l)}\Big) \quad \text{where } \sum_k L^{(k,l)} = 0 \quad \forall l,\\
\mu^{(l)} &= \sum_{i<j}\Big(-\varepsilon\nabla\cdot\big(\sigma_{i,j}\partial_{\nabla\phi^{(l)}}a_{i,j}\big) + \varepsilon\sigma_{i,j}\partial_{\phi^{(l)}}a_{i,j} + \frac{1}{\varepsilon}\sigma_{i,j}\partial_{\phi^{(l)}}w_{i,j}\Big)\\
&\quad + \xi_l'\big(G_l - c^{(l)}G_l'\big)
\end{aligned}$$

where $\delta_{i,j} = \varepsilon a_{i,j} + \frac{1}{\varepsilon}w_{i,j}$ and the coefficient matrix $(L^{(k,l)})_{k,l}$ is symmetric. As $\varepsilon \to 0$ these equations formally yield the incompressible Navier-Stokes equations in the bulk domains while the interfaces are transported with the flow and the jump of the stress from the adjacent fluids is counterbalanced by interfacial forces including surface tension and the Marangoni force,

$$[-p\boldsymbol{I} + 2\eta^{(\cdot)}D(\boldsymbol{v})]_j^i\boldsymbol{\nu}^{(i,j)} = \sigma_{i,j}(c^{(i,j)})\kappa_{i,j}\boldsymbol{\nu}^{(i,j)} + \nabla_{\Gamma^{(i,j)}}\sigma_{i,j}(c^{(i,j)}) \qquad \text{in } \Gamma^{(i,j)}.$$

In the triple junctions the forces by which the interfaces pull sum up to zero,

$$0 = \sigma_{i,j}\boldsymbol{\mu}^{(i,j,k)} + \sigma_{j,k}\boldsymbol{\mu}^{(j,k,i)} + \sigma_{k,i}\boldsymbol{\mu}^{(k,i,j)} \qquad \text{in } T^{(i,j,k)}.$$

Note that this condition does not allow for wetting though the phase field model itself can deal with this situation, see [3, 4].

The ansatz for the surfactant equations in the diffuse interface setting reads

$$\partial_t^\bullet\big(\xi_i c^{(i)}\big) - \nabla\cdot\big(\xi_i M_c^{(i)}\nabla G_i'(c^{(i)})\big) = \delta_{i,j}\alpha^{(i,j)}\big(\gamma_{i,j}'(c^{(i,j)}) - G_i'(c^{(i)})\big),$$

$$\partial_t^\bullet\big(\delta_{i,j}c^{(i,j)}\big) - \nabla\cdot\big(\delta_{i,j}M_c^{(i,j)}\nabla\gamma'_{i,j}(c^{(i,j)})\big)$$
$$= \delta_{i,j}\alpha^{(i,j)}\big(G_i'(c^{(i)}) - \gamma'_{i,j}(c^{(i,j)})\big) + \delta_{i,j}\alpha^{(j,i)}\big(G_j'(c^{(j)}) - \gamma'_{i,j}(c^{(i,j)})\big)$$
$$+ \sum_{k\neq i,j}\tau_{i,j,k}\beta_{(i,k)\leftrightarrow(i,j)}\big(\gamma'_{i,k}(c^{(i,k)}) - \gamma'_{i,j}(c^{(i,j)})\big)\big).$$

The asymptotic analysis then indeed yields the desired bulk and interface advection-diffusion equations and the closing condition (2). The challenge is the realisation of the triple junction fluxes (3).

The $\tau_{i,j,k}$ are approximations to the triple junction distributions and may be chosen of the form

$$\tau_{i,j,k} = C_\tau\frac{1}{\varepsilon^2}(\phi^{(i)}\phi^{(j)}\phi^{(k)})^2.$$

If phase field potentials a and w are used then these functions have exponentially decaying tails away from the triple junction. The asymptotic analysis around the triple junction yields that the calibration constant C_τ depends on the phase field solution to lowest order around the junction – for which no closed solution formula is known. However, the value can be assessed numerically. Our investigations indicate a dependence on the tensions $\sigma_{i,j}$ or, equivalently, the equilibrium angles at the triple junction.

Further numerical tests in the stationary case (no fluid flow, only the surfactant equations) show convergence of the phase field solutions to the sharp interface solutions for the numerically obtained value for C_τ. Further simulations display the applicability of the approach to the full problem where, in 2D, Marangoni effects, bulk-surface coupled problems, and problems with surfactant mixtures can be dealt with.

References

[1] H. Abels, H. Garcke, and G. Grün, *Thermodynamically consistent, frame indifferent diffuse interface models for incompressible two-phase flows with different densities*, Math. Models Methods Appl. Sci. **22** (201), 1150013, 40pp.

[2] G. Bellettini, A. Braides, and G. Riey, *Variational approximation of anisotropic functionals on partitions*, Annali di Matematica Pura ed Applicata **184** (2005), 75–93.

[3] F. Boyer and C. Lapuerta, *Study of a three component Cahn-Hilliard flow model*, Math. Model. Numer. Anal. **40** (2006), 653–687.

[4] F. Boyer and S. Minjeaud. Hierarchy of consistent n-component Cahn-Hilliard systems. *Math. Models Methods Appl. Sci.*, 24(14):2885–2928, 2014.

[5] H. Garcke, K.F. Lam, B. Stinner, *Phase-field modelling of two-phase flow with soluble surfactant*, *Interfaces and Free Boundaries: Analysis, Control and Simulation*, Oberwolfach Report **10** (2013), 867–950.

[6] H. Garcke, K.F. Lam, B. Stinner, *Diffuse interface modelling of soluble surfactants in two-phase flow*, Commun. Math. Sci. **12** (2014), 1475–1522.

[7] H. Garcke, B. Stoth, and B. Nestler, *Anisotropy in multi-phase systems: a phase field approach*, Interfaces Free Bound. *1* (1999), 175–198.

[8] B. Stinner, *Surface energies in multi-phase systems with diffuse phase boundaries*, *Free boundary problems*, Internat. Ser. Numer. Math. **154** (2007), 413–423.

On anisotropic Willmore flow

Paola Pozzi

In recent years the Willmore energy and its associated gradient flow have attracted a lot of attention. Indeed the Willmore functional plays a role in the modeling of biological membranes and in certain problems arising in image processing. Moreover it is a prototype for fourth order PDEs, which are well known to exhibits quite a different behavior when compared to the second order ones.

Although there is a huge literature concerning analytical and numerical studies of the Willmore energy, very little can be found when one considers its anisotropic counterpart. This is quite surprising if one thinks that anisotropy should be taken into account when describing several physical phenomena. On the other hand introduction of anisotropy gives rise to some very interesting but in some sense fairly complicated mathematics.

Here we first of all present *a geometrically consistent formulation* of anisotropic Willmore energy and anisotropic Willmore flow for closed parametric hypersurfaces in $\mathbb{R}^n$. When working with anisotropy, one is left with many possible choices for the definition of an anisotropic energy and its associated flow. By geometrically consistent we mean that the formulation is derived in such a way that relevant features of the isotropic case carry over to the anisotropic setting.

The next task is to discretize the flow by finite elements and discover interesting (numerical) anisotropic Willmore surfaces. Our goal is to derive a finite element scheme that extends the one proposed by Dziuk [2] in the isotropic case.

Due to the highly nonlinear character of the PDE we are studying, we opt for discretizing a geometrically equivalent flow. This steps simplify the numerical computation in that for instance only knowledge of the anisotropy map γ and its derivatives are needed, whereas information about its dual map γ^* and its derivatives are no longer necessary. Subsequently we provide a mixed formulation of the flow under consideration, discretize it using piecewise linear finite elements and show stability of the semi-discrete scheme.

Finally a fully discrete semi-implicit model is presented, that treats nonlinearities in an explicit way. In the isotropic case we recover the algorithm proposed by Dziuk in [2]. In the anisotropic setting, however, we are faced with high instability of the scheme. Experimental stability of the fully discrete scheme is achieved through the introduction of a carefully chosen stability term. Although the numerical tests support the choice of the proposed stability term, a rigorous proof is still missing. In fact there is no proof of stability of the fully discrete scheme even in the isotropic case.

We conclude with several tests and simulations for curves and surfaces. In particular we show a very interesting example of evolution towards a toroidal anisotropic Willmore surface. This is, as far as we know, the first of its kind.

We refer to [1] (and reference in there) for more details.

References

[1] P. Pozzi, *Computational anisotropic Willmore flow* Interfaces Free Bound. **17** (2015), no. 2, 189–232.

[2] G. Dziuk, *Computational parametric Willmore flow* Numer. Math. **111**, 1 (2008), 55–80.

Potential flow with free boundaries using the level set method. A review of some electro-hydrodynamic applications

Maria Garzon

(joint work with James A. Sethian, Len J. Gray, August Johanssen)

Many interesting fluid interface problems, such as wave propagation and breaking, droplet and bubble break-up, electro-jetting, rain drops, etc. can be modeled using the assumption of potential flow. In these problems, an interface needs to be advanced by a velocity determined by the solution of a surface partial differential equation posed on this moving boundary. A standard approach comes from a Lagrangian-Eulerian formulation of the potential flow equations together with some sort of front tracking method.

This Lagrangian approach is prone to fail when break-up or merging processes appear. Both mathematical and computational difficulties occur when the free boundary changes topology. By using ideas from a level set formulation, the two surface equations of the Lagrangian formulation can be implicitly embedded in PDEs posed in one higher dimension on a fixed domain, [1, 2]. The advantage of this approach is that it seamlessly allows topologically breakup or merging of the fluid domain.

Let $\Omega_1(t)$ be a fluid domain immersed in an infinite exterior fluid $\Omega_2(t)$, Γ_t be the free boundary separating both domains, and Ω_D be a fixed domain that should contain the free boundary for all $t \in [0, T]$. The level set/extended potential flow model may be then written as:

$$\mathbf{u} = \nabla\phi \text{ in } \Omega_1(t) \tag{1}$$

$$\Delta\phi = 0 \text{ in } \Omega_1(t) \tag{2}$$

$$\Psi_t + \mathbf{u}_{\text{ext}} \cdot \nabla\Psi = 0 \text{ in } \Omega_D \tag{3}$$

$$G_t + \mathbf{u}_{\text{ext}} \cdot \nabla G = f_{\text{ext}} \text{ in } \Omega_D. \tag{4}$$

Here, ϕ is the velocity potential, $\mathbf{u}$ the velocity field, Ψ the level set function, G the extended potential function, f accounts for the surface forces, and the subscript "ext" refers to the extended quantities off the front into Ω_D. This hydrodynamic problem can be coupled with any other exterior problem on $\Omega_2(t)$. In particular, assuming a uniform electric field $\mathbf{E}$ in $\Omega_2(t)$, acting in the direction of the z axis

and $\mathbf{E} = 0$ in $\Omega_1(t)$ (perfect conductor fluid) then:

$$\mathbf{E} = -\nabla U \text{ in } \Omega_2(t) \tag{5}$$

$$\Delta U = 0 \text{ in } \Omega_2(t) \tag{6}$$

$$U = U_0 \text{ on } \Gamma_t \tag{7}$$

$$U = -E_\infty z \text{ at the far field,} \tag{8}$$

where U is the electric potential and E_∞ is the electric field intensity.

Let be ϵ an infinitesimal number and τ the time at which a flow singularity occurs, *i.e.* break-up or merging. It has been numerically shown [2] that, away from $t \in [\tau - \epsilon, \tau + \epsilon]$, the level set/extended potential flow model given by Eqns. (1) to (4) matches the classical Eulerian-Lagrangian formulation. For practical purposes it makes sense to set ϵ as the time at which the inviscid assumptions are no longer valid, which happens at length scales of few nanometers.

By combining finite difference schemes in time and space for Eqns. (3) and (4) with boundary integral methods, we have numerically approximated problems in 2D and 3D axi-symmetric geometries, see [1, 2, 4]. For the fully 3D approximation, we used coupled finite difference level set methods to non-conforming Nitsche finite element method for the Laplace equations, see [6].

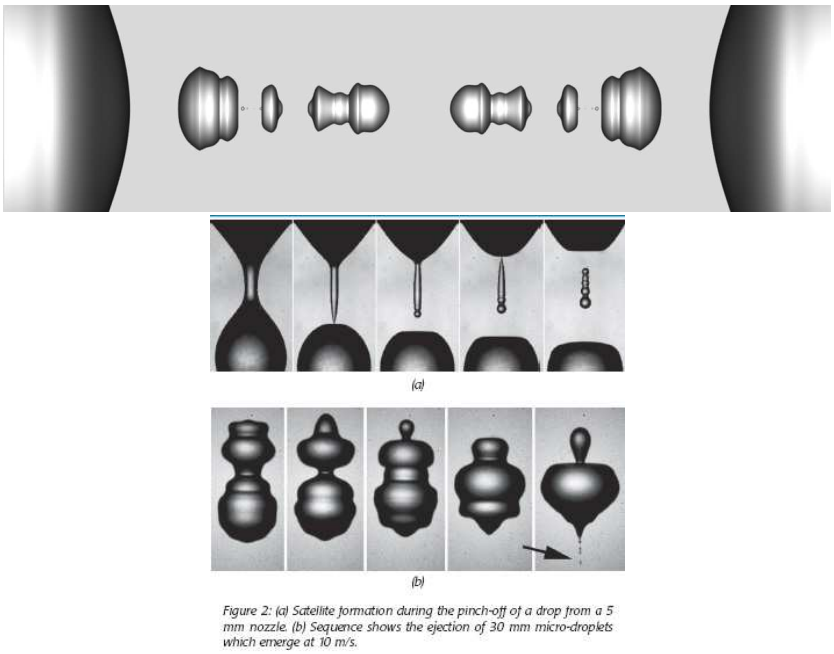

FIGURE 1. Computed profiles (top) and laboratory photographs (bottom)

As examples, we have reported numerical results regarding wave breaking [1], the Rayleigh-Taylor instability of an infinite fluid jet [2], droplet and bubble evolution in a two fluid system [3], electric drop distortion and jetting [5] and a fully 3D computation of film destabilization and tip streaming [6]. To validate these

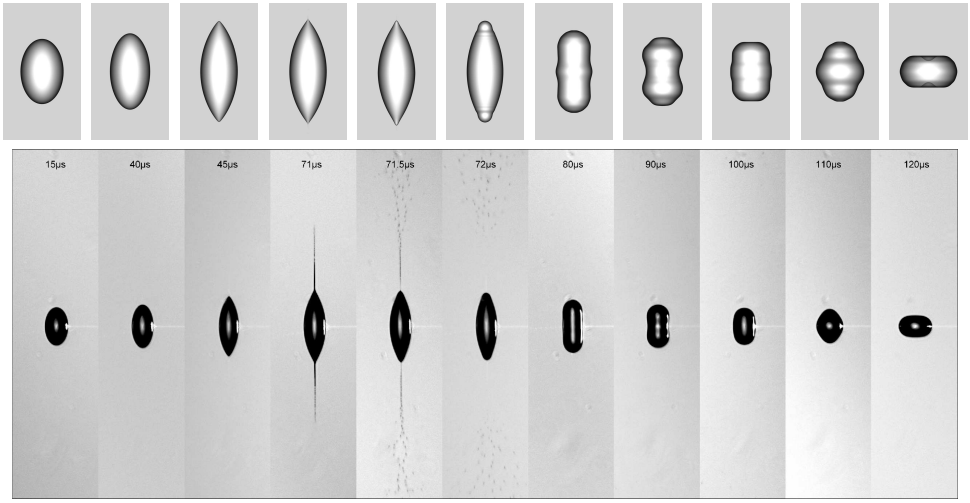

FIGURE 2. Laboratory snapshots at indicated times of the evolution of a surface charged super-cooled water droplet, Reprinted figure with permission from E. Giglio, D. Duft and T. Leisner, Phys. Rev. E, 77, 036319 (2008). Copyright(2008) by the American Physical Society (bottom); and computed profiles at times $80, 101.2, 108.1, 108.5, 109.8, 112.1, 124.2, 133.4, 138, 142, 154.1\mu$s (top), here the symmetry axis is located vertical for comparison.

numerical results, we have tested convergence with respect an analytical solution, when possible; convergence with respect the discretization parameters; self similar scaling laws near singularities; and comparison with available laboratory experiments. In Fig. 1 a snapshot of the Rayleigh-Taylor instability simulation [2] is shown. We show the computed profiles at $t = 22.9$ (top) and compare it with laboratory experiments by Thoroddsen [7] (bottom), and observe the close similarities between the calculated drop shapes and the experimental shapes. A 3D axi-symmetric electro-hydrodynamic simulation is shown in Fig. 2, see [5]. Here, a free charged droplet undergoes distortion, cone-jetting and back to equilibrium shape (when enough charge is lost). We compare computed profiles (top) with laboratory photographs (bottom). Computed drop shapes and time occurrences are in very good agreement with the experimental ones.

REFERENCES

[1] M. Garzon, D. Adalsteinsson, L. J. Gray, J. A. Sethian,*A coupled level set-boundary integral method for moving boundary simulations*, Interfaces and Free Boundaries **7** (2005) 277–302.

[2] M. Garzon, L. J. Gray, J. A. Sethian, *Numerical simulation of non-viscous liquid pinch-off using a coupled levelset-boundary integral method*, J. Comput. Phys. **228** (2009) 6079–6106.

[3] M. Garzon, L. J. Gray, J. A. Sethian, *Simulation of the droplet-to-bubble transition in a two-fluid system*, Phys. Rev. E **83** (2011) 046318.

[4] M. Garzon, L. J. Gray, J. A. Sethian, *Axisymmetric boundary integral formulation for a two-fluid system*, Int. J. Numer. Meth. in Fluids **69** (2012) 1124–1134.

[5] M. Garzon, L. J. Gray, J. A. Sethian, *Numerical simulations of electrostatically driven jets from nonviscous droplets*, Phys. Rev. E **89** (2014) 033011.

[6] Johanssen A., M. Garzon, J. A. Sethian, *A three-dimensional coupled Nitsche and level set method for electrohydrodynamic potential flows in moving domains*, J. Comput. Phys. Accepted for publication.
[7] Thoroddsen S. T., *Micro-droplets and micro-bubbles imaging motion at small scales*, Nus. Eng. Res. News **22** (2007).

A variational approach to particles in lipid membranes

Carsten Gräser
(joint work with C. M. Elliott, G. Hobbs, T. Kies, R. Kornhuber, M.-W. Wolf)

A variety of models for the membrane mediated interaction of particles in lipid membranes are discussed in the literature. Several of them are well established in theoretical physics but lack a rigorous mathematical analysis.

We present mathematically consistent variational formulations for such models [1]. The root model is based on the classic biharmonic-type energy

$$J(u) = \frac{\kappa}{2}\int_\Omega |\Delta u|^2 + \frac{\sigma}{2}\int_\Omega |\nabla u|^2.$$

We consider minimization problems for such functionals in suitable subspaces of $H^2(\Omega)$ under additional constraints of the form

$$u = h_i, \qquad \frac{\partial}{\partial n}u = s_i \qquad \text{on } \partial B_i(x_i) \tag{1}$$

for N particles $B_i(x_i) \subseteq \Omega$, $i = 1, \dots, N$, with centers $x_i \in \Omega$. This can e. g. be viewed a model for conical inclusions in the membrane as depicted in Figure 1.

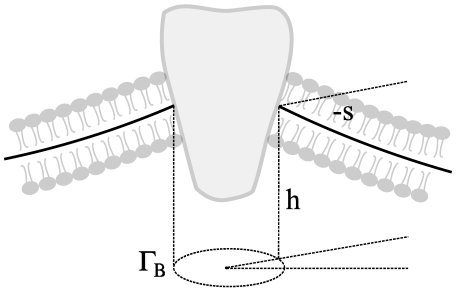

Figure 1. A conical inclusion in a membrane

For fixed particle positions x_i this leads to variational problems that can be treated by classical linear theory. The same is true if particles are allowed to tilt and adjust their average height freely. In the more general case we look for energy minimizing particle positions leading to nonlinear coupled problems for u and the N positions $x_i \in \mathbb{R}^2$. Using an equivalent formulation we show existence of minimizers $(u, x) \in H^2(\Omega) \times (\mathbb{R}^2)^N$ [2].

By relaxing the curve constraints (1) we arrive at new models with averaged curve constraints that bridge (1) to another common class of models based on point curvature constraints. The presented approach allows to view those seemingly

unrelated models as a hierarchy and to show new existence and uniqueness results. It also makes those problems accessible to effective numerical methods. This is illustrated by numerical results that examine the repulsive or attractive nature of different particle configurations for curve and point constraints [1].

References

[1] C. M. Elliott, C. Gräser, G. Hobbs, R. Kornhuber, and M.-W. Wolf. A variational approach to particles in lipid membranes. Technical report, 2015, arxiv:1512.02375.
[2] C. Gräser, T. Kies, and M.-W. Wolf. Optimal position and orientation of particle embedded in lipid membranes. Technical report, 2016. in preparation.

Curvature elasticity of membranes and vesicles: Stability relations

Reinhard Lipowsky

Biological membranes consist of fluid bilayers with many lipid and protein components. The fluidity implies a high flexibility that allows the membranes to attain a large variety of different shapes. [1] This polymorphism can be understood in the framework of the spontaneous curvature model. [2, 3] As shown recently, the model also provides important insight into the engulfment of nanoparticles [4] and the formation of membrane nanotubes [5].

One intriguing aspect of the spontaneous curvature model are relatively simple stability relations that express the mean curvature of certain membrane segments in terms of the model parameters. Three such stability relations are discussed in some detail. These relations describe the stability of closed membrane necks after budding [3]; the onset of membrane adhesion [4]; and the stability of necks for completely engulfed nanoparticles [4]. The relations are intuitively appealing and have been confirmed my extensive numerical calculations but, so far, have not been proved in a rigorous manner.

References

[1] R. Lipowsky, Biol. Chem. 395, 253–274 (2014)
[2] W. Helfrich, Z. Naturforsch. 28c, 693–703 (1973)
[3] U. Seifert, K. Berndl, R. Lipowsky, Phys. Rev. A 44, 1182–1202 (1991)
[4] J. Agudo-Canaleijo and R. Lipowsky, ACS Nano 9, 3704 (2015); and Nano Letters 15, 7168 (2015)
[5] Y. Liu, J. Agudo-Canaleijo, A. Grafmller, R. Dimova and R. Lipowsky, ACS Nano (in press) DOI: 10.1021/acsnano.5b05377

Wrinkling of thin elastic sheets

Oliver Sander

The wrinkling behavior of thin elastic structures is of much interest both to engineers and mathematicians. Recently, Wong and Pellegrino [9] conducted systematic experimental tests of the wrinkling of a rectangular polyimide sheet under shear displacements. One of their results is shown in Figure 1. One observes a pattern of wrinkles at a 45° angle, but also secondary features like higher-frequency wrinkles near the horizontal boundaries, and irregular low-frequency wrinkles near the vertical edges.

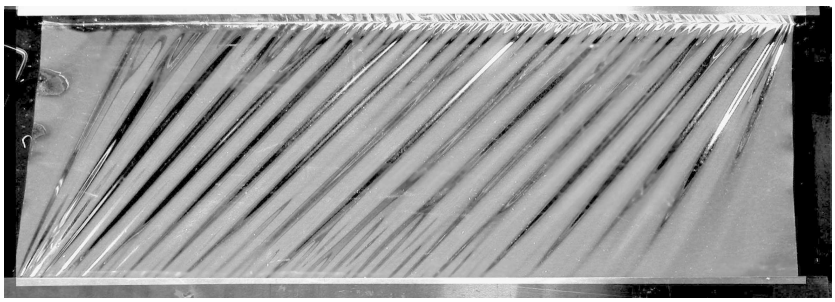

Figure 1. Photo of a thin polyimide sheet under a shearing displacement (taken from [9])

Various models and simulation approaches have been proposed to numerically reproduce these wrinkling patterns [8, 10]. A suitable mathematical model is the geometrically exact hyperelastic Cosserat shell proposed by Neff [4]. In this model, configurations of a shell are pairs of functions

$$(m, \overline{R}) : \mathbb{R}^2 \supset \omega \to \mathbb{R}^3 \times \mathrm{SO}(3).$$

The function m describes the displacement of the shell midsurface, and the microrotation field $\overline{R}$ models the direction and drilling of a transversal unit vector. Stable states of the shell are minimizers of the energy functional

$$I(m, \overline{R}) = \int_\omega h\, W_{\mathrm{mp}}(\overline{U}) + h\, W_{\mathrm{curv}}(\mathfrak{K}_s) + \frac{h^3}{12}\, W_{\mathrm{bend}}(\mathfrak{K}_b)\, \mathrm{d}\omega + \text{loads}, \tag{1}$$

subject to suitable boundary conditions for the deformation and rotation. The quantities $\overline{U}$, $\mathfrak{K}_s$, and $\mathfrak{K}_b$ are the strain measures, defined as

$$\overline{U} = \overline{R}^T \hat{F} \qquad \text{with} \qquad \hat{F} = (\nabla m | \, \overline{R}_3) \in \mathbb{R}^{3\times 3},$$

and

$$\mathfrak{K}_s := \left(\overline{R}^T (\nabla \overline{R}_1 | \, 0), \overline{R}^T (\nabla \overline{R}_2 | \, 0), \overline{R}^T (\nabla \overline{R}_3 | \, 0) \right) =: \left(\mathfrak{K}_s^1, \mathfrak{K}_s^2, \mathfrak{K}_s^3 \right) \in \mathbb{R}^{3\times 3\times 3},$$

$$\mathfrak{K}_b := \overline{R}^T (\nabla \overline{R}_3 | \, 0) = \mathfrak{K}_s^3 \in \mathbb{R}^{3\times 3}.$$

The three parts of the elastical energy density of the shell correspond to membrane-strain W_{mp}, total curvature-strain W_{curv} and specific bending-strain W_{bend}. They have the expressions

$$\begin{aligned} W_{\mathrm{mp}}(\overline{U}) &= \mu \| \operatorname{sym}(\overline{U} - \mathbb{1})\|^2 + \mu_c \| \operatorname{skew}(\overline{U} - \mathbb{1})\|^2 \\ &\quad + \frac{\mu\lambda}{2\mu+\lambda}\,\frac{1}{2}\left((\det \overline{U} - 1)^2 + \left((\det \overline{U})^{-1} - 1\right)^2\right), \\ W_{\mathrm{curv}}(\mathfrak{K}_s) &= \mu\, L_c^q\, \|\mathfrak{K}_s\|^q\,, \\ W_{\mathrm{bend}}(\mathfrak{K}_b) &= \mu\, \| \operatorname{sym}(\mathfrak{K}_b)\|^2 + \mu_c \| \operatorname{skew}(\mathfrak{K}_b)\|^2 + \frac{\mu\lambda}{2\mu+\lambda}\, \operatorname{tr}\left[\operatorname{sym}(\mathfrak{K}_b)\right]^2, \end{aligned}$$

where λ, μ are the Lamé parameters, $\mu_c \geq 0$ is called the Cosserat couple modulus, and the parameter $L_c > 0$ is an internal length of the material, which is responsible for size effects. Existence of such minimizers in $W^{1,p}$ has been shown in [4, 5].

Discretization of such a model by finite elements is difficult, because the function spaces $W^{1,p}(\omega, \mathrm{SO}(3))$ do not have a vector space structure. In [6], the author has generalized standard Lagrangian finite elements to such nonlinear spaces. This generalization, termed *geodesic finite elements*, uses functions that are continuous, and piecewise given by the interpolation rule

$$\Upsilon \;:\; T_{\mathrm{ref}} \to \mathrm{SO}(3), \qquad \Upsilon(\xi) = \operatorname*{arg\,min}_{R \in \mathrm{SO}(3)} \sum_{i=1}^{m} \lambda_i(\xi)\, \operatorname{dist}(R_i, R)^2, \tag{2}$$

where $\{\lambda_i\}_{i=1}^m$ is a set of p-th order scalar Lagrangian shape functions on the reference element T_{ref}, and $R_i \in \mathrm{SO}(3)$, $i = 1, \ldots, m$ are values at the corresponding Lagrange nodes. Properties of these interpolation functions are discussed in [6]. A priori H^1 error bounds have been shown in [2], but it currently appears that the energy functional (1) does not satisfy the assumptions of this theory.

Geodesic finite element functions are H^1 Sobolev functions, and therefore the continuous minimization problem for the functional I directly leads to a minimization problem on a product space $(\mathbb{R}^3)^{n_1} \times \mathrm{SO}(3)^{n_2}$. We solve this problem with a Riemannian trust-region method as proposed in [1]. For the inner solver we use a monotone multigrid method [3]. Convergence speed of this methods leaves to be desired, because, with realistic parameter choices, the tangent matrices of the functional I can be very ill-conditioned. A good structure-exploiting preconditioner for these systems would be a major step forward.

Using the energy (1) and the discretization based on (2) to reproduce the wrinkling experiment from Figure 1, we obtained the result shown in Figure 2 [7]. Both the diagonal wrinkles as well as the secondary features can be clearly seen. Wong and Pellegrino also measured the transversal deflection at the horizontal midline of the sheet. Figure 2 shows their results, together with the corresponding data from our simulation. The number of wrinkles is almost identical in experiment and simulation. The difference may be explained by the fact that the energy functional can be expected to have several local minima. Also, one can see that the simulation overestimates the wrinkle amplitudes. The reason for this is unclear. One

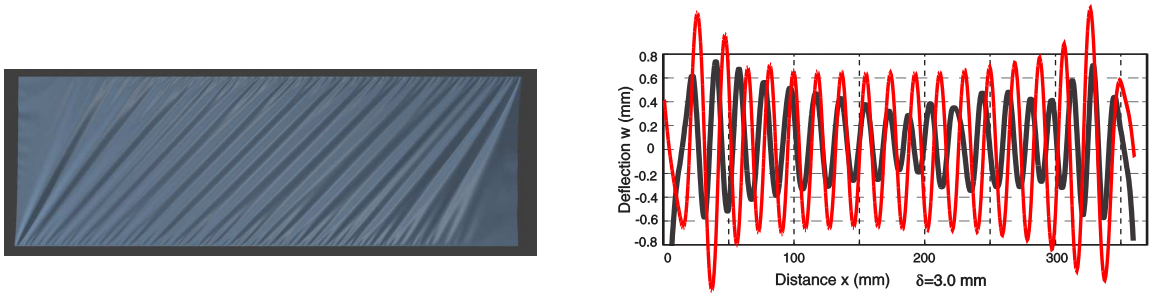

FIGURE 2. Left: Numerical simulation of the experiment from Figure 1. Right: Transversal displacement at the horizontal midline. Black: measured results from [9]. Red: simulation results from [7]

hypothesis is that the actual sheets show plastic behavior, which is not included in the numerical model.

REFERENCES

[1] P.-A. Absil, R. Mahony, and R. Sepulchre. *Optimization Algorithms on Matrix Manifolds*. Princeton University Press, 2008.

[2] P. Grohs, H. Hardering, and O. Sander. Optimal a priori discretization error bounds for geodesic finite elements. *Found. Comput. Math.*, 2014. online, doi: 10.1007/s10208-014-9230-z.

[3] R. Kornhuber. *Adaptive Monotone Multigrid Methods for Nonlinear Variational Problems*. B.G. Teubner, 1997.

[4] P. Neff. A geometrically exact Cosserat-shell model including size effects, avoiding degeneracy in the thin shell limit. Part I: Formal dimensional reduction for elastic plates and existence of minimizers for positive Cosserat couple modulus. *Continuum Mech. Thermodyn.*, 16:577–628, 2004.

[5] P. Neff. A geometrically exact planar Cosserat shell-model with microstructure: Existence of minimizers for zero Cosserat couple modulus. *Math. Models Methods Appl. Sci.*, 17:363–392, 2007.

[6] O. Sander. Geodesic finite elements of higher order. *IMA J. Numer. Anal.*, 2015. online, doi: 10.1093/imanum/drv016.

[7] O. Sander, P. Neff, and M. Bîrsan. Numerical Treatment of a Geometrically Nonlinear Planar Cosserat Shell Model. arXiv: 1412.3668, 2014.

[8] M. Taylor, K. Bertoldi, and D. J. Steigmann. Spatial resolution of wrinkle patterns in thin elastic sheets at finite strain. *J. Mech. Phys. Solids*, 62:163–180, 2014.

[9] Y. W. Wong and S. Pellegrino. Wrinkled membranes part I: Experiments. *J. Mech. Mater. Struct.*, 1(1):1–23, 2006.

[10] Y. W. Wong and S. Pellegrino. Wrinkled membranes part III: Numerical simulations. *J. Mech. Mater. Struct.*, 1(1):63–95, 2006.

Cahn–Hilliard–Darcy models for tumour growth with chemotaxis and active transport

Harald Garcke
(joint work with Kei Fong Lam, Emanuel Sitka, Vanessa Styles)

In recent years several phase field type models for tumour growth have been introduced. We propose a new model which is derived with the help of basic thermodynamical principles and leads to a Cahn–Hilliard–Darcy system. The model takes nutrient diffusion, chemotaxis, apoptosis, proliferation, adhesion and as a new aspect active transport into account. An additional new feature of the model is that it is based on a volume averaged velocity which leads to particular simple equations for the flow velocity and the pressure.

The overall system is given as

$$\begin{aligned}
\operatorname{div} \mathbf{v} &= \alpha\Gamma\,,\\
\mathbf{v} &= -K(\nabla p - \mu\nabla\varphi - \chi\sigma\nabla\varphi)\,,\\
\partial_t\varphi + \operatorname{div}(\varphi\mathbf{v}) &= m\Delta\mu + \overline{\rho}_s\Gamma\,,\\
\mu &= \frac{\beta}{\varepsilon}W'(\varphi) - \beta\varepsilon\Delta\varphi - \chi\sigma\,,\\
\partial_t\sigma + \operatorname{div}(\sigma\mathbf{v}) &= \operatorname{div}(n(\chi_\sigma\nabla\sigma - \chi\nabla\varphi)) - \mathcal{C}\sigma h(\varphi)\,,\\
\Gamma &= (\mathcal{P}\sigma - \mathcal{A})h(\varphi)\,.
\end{aligned}$$

Here, $\mathbf{v}$ is the velocity, p the pressure, φ is related to the tumour density, μ is the chemical potential and σ is the nutrient density. Furthermore K, $\overline{\rho}_s$, m, β, ε, n, $\mathcal{C}$, $\mathcal{P}$, $\mathcal{A}$ are positive constants, W is a double well potential and α is a real number. The phase field φ takes the value $+1$ in the tumour region and the value -1 in the region occupied by healthy cells. The function h is an interpolation function with $h(1) = 1$ and $h(-1) = 0$.

A sharp interface limit in the limit $\varepsilon \to 0$ can be identified. For the simplified model (no Darcy flow, quasi-static nutrient diffusion)

$$\begin{aligned}
\partial_t\varphi &= \Delta\mu + h(\varphi)(\mathcal{P}\sigma - \mathcal{A})\,,\\
\mu &= \frac{1}{\varepsilon}W'(\varphi) - \varepsilon\Delta\varphi - \chi\sigma\,,\\
0 &= \Delta\sigma - \eta\Delta\varphi - h(\varphi)\mathcal{B}\sigma
\end{aligned}$$

we obtain the sharp interface limit

$$-\Delta\mu = \begin{cases} \mathcal{P}\sigma - \mathcal{A} & \text{in } \Omega_T\,,\\ 0 & \text{in } \Omega_H\,, \end{cases} \qquad \Delta\sigma = \begin{cases} \mathcal{B}\sigma & \text{in } \Omega_T\,,\\ 0 & \text{in } \Omega_H\,, \end{cases}$$

$$\begin{aligned}
[\mu]_H^T &= 0, [\sigma]_H^T = 2\eta && \text{on } \Gamma\,,\\
2\mu &= \gamma\kappa - \chi(\sigma_H + \sigma_T) && \text{on } \Gamma\,,\\
0 &= [\nabla\sigma]_H^T \cdot \nu && \text{on } \Gamma\,,\\
-\mathcal{V} &= [\nabla\mu]_H^T \cdot \nu && \text{on } \Gamma\,,
\end{aligned}$$

where Ω_T and Ω_H are the regions occupied by the tumour and the healthy cells, $[.]_H^T$ denote the jump across the interface $\Gamma = \partial\Omega_T \cap \partial\Omega_H$ and κ is the mean curvature of the interface. A particular feature is that the presence of the active transport leads to a jump of the nutrient concentration across the sharp interface Γ. For details and for the asymptotic limit of the full Cahn–Hilliard–Darcy system we refer to [1] where the sharp interface limit is derived with the help of formally matched asymptotic expansions. A well-posedness result for Cahn–Hilliard systems modelling tumour growth with chemotaxis and active transport is given in [2].

Well-posedness results for the full Cahn–Hilliard–Darcy system and for the sharp interface problem are missing so far. In addition, no rigorous results on the sharp interface limit are known so far. It would also be interesting to study optimal control problems related to the above Cahn–Hilliard–Darcy system.

References

[1] H. Garcke, K.F. Lam, E. Sitka, V. Styles, *A Cahn–Hilliard–Darcy model for tumour growth with chemotaxis and active transport*, (2015) to appear in M^3AS, arXiv:1508.00437.

[2] H. Garcke, K.F. Lam *Well-posedness of a Cahn-Hilliard system modelling tumour growth with chemotaxis and active transport*, (2015), arXiv:1511.06143

Numerical study of liquid droplets propelled by Marangoni flow

Laura Stricker

(joint work with Jürgen Vollmer)

In order to understand the collective behaviour of biological microswimmers, such as bacteria and spermatozoa, it is important to know which aspects are governed merely by the physics of the system and which aspects are biology-related. In the present study we address the mechanisms of locomotion of non-biological swimmers. We focus on artificial swimmers consisting in active droplets moving by Marangoni flow [1]. In such droplets, a non-uniform surface tension distribution arises on the droplet surface, due to a non-uniform distribution of surfactants (polar molecules dissolved in the solution and migrating to the surface). To satisfy the local forces balance at the interface, a Marangoni stress originates, tangent to the surface, from the area with a lower surface tension to the one with a higher surface tension. From this, a convective fluid motion is set inside and outside the droplet and the droplet starts moving, by momentum conservation (Fig. 1).

In our study, we consider two kinds of systems: nematic liquid crystal droplets immersed in an aqueous solution of ionic surfactant [2], and self-propelled droplets driven by Belousov-Zhabotinsky (BZ) reactions [3]. We numerically study the flow field outside and inside a single droplet, by means of a level set method [4], in order to account for both the deformation of the droplet and the interaction with a small number of neighboring droplets. Further mechanisms that influence the locomotion, such as mass transport, chemical reactions and the coupling between the bulk and the surface concentration of the surfactants, are also specifically

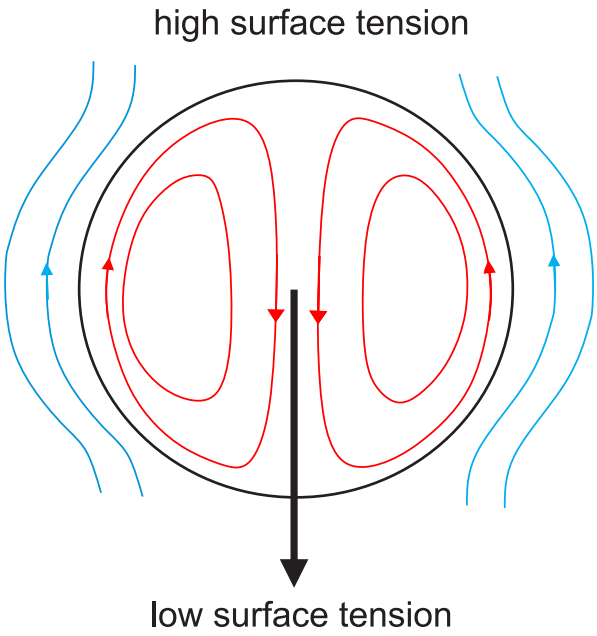

FIGURE 1. Sketch of droplet moving by Marangoni flow. The thin grey arrows represent the direction of the induced motion, the curved lines represent the flow profile. The thick black arrow represents the direction of the droplet's motion.

addressed. From the surface distribution of the surfactants we derive the local surface tension, by means of a Langmuir equation of state [5].

We considered both the case of soluble and insoluble surfactant. In the case of insoluble surfactants, the two concentration fields, in the bulk and on the surface, are decoupled. The dynamics and the kinematics were tested by prescribing a surface tension field, instead of deriving it from the Langmuir equation. In Fig. 2 we show the motion resulting from a surface tension field $\sigma(\theta) = \sigma_0(1 + \epsilon \cos\theta \pm \sin(2\theta))$, where θ is the angular position with respect to the radial axis, σ_0 is a constant and $\epsilon = 0.4$. We reproduce the typical behavior of squirmers acting as pullers (left figure, corresponding to the sign $+$) and pushers (right figure, corresponding to the sign $-$). The dark-grey lines represent the initial position, the light-grey line represents the position of the droplet at time $t^* = t/t_0 = 0.12$, where the time scale $t_0 = \sqrt{\pi R_0^3 \rho / 2\epsilon\sigma_0}$ gives an estimate of the time required to displace a droplet of density ρ and radius R_0 along a distance of one time its radius, only due to Marangoni flow. The arrows represent the velocity field in the co-moving frame of reference r-z, shifting with the droplet.

In the case of soluble surfactants, we simulate a possible mechanism giving origin to self-propulsion, as a consequence of a random initial displacement of the droplet.

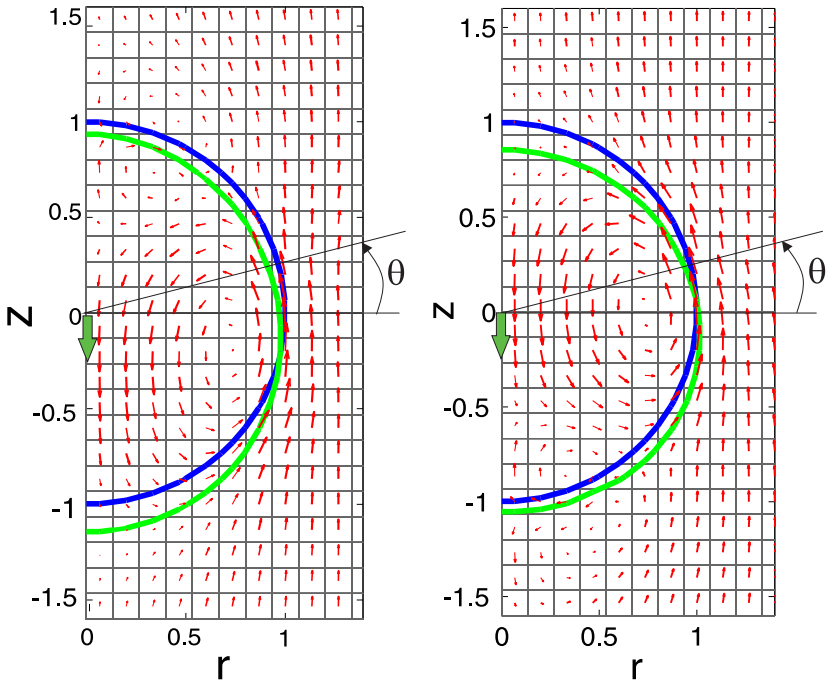

FIGURE 2. Numerical simulation of a droplet moving by Marangoni flow, when a surface tension field is prescribed as $\sigma(\theta) = \sigma_0(1 + \epsilon\cos\theta \pm \sin(2\theta))$. The sign + corresponds to the figure on the left, the − to the figure on the right. Parameters: $R_0 = 25\mu m$, $\epsilon = 0.4$. The dark-grey lines represent the initial position, the light-grey lines the position of the droplet at time $t^* = t/t_0 = 0.12$. The arrows depict the velocity of the flow in the co-moving frame, shifting with the droplet. The two droplets reproduce the typical puller (left), pusher (right) behavior exhibited by squirmers.

REFERENCES

[1] D. A. Saville, *The effects of interfacial tension gradients on the motion of drops and bubbles*, Chem. Eng. J., vol. 5 **3** (1973), 251–259.

[2] K. Peddireddy, P. Kumar, S. Thutupalli, S. Herminghaus, and C. Bahr, *Solubilization of thermotropic liquid crystal compounds in aqueous surfactant solutions*, Langmuir **28** (2012), 12426–12431.

[3] M. M. Hanczyc, T. Toyota, T. Ikegami, N. Packard, and T. Sugawara, *Fatty acid chemistry at the oil-water interface: Self-propelled oil droplets*, J. Am. Chem. Soc. **129** (2007), 9386–9391.

[4] J. A. Sethian, *Level set methods and fast marching methods*, Cambridge (1999), Cambridge University Press.

[5] Y. Pawar and K. Stebe, *Marangoni effects on drop deformation in an extensional flow: The role of surfactant physico-chemistry. I. Insoluble surfactants*, Phys. Fluids **8** (1996), 1738–1751.

Cell membrane interaction with membrane proteins and with the cytoskeleton

Christian Schmeiser
(joint work with Gaspard Jankowiak, Christoph Winkler)

Biological cells and intracellular compartments are enclosed by the cell membrane, a lipid bilayer, which resists bending and has the tangential behavior of a two-dimensional incompressible fluid. It strongly interacts with other cellular compartments and it is important for the regulation of various cellular processes.

An example is the leading edge of the lamellipodium, a flat cell protrusion important for cell spreading and crawling on flat surfaces. The protein IRSp53 has an I-BAR domain, binding to the cell membrane and promoting convex membrane deformation, and an SH3 domain, binding to the machinery which regulates growth of the cytoskeleton network supporting the lamellipodium. In [3] the flat shape of the lamellipodium has been attributed to this coupling of membrane geometry with cytoskeleton dynamics. A quasistationary model for membrane deformation driven by cytoskeleton growth and including an IRSp53-cluster has been coupled to a stochastic model for the cytoskeleton dynamics (for details see [3]). Snapshots from a simulation showing stable growth of a flat lamellipodium are depicted in Fig. 1.

The model of [3] is incomplete in the sense that it does not describe the formation of clusters of BAR domains. As a first step in this direction, we formulate a model for the dynamics of a distribution of BAR domains along a one-dimensional deforming membrane in a two-dimensional environment. The membrane is described as a smooth closed curve of fixed length L in terms of its curvature $\kappa(s,t)$, depending on arclength s and time t, and minimizing (at each time t) the modified Helfrich energy [2]

$$E[\kappa] = \int_0^L (\kappa^2 + \rho(\kappa - \kappa^*)^2) ds\,,$$

where $\rho(s,t)$ is the BAR domain distribution and κ^* is the equilibrium curvature of the BAR domain. For closedness and smoothness of the curve, κ has to satisfy the constraints

$$\int_0^L \kappa\, ds = 2\pi\,, \qquad \int_0^L \sin\left(\int_0^s \kappa\right) ds = \int_0^L \cos\left(\int_0^s \kappa\right) ds = 0\,.$$

For ρ we propose the convection-diffusion model

$$\partial_t \rho = \partial_s \left(D\partial_s \rho + \rho(1-\rho)\partial_s \frac{(\kappa - \kappa^*)^2}{2} \right)$$

with diffusivity D and the volume filling factor $(1-\rho)$ turning off the tendency of BAR domains to migrate towards regions of favorable curvature, when the maximal density 1 is reached.

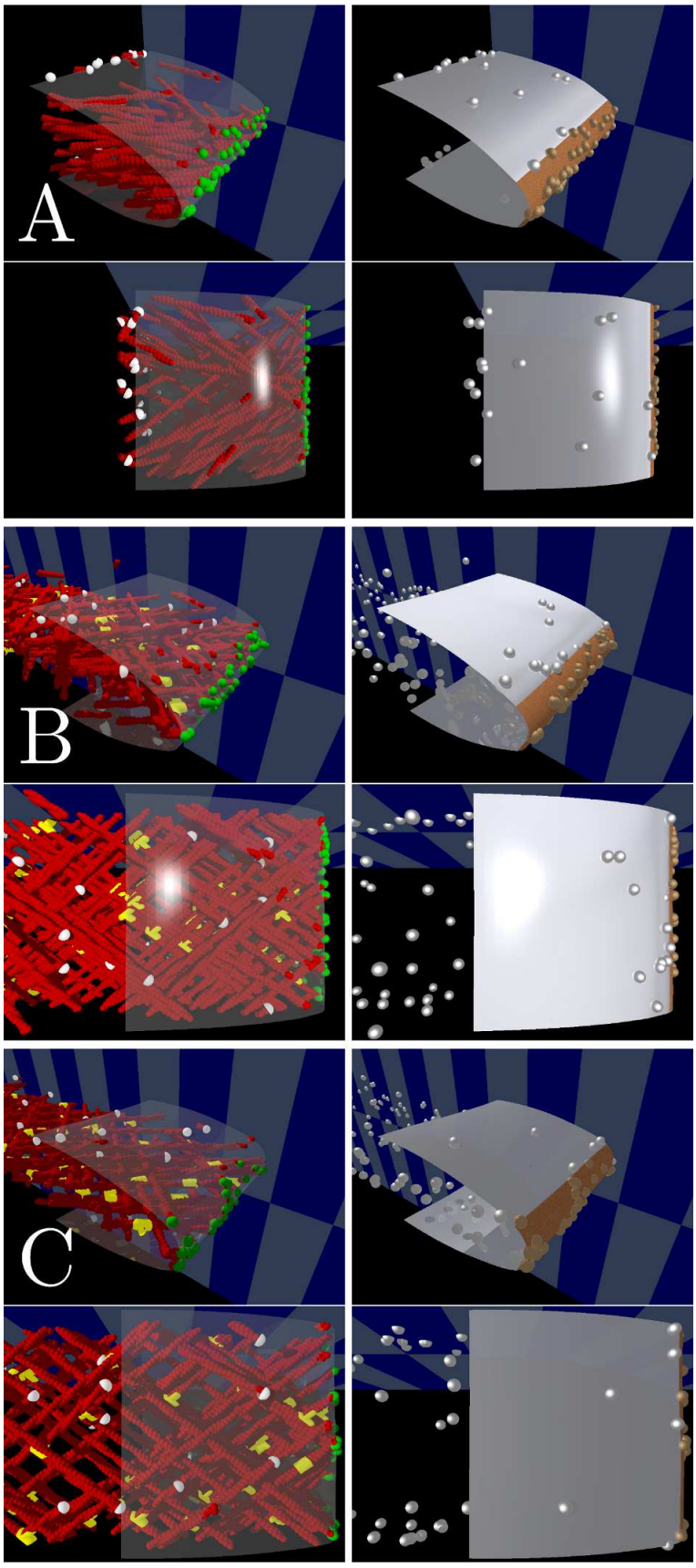

FIGURE 1. Time series of a lamellipodium simulation from [3]

Unfortunately this model seems to be ill posed in certain situations. Using the Euler-Lagrange equation for κ, the equation for ρ can be written as

$$\partial_t \rho = \partial_s \left(\left(D - \frac{\rho(1-\rho)F^2}{(1+\rho)^3} \right) \partial_s \rho + \frac{\rho(1-\rho)F\partial_s F}{(1+\rho)^2} \right)$$

with an unknown nonlocal operator $F[\rho]$. It is possible that the nonlinear diffusivity in this equation becomes negative, at least for intermediate density values (away from $\rho = 0$ and $\rho = 1$). A similar model has been derived as formal macroscopic limit of a microscopic model for cell-cell adhesion [1]. In simulations with the microscopic model, many small clusters have been observed as a consequence of oscillatory solution behavior, followed by a coarsening process, similar to phase change models.

References

[1] K. Anguige, C. Schmeiser, *A one-dimensional model for cell diffusion and aggregation, incorporating volume filling and cell-to-cell adhesion*, J. Math. Biol. **58** (2009), 395–427.

[2] W. Helfrich, *Elastic Properties of Lipid Bilayers: Theory and Possible Experiments*, Z. Naturforsch. C **28** (1973), 693–703.

[3] C. Schmeiser, C. Winkler, *The Flatness of Lamellipodia Explained by the Interaction Between Actin Dynamics and Membrane Deformation*, J. Theoret. Biol. **380** (2015), 144–155.

On algorithms with good mesh properties based on the harmonic map heat flow and the DeTurck trick

Hans Fritz

(joint work with Charles M. Elliott)

In the first part, novel numerical schemes for the computation of the curve shortening and mean curvature flows are introduced. These schemes are based on special reparametrizations of the evolution equations. The main idea is to use solutions to the harmonic map heat flow for the reparametrization. This idea is known from the Ricci flow as the DeTurck trick; see [4, 6]. The reparametrization is done in two steps. Firstly, the mean curvature and the harmonic map heat flows are coupled in the following way

$$(P) = \begin{cases} \dfrac{\partial}{\partial t} x = -(H\nu) \circ x, \quad \text{with } x(\cdot, 0) = x_0 \text{ on } \mathcal{M}, \\ \dfrac{\partial}{\partial t} \psi_\alpha = \dfrac{1}{\alpha} \Delta_{g(t),h} \psi_\alpha, \quad \text{with } g(t) := x(t)^* \mathfrak{e} \text{ and } \psi_\alpha(\cdot, 0) = id(\cdot) \text{ on } \mathcal{M}. \end{cases}$$

Here, $x : \mathcal{M} \times [0, T) \to \mathbb{R}^{n+1}$ is a time-dependent embedding of the n-dimensional, closed reference manifold $\mathcal{M}$. The velocity of $x(t)$ in the normal direction $\nu(t)$ is proportional to the mean curvature $H(t) := \nabla_{\Gamma(t)} \cdot \nu(t)$ of the hypersurface $\Gamma(t) := x(\mathcal{M}, t)$. The harmonic map heat flow $\psi_\alpha : \mathcal{M} \times [0, T) \to \mathcal{M}$ depends on the pull-back metric $g(t) := x(t)^* \mathfrak{e}$ of the Euclidean metric $\mathfrak{e}$ and on the fixed yet arbitrary background metric h on $\mathcal{M}$. $\Delta_{g(t),h}$ is the so-called map Laplacian with respect to these metrics. The inverse diffusion constant $\alpha > 0$ determines the time

scale of the harmonic map heat flow. In the second step, the embedding $x(t)$ is reparametrized by $\hat{x}_\alpha(t) := x(t) \circ \psi_\alpha(t)^{-1}$. A direct calculation shows that $\hat{x}_\alpha(t)$ satisfies the following PDE, which is called the mean curvature-DeTurck flow,

$$\frac{\partial}{\partial t}\hat{x}_\alpha = \Delta_{\hat{g}_\alpha(t)}\hat{x}_\alpha - \frac{1}{\alpha}\nabla\hat{x}_\alpha(V_\alpha),$$

with $\hat{g}_\alpha := \hat{x}_\alpha(t)^*\mathfrak{e}$ and $V_\alpha^j := \hat{g}_\alpha^{kl}(\Gamma(h)_{kl}^j - \Gamma(\hat{g}_\alpha)_{kl}^j)$, where $\Gamma(h)$ and $\Gamma(\hat{g}_\alpha)$ denote the corresponding Christoffel symbols. It is important for our numerical approach that this equation does not depend on the harmonic map heat flow $\psi_\alpha(t)$ any more. The reparametrization leads to an additional tangential velocity, which induces the advantageous mesh redistributions in the discrete setting. In the one-dimensional case, that is for the curve shortening flow, it is possible to rewrite the above PDE in divergence form by using a certain splitting of the time derivative. The spatial discretization of the corresponding weak formulation leads to a semi-discrete scheme for which we can prove the following error estimates.

Theorem 1. *Let $\alpha \in (0,1]$ and suppose that $\hat{X} \in C^{2,1}(\mathbb{R}/2\pi \times [0,T], \mathbb{R}^2)$ is a solution of*

$$\alpha\hat{X}_t + (1-\alpha)(\nu \cdot \hat{X}_t)\nu = |\hat{X}_\theta|^{-2}\hat{X}_{\theta\theta}, \quad \text{in } \mathbb{R}/2\pi \times (0,T),$$
$$\hat{X}(\cdot,0) = X_0(\cdot), \quad \text{on } \mathbb{R}/2\pi,$$

with $\hat{X}_t \in L^\infty((0,T), H^{1,2}(\mathbb{R}/2\pi,\mathbb{R}^2)) \cap L^2((0,T), H^{2,2}(\mathbb{R}/2\pi,\mathbb{R}^2))$, and $|\hat{X}_\theta| \geq c_0 > 0$ in $\mathbb{R}/2\pi \times [0,T]$. Then there exists a constant $h_0 > 0$ depending on $\hat{X}$, T and α such that for every $0 < h \leq h_0$ there is a unique solution $\hat{X}_h \in H^{1,2}((0,T), \mathcal{S}_h^2)$ of the non-linear, semi-discrete problem

$$\int_0^{2\pi} \Big(\alpha\hat{X}_{ht} \cdot \varphi_h + (1-\alpha)(\hat{X}_{ht} \cdot \nu_h)(\nu_h \cdot \varphi_h)\Big)|\hat{X}_{h\theta}|^2 d\theta + \int_0^{2\pi} \hat{X}_{h\theta} \cdot \varphi_{h\theta} d\theta = 0,$$

$\forall \varphi_h \in \mathcal{S}_h^2, 0 < t < T$, with initial data $\hat{X}_h(\cdot,0) = (I_h X_0)(\cdot)$ on $\mathbb{R}/2\pi$, and

$$\alpha \int_0^T \|(\hat{X}_t - \hat{X}_{ht})(t)\|_{L^2(0,2\pi)}^2 dt + (1-\alpha)\int_0^T \|\nu_h \cdot (\hat{X}_t - \hat{X}_{ht})(t)\|_{L^2(0,2\pi)}^2 dt$$
$$+ \max_{t\in[0,T]} \|(\hat{X} - \hat{X}_h)(t)\|_{H^{1,2}(0,2\pi)}^2 \leq Ce^{\frac{M}{\alpha}T}h^2.$$

The constants C and M depend on the continuous solution $\hat{X}$ and on T.

Here, $\mathcal{S}_h$ denotes the space of periodic, continuous and piecewise linear functions on the computational grid of $[0, 2\pi]$. The proof is based on Schauder's fixed point theorem. We use the time discretization to linearize the problem in each time step.

Algorithm 1. *Let $\alpha \in (0,\infty)$. For a given initial polygonal curve $\Gamma_h^0 = \hat{X}_h^0(\mathbb{R}/2\pi)$ with $\hat{X}_h^0 \in \mathcal{S}_h^2$, determine for $m = 0, \ldots, M_\tau - 1$ the solution $\hat{X}_h^{m+1} \in \mathcal{S}_h^2$ of*

$$\int_0^{2\pi} \left(\frac{\alpha}{\tau}\hat{X}_h^{m+1} \cdot \varphi_h + \frac{1-\alpha}{\tau}(\hat{X}_h^{m+1} \cdot \nu_h^m)(\nu_h^m \cdot \varphi_h)\right)|\hat{X}_{h\theta}^m|^2 d\theta + \int_0^{2\pi} \hat{X}_{h\theta}^{m+1} \cdot \varphi_{h\theta} d\theta$$
$$= \int_0^{2\pi} \left(\frac{\alpha}{\tau}\hat{X}_h^m \cdot \varphi_h + \frac{1-\alpha}{\tau}(\hat{X}_h^m \cdot \nu_h^m)(\nu_h^m \cdot \varphi_h)\right)|\hat{X}_{h\theta}^m|^2 d\theta, \quad \forall \varphi \in \mathcal{S}_h^2,$$

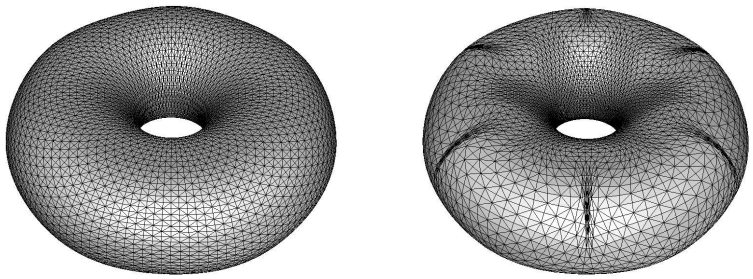

(A) (B)

FIGURE 1. Simulation of the mean curvature flow. The left image shows the result of our new approach at $t = 0.11$. The right image shows the result of Algorithm (2.25) in [1] for the same number of vertices.

where ν_h^m is a piecewise constant unit normal field to the polygonal curve Γ_h^m, and set

$$\Gamma_h^{m+1} := \hat{X}_h^{m+1}([0, 2\pi]).$$

The above family of numerical schemes for the curve shortening flow unveils a surprising geometric connection between the numerical schemes in [2] and [3]. Numerical experiments show that the above schemes have good mesh properties for sufficiently small α, which means that the ratio of the maximal to the minimal segment length is usually close to one. For the higher-dimensional case, that is for the mean curvature-DeTurck flow, we also obtain families of schemes with good mesh properties, which means that the quotient of the diameter of a simplex and of the radius of the largest ball contained in it remains reasonable small for all simplices of the corresponding triangulation. Figure 1 shows the comparison of our approach to the BGN-scheme (2.25) in [1] for the initial surface $\Gamma(0) \subset \mathbb{R}^3$ given by $X_0(\theta, \phi) := \big((r_1 + r_2 \cos\varphi)\cos\theta, (r_1 + r_2\cos\varphi)\sin\theta, r_2 \sin\varphi + \frac{1}{5}\sin(6\theta)\big)$, for $\theta \in [0, 2\pi), \varphi \in [0, 2\pi)$ with radii $r_1 = 1.0$ and $r_2 = 0.65$.

In the second part, we generalize the above approach in order to obtain numerical schemes with good mesh properties for evolving submanifolds with boundaries. This includes moving domains and surfaces with boundaries. In this part, the submanifold does not necessarily evolve according to the mean curvature flow. In order to incorporate the motion of the boundary, we choose the following boundary conditions for the harmonic map heat flow,

$$(BC) := \begin{cases} \nabla_{\mu(t)}\psi \perp_h \partial\mathcal{M} & \text{on } \partial\mathcal{M} \times (0,T), \\ \psi(\partial\mathcal{M}, t) \subset \partial\mathcal{M} & \text{for all } t \in [0,T), \end{cases}$$

where $\mu(t)$ is a unit co-normal field to $\partial\mathcal{M}$ with respect to the pull-back metric $g(t)$; see [5]. The reparametrization of the evolution of the submanifold with boundary by solutions to the harmonic map heat flow of manifolds with boundary leads to a

new velocity field for the motion of the submanifold. An algorithm which is based on the idea to move the mesh vertices according to this velocity field is able to improve or maintain the mesh quality in various circumstances. We show that this idea can be easily built into algorithms for the computation of physical problems with moving boundaries by using the ALE-method in [7].

References

[1] J. W. Barrett, H. Garcke and R. Nürnberg, *On the parametric finite element approximation of evolving hypersurfaces in* $\mathbb{R}^3$, J. Comput. Phys. **227** (2008), 4281–4307.

[2] J. W. Barrett, H. Garcke and R. Nürnberg, *The Approximation of Planar Curve Evolutions by Stable Fully Implicit Finite Element Schemes that Equidistribute*, Numer. Methods Partial Differential Equations **27** (2011), 1–30.

[3] K. Deckelnick and G. Dziuk, *On the approximation of the curve shortening flow*, Calculus of Variations, Applications and Computations: Pont-à-Mousson, Pitman Research Notes in Mathematics Series (1994), 100–108.

[4] D. M. DeTurck, *Deforming metrics in the direction of their Ricci tensor*, J. Differential Geometry **18**, no. 11 (1983), 157–162.

[5] R. S. Hamilton, *Harmonic maps of manifolds with boundary*, Springer Lecture Notes **471** (1975).

[6] R. S. Hamilton, *The formation of singularities in the Ricci flow*, Surveys in Differential Geometry **227** (1995), 7–136.

[7] C. M. Elliott and V. M. Styles, *An ALE ESFEM for solving PDEs on evolving surfaces*, Milan Journal of Mathematics **80** (2012), 469–501.

The Locally Adaptive Time Stepping (LATS) Method: From Hodgkin-Huxley to Cahn-Hilliard

David L. Chopp

(joint work with Michael Rempe, Richard Kublik, Narut Sereewattanawoot)

The Locally Adaptive Time Stepping Method (LATS) [2] is a numerical method for solving systems of reaction diffusion equations of the form

$$\frac{\partial \vec{u}}{\partial t} = \nabla^2 \vec{u} + \vec{R}(\vec{u}).$$

The method is designed for systems where there are large variations in time scales between different regions in the computational domain. One example of such a system is the Hodgkin-Huxley model for studying the propagation of action potentials in neurons, which is a single reaction diffusion equation in the membrane potential, V, of the form

$$C\frac{\partial V}{\partial t} = \frac{1}{2\pi a}\frac{\partial}{\partial x}\left(\frac{\pi a^2}{R}\frac{\partial V}{\partial x}\right) - g_{Na}m^3h(V-E_{Na}) - g_K n^4(V-E_K) - g_L(V-E_L),$$

where m, h, and n are functions of the voltage that indicate the state of voltage regulated ion channels for transport of ions across the cell membrane.

The localized variation in time scales is exemplified by the propagation of an action potential as illustrated in Figure 1(a). In that figure, the action potential is traveling to the right and spans three subdomains. Ahead of the action potential

to the right, the voltage is at rest, and behind the action potential the voltage undergoes a gradual recovery phase back toward the resting voltage. Panel (b)

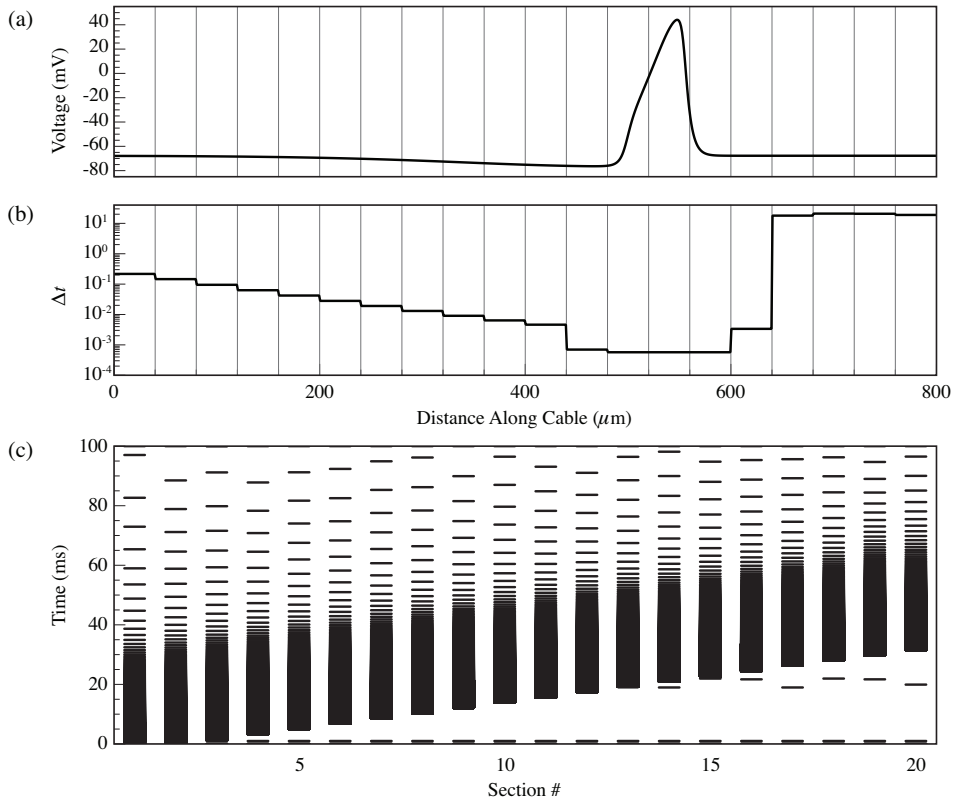

FIGURE 1. Illustration of the LATS method. (a) plot of the voltage for a propagating action potential at a fixed point in time. Vertical lines indicate the boundaries between subdomains. (b) The time step size for each subdomain at the same time point for the plot in (a). (c) Update time points for each subdomain. Each horizontal mark indicates a time point where the voltage is updated.

shows how the local time step sizes adjusts to the relative time scales. Subdomains at rest take the largest time steps, and subdomains in the rapidly varying action potential take the smallest steps. The steps gradually increase in the recovery phase as the variation decays exponentially back to rest. Panel (c) illustrates the time points when each subdomain is updated. From this it is clear that the time step sizes adjust locally according to the current location of the action potential.

By concentrating small time steps only in the subdomains where it is needed and allowing slower evolving subdomains to have less frequent updates, this strategy effectively concentrates computational resources on the subdomains where the activity is localized making the method more efficient. We demonstrate this results in a method that scales one order lower than traditional non-localized methods.

After demonstrating success for the Hodgkin-Huxley model, we are also applying the method to solving the Cahn-Hilliard equation for phase field models. The

purpose of this approach is to facilitate more efficient computation when computing evolution over longer time periods than are currently practical. In that setting, large swaths will be of a single phase and can have large time steps, while a significantly smaller region where the phase transitions occur will require smaller steps. We present preliminary results showing that the method does not alter the computational results. Optimizing the algorithm for efficiency and benchmarking the comparable advantage of this approach are topics for future work.

References

[1] M.J. Rempe and D.L. Chopp, *A predictor-corrector algorithm for reaction-diffusion equations associated with neural activity on branched structures*, SIAM Journal of Scientific Computing **28**(6) (2006), 2139–2161.

[2] R. Kublik and D.L. Chopp, *A locally adaptive time-stepping algorithm for the solution to reaction-diffusion equations on branched structures*, Advances in Computational Mathematics, to appear (2015).

An approximate curvature energy for bilayer membranes

Matthias Röger

(joint work with Luca Lussardi, Mark Peletier)

Artificial membranes are formed by amphiphilic lipid molecules (with a water-attracting head and two water-repelling tails) that self-organize into bilayer structures, where the head parts shield the lipid tails from the contact with water. The resulting structures resist stretching and bending but still allow the lipids to freely move in the in-plane direction. On a macroscale, membranes are modeled as two-dimensional surfaces and shapes have been described quite successfully using curvature energies of Canham–Helfrich type.

We discuss a certain 'mesoscale' energy for lipid bilayer membranes, introduced in [6]. We demonstrate that this energy can select bilayer structures as preferred configurations and carries a contribution that in the macroscale limit converges to a specific curvature energy. The model in [6] takes the form of an energy for idealized and rescaled tail and head densities, u and v,

$$\mathcal{F}_\varepsilon(u,v) := \begin{cases} \varepsilon \int_{\mathbb{R}^n} |\nabla u| + \frac{1}{\varepsilon} d_1(u,v) & \text{if } (u,v) \in \mathcal{K}_\varepsilon, \\ +\infty & \text{otherwise in } L^1(\mathbb{R}^n) \times L^1(\mathbb{R}^n). \end{cases}$$

Here $n \in \{2,3\}$, $M > 0$ are fixed, $\varepsilon > 0$ represents a small parameter, and $\mathcal{K}_\varepsilon$ denotes the admissible set of configurations (u,v), $u \in BV(\mathbb{R}^n; \{0, \varepsilon^{-1}\})$, $v \in L^1(\mathbb{R}^n; \{0, \varepsilon^{-1}\})$ such that $\int u = \int v = M$ and $uv = 0$ almost everywhere in $\mathbb{R}^n$. The first term in the energy describes the repulsive forces between tail particles and water or head particles; the respective expression measures the boundary size of the u support. The second term in the energy is given by the Monge–Kantorovich distance between u and v and is a remnant of an implicit implementation of the head-tail connection.

In [6] a Gamma-convergence result in the limit $\varepsilon \to 0$ was presented for the two-dimensional case $n = 2$. This asymptotic analysis rigorously shows the preference for uniformly thin and closed structures and identifies a generalized Euler elastica bending energy as an asymptotic contribution to the mesoscale energy.

In this talk we report on the extension of key parts of the previous analysis to three space dimensions: In [4] a general lower bound estimate, a formal derivation of the macroscopic limit $\varepsilon \to 0$ and a rigorous upper bound that matches the formal limit is presented. For the lower estimate we show that the mass transport problem that defines the d_1 distance induces a unit-length vector field θ on the boundary S of the support of the tail density u, related to the direction of transport rays through the corresponding point. A function $\mathfrak{m}$ on S describes the mass transported through that point. The following theorem states the key lower estimate.

Theorem 1. *Let $(u, v) \in \mathcal{K}_\varepsilon$ and assume that the boundary of $\operatorname{spt} u$ is given by a finite union of pairwise disjoint, compact, orientable surfaces S_j of class C^1 in $\mathbb{R}^3$. Then $M = \sum_{j=1}^{L} \int_{S_j} \mathfrak{m}\, d\mathcal{H}^2$, θ and the inner unit normal field ν of $\operatorname{spt}(u)$ on S_j satisfy $\theta \cdot \nu > 0$ and the following lower bound holds,*

$$\mathcal{F}_\varepsilon(u, v) \geq 2M + \sum_{j=1}^{L} \int_{S_j} (\mathfrak{m} - 1)^2 \, d\mathcal{H}^2 + \int_{S_j} \left(\frac{1}{\theta \cdot \nu} - 1 \right) \mathfrak{m}^2 \, d\mathcal{H}^2 + \sum_{j=1}^{L} \int_{S_j} \frac{\mathfrak{m}^4}{(\theta \cdot \nu)^3} Q(D\theta) \, d\mathcal{H}^2, \tag{1}$$

where the quadratic form Q is defined for an arbitrary square matrix A by

$$Q(A) := \frac{1}{4} (\operatorname{tr} A)^2 - \frac{1}{6} \operatorname{tr}(\operatorname{cof} A)$$

with $\operatorname{cof} A$ denoting the cofactor matrix of A.

From this estimate, we can formally identify the limit of the mesoscale energy: moderate energy configuration concentrate on a collection of surfaces with uniform density ($\mathfrak{m} = 1$, also indicating a uniform thickness of the mesoscale structures), the ray directions asymptotically coincide with the inner normal fields ν and the rescaled energy $\varepsilon^{-2}(\mathcal{F}_\varepsilon - 2M)$ converges to an energy that is given by a surface integral over $Q(D\nu)$, which just corresponds to the expression $\frac{1}{4}H^2 - \frac{1}{6}K$, where H and K denote mean and Gaussian curvature, respectively.

A second result in [4] gives a first step towards the rigorous justification of this formal considerations and presents the construction of a recovery sequence.

Theorem 2. *Fix a smooth compact orientable surface $S \subset \mathbb{R}^3$ without boundary such that $\mathcal{H}^2(S) = \frac{1}{2}M$. Then there exists a sequence $(u_\varepsilon, v_\varepsilon)_{\varepsilon > 0}$ in $\mathcal{K}_\varepsilon$ such that*

$$u_\varepsilon \mathcal{L}^3 \overset{*}{\rightharpoonup} 2\mathcal{H}^2 \lfloor S \quad \text{as } \varepsilon \to 0,$$

$$\frac{1}{\varepsilon^2} \Big(\mathcal{F}_\varepsilon(u_\varepsilon, v_\varepsilon) - 2M \Big) \to 2 \int_S \left(\frac{1}{4} H^2 - \frac{1}{6} K \right) d\mathcal{H}^2$$

where $\overset{*}{\rightharpoonup}$ is the usual weak-$*$ convergence of Radon measures.

Concerning a corresponding compactness and lower bound property of the limit energy the estimate (1) shows two main difficulties: firstly the control in the estimate is not on the derivative of the inner normal field ν, but on a direction field that is only close (in an L^2 sense) to ν. Secondly, the mass density $\mathfrak{m}$ could degenerate on a (small) portion of the surfaces, where one thus looses control over $Q(D\theta)$.

In [5] we address one of these issues and first assume that the mass density satisfies $\mathfrak{m} \equiv 1$. We then deal with the following simplified setting: Let $\mathcal{M}$ be the set of tuples (S, θ), S a compact and orientable surface of class C^2 in $\mathbb{R}^3$ with a C^1 unit normal field ν, and $\theta \colon S \to \mathbb{R}^3$ a Lipschitz vector field such that

$$|\theta| = 1 \text{ and } \theta \cdot \nu > 0 \text{ on } S, \quad L(p) \in \mathbb{R}^{3\times 3} \text{ is symmetric for all } p \in S,$$

where $L(p) : \mathbb{R}^3 \to \mathbb{R}^3$ is the extension of $D\theta(p) : T_pS \to \mathbb{R}^3$ with $L(p)\theta(p) = 0$. Then consider the functional $\mathcal{Q}_\varepsilon : \mathcal{M} \to \mathbb{R}^+_0$,

$$\mathcal{Q}_\varepsilon(S, \theta) = \int_S \varepsilon^{-2}\Big(\frac{1}{\theta \cdot \nu} - 1\Big)\, d\mathcal{H}^2 + \int_S Q(L(p))\, d\mathcal{H}^2(p).$$

This setting and the corresponding analysis might also be of independent interest for similar problems, where curvature information is provided by a control on a director field with asymptotically vanishing tilt from the normal direction. The main result in [5] is the following compactness and lower bound property.

Theorem 3. *Let $(\varepsilon_j)_{j\in\mathbb{N}}$ be an infinitesimal sequence of positive numbers and $(S_j, \theta_j)_{j\in\mathbb{N}}$ be a sequence in $\mathcal{M}$ such that for a fixed $\Lambda > 0$*

$$\sup_j \mathcal{H}^2(S_j) + \sup_j \mathcal{Q}_{\varepsilon_j}(S_j, \theta_j) \le \Lambda, \qquad \bigcup_j S_j \subset\subset \mathbb{R}^3.$$

Assume furthermore that in the sense of Radon measures on Ω

$$\mathcal{H}^2 \llcorner S_j \to \mu \quad \text{as } j \to \infty.$$

Then $\mu = \mu_V$ where V is an integral varifold with generalized second fundamental form in L^2 and

$$\int \left(\frac{1}{4}H^2 - \frac{1}{6}K\right) dV \le \liminf_{j\to+\infty} \mathcal{Q}_{\varepsilon_j}(S_j, \theta_j)$$

holds, where H and K are, respectively, the mean curvature and the Gauss curvature of V in the sense of Hutchinson [3].

We remark that the limit varifolds in particular do not have a boundary. The main challenge in the proof is that the functionals $\mathcal{Q}_\varepsilon$ do not allow to control the curvature or first variation of the surfaces S_j. Compared to the case $n = 2$ completely different methods are necessary. We consider the limit of the graphs of the director fields θ_j over S_j and show that these converge in the sense of currents to generalized Gauss graphs as introduced in [1] and further studied in particular in [2]. We reformulate the energy as energies of the graph currents and first obtain

compactness and lower bound properties in this setting. Finally we deduce the estimate in the framework of Hutchinson varifolds.

References

[1] G. Anzellotti, R. Serapioni, I. Tamanini. Curvatures, functionals, currents. *Indiana Univ. Math. J.*, 39(3):617–669, 1990.

[2] S. Delladio. Special generalized Gauss graphs and their application to minimization of functionals involving curvatures. *J. Reine Angew. Math.*, 486:17–43, 1997.

[3] J. E. Hutchinson. Second fundamental form for varifolds and the existence of surfaces minimising curvature. *Indiana Univ. Math. J.*, 35:45–71, 1986.

[4] L. Lussardi, M. A. Peletier, M. Röger. Variational analysis of a mesoscale model for bilayer membranes. *J. Fixed Point Theory Appl.*, 15(1):217–240, 2014.

[5] L. Lussardi, M. Röger. Gamma Convergence of a Family of Surface-Director Bending Energies with Small Tilt. *Arch. Ration. Mech. Anal.*, online first, 2015.

[6] M. A. Peletier, M. Röger. Partial localization, lipid bilayers, and the elastica functional. *Arch. Ration. Mech. Anal.*, 193(3):475–537, 2009.

A Computational Method for the Coupled Solution of Reaction-Diffusion Equations on Evolving Domains and Surfaces: Application to Model of Cell Migration and Chemotaxis

John Mackenzie

(joint work with Michael Nolan, Grant MacDonald, Robert Insall, Matthew Neilson)

1. Introduction

The motivation for the work presented in this talk is the computational modelling of eukaryotic cell migration and chemotaxis. In this talk I presented details of an adaptive moving mesh finite element algorithm for the coupled bulk-surface solution of reaction-diffusion equations. In the biological applications in mind, the bulk region corresponds to either the intracellular or extracellular region and the surface corresponds to the cell membrane. A major issue to be tackled for this class of problems is the efficient and accurate generation of bulk and surface meshes to enable the numerical solution of the model equations.

2. Adaptive moving mesh generation

2.1. **Bulk mesh generation.** Adaptive moving meshes for time-dependent bulk regions are generated using so-called moving mesh partial differential equations (MMPDEs). These PDEs are derived as gradient flow equations of a variational formulation which includes the ability to cluster mesh elements in regions of particular interest. Examples of good quality bulk meshes adapted to evolve cell morphologies were presented (see also [1]).

2.2. **Boundary mesh generation.** We consider the class of boundary movements given by the following evolution law for the normal velocity

$$\mathcal{V}(\boldsymbol{x},t) = \alpha\kappa + \beta, \quad \boldsymbol{x} \in \Gamma(t), \tag{1}$$

where κ is the curvature. Within the context of biological cell applications, the functions α and β could model the physical forces exerted on the membrane by cortical tension, and protrusions caused by actin polymerisation, respectively.

In our previous work (1) was solved numerically in [2] using an efficient adaptive level set method. Further improvements in the robustness and efficiency in the solution of (1) was obtained using the so-called BGN parameterised finite element scheme [4]. In this talk I presented a novel adaptive moving mesh method based on a Lagrangian approach, where the main idea is to represent the flow of curves by the position vector $\boldsymbol{x}$ which is the solution of the geometric evolution equation

$$\dot{\boldsymbol{x}} = \mathcal{V}\boldsymbol{n} + \mathcal{B}\boldsymbol{t}, \tag{2}$$

where $\boldsymbol{n}$ and $\boldsymbol{t}$ are unit normal and tangent vectors, respectively. Note that the presence of the tangential velocity $\mathcal{B}$ has no effect on the shape of the evolving curve but it is well known that the incorporation of a suitably chosen non-zero value of $\mathcal{B}$ can avoid the major drawback of the Lagrangian approach which is the possibility that grid points merge, resulting in a loss of stability and accuracy.

To implement an adaptive moving mesh strategy, the tangential velocity is assumed to satisfy the equation

$$\mathcal{B} = \dot{\boldsymbol{x}} \cdot \boldsymbol{t} = \frac{P}{\tau}(M||\boldsymbol{x}_\sigma||)_\sigma, \tag{3}$$

where, τ and P are a temporal smoothing parameter and spatial balancing operator, respectively and M is a postive monitor function, or adaptivity criterion. This could, for example, be based on a suitable a posteriori error estimate if available. Details of the numerical discretisation of the boundary moving mesh equations can be found in [1].

Examples were presented showing the performance of the adaptive moving mesh scheme for curve shortening flow. Using a suitable monitor function it was shown that improved accuracy could be achieved using our adaptive moving mesh method compared to the use of the BGN scheme which delivers an equidistributed arc-length mesh.

3. Cell migration and chemotaxis

The developed algorithm was applied to a "pseudopod-centred" model based on a set of reaction-diffusion equations that gives rise to an appropriate spatial-temporal activator profile to be used to move the cell membrane. The model is derived from a well-established discrete model of Meinhardt and describes the dynamic interaction between a membrane-bound local activator a, a rapidly distributed global inhibitor b and a local inhibitor c [2, 3].

To move the cell membrane we assume that actin polymerization creates a protrusive pressure that pushes the cell membrane outward in the normal direction

giving rise to the normal velocity

$$\mathcal{V}(\boldsymbol{x},t) = K_{prot}a(\boldsymbol{x},t) - \lambda(t)\kappa, \quad \boldsymbol{x} \in \Gamma(t), \tag{4}$$

where K_{prot} is a positive parameter. To control the area enclosed by $\Gamma(t)$, we have used a spatially constant but time dependent cortical tension factor $\lambda(t)$ (details can be found in [2]).

In the extracellular region, $\Omega(t)$, we assume that the concentration of ligand molecules evolves according to a linear diffusion equation. At the cell membrane, $\Gamma(t)$, we assume that a chemoattractant ligand L binds reversibly to a receptor R to form a receptor-ligand complex LR. It is also assumed that membrane-bound enzymes locally degrade the ligand field. The coupled bulk-surface system for the evolution of the ligand concentration, l, and the concentration of bound receptors, l_s, therefore takes the form

$$\frac{\partial l}{\partial t} = D\Delta l, \qquad \boldsymbol{x} \in \Omega(t) \tag{5}$$

$$\frac{\partial l_s}{\partial t} + \nabla_\Gamma \cdot (\boldsymbol{u} l_s) = D_s \Delta_\Gamma l_s + k_1(R_{tot} - l_s)l - k_{-1}l_s, \qquad \boldsymbol{x} \in \Gamma(t). \tag{6}$$

Here, D and D_s are the diffusion coefficients for the ligand and receptor-ligand complex, respectively. We assume that the total concentration of bound and unbound receptors is constant and takes the value R_{tot}. The constant k_1 is the rate of ligand association and k_{-1} the rate of disassociation. The normal flux boundary condition between the extracellular region and the cell membrane takes the form

$$-D\frac{\partial l}{\partial n} - [(\boldsymbol{u} \cdot \boldsymbol{n})]l = k_1(R_{tot} - l_s)l - k_{-1}l_s + \frac{V_{max}l}{K_m + l}, \qquad \boldsymbol{x} \in \Gamma(t). \tag{7}$$

Determining the concentration of bound receptors, l_s allows the estimation of the local fractional receptor occupancy

$$R_o(\boldsymbol{x},t) = \frac{l_s(\boldsymbol{x},t)}{R_{tot}}.$$

The combined effect of the response to the external signal and random intrinsic noise is modelled by the term

$$s(\boldsymbol{x},t) = r_a(\eta^t + R_o(\boldsymbol{x},t)),$$

which feeds in multiplicatively to the autocatalytic activator equation. The coupled bulk-surface reaction diffusion systems are discretised using a conservative ALE finite element method and a novel iterative solution algorithm [1].

Simulations were presented that demonstrate that the developed algorithm can predict effective chemotaxis in a linear gradient (see simulations in [1]). Furthermore, some preliminary experiments were shown to indicate that the simulated motile cells could self-generate gradients in initially homogeneous environments. This self-generated chemotaxis is thought to be potentially important in cancer cell metastasis.

4. Further work

Extensions of the work presented in the talk include the derivation of a suitable tangential velocity based on adaptive moving mesh principles for evolving surfaces. Further investigation of the cell model to predict self-chemotaxis will also hopefully provide insights to this important biological process.

References

[1] G. MacDonald, J.A. Mackenzie, M. Nolan, R.H. Insall *A computational method for the coupled solution of reaction-diffusion equations on evolving domains and manifolds: Application to a model of cell migration and chemotaxis*, J. Comput. Phys. **In press** (2015), http://dx.doi.org/10.1016/j.jcp.2015.12.038.

[2] M.P. Neilson, J.A. Mackenzie, S.D. Webb, R.H. Insall *Modelling cell movement and chemotaxis using pseudopod-based feedback*, SIAM J. Sci. Comput **33(3)** (2011), 1035–1057.

[3] M.P. Neilson, D.M Veltman, P.J.M van Haastert, S.D. Webb, J.A. Mackenzie, R.H. Insall *Chemotaxis: a feedback-based computational model robustly predicts multiple aspects of real cell behaviour*, PLoS Biol. **9(5)** (2011), e1000618.

[4] M.P. Neilson, J.A. Mackenzie, S.D. Webb, R.H. Insall *Use of the parameterised finite element method to robustly and efficiently evolve the edge of a moving cell*, Integr. Biol. **2** (2010), 687–695.

Optimal control of multiphase fluids and droplets

Michael Hintermüller

(joint work with H. Antil, T. Keil, R. Nochetto, T.M. Surowiec, and D. Wegner)

1. Optimal control of the Cahn-Hilliard/Navier-Stokes system with variable densities

For the optimal control of multiphase fluids in the liquid-liquid case we consider a phase-field model with two fluids being immiscible on a macroscopic scale but which are allowed to mix in a small interface region. For fluids having variable densities, the evolution of the system can be modeled by the Cahn–Hilliard/Navier–Stokes type equations [1]:

$$\begin{aligned} \partial_t(\rho\mathbf{u}) + \operatorname{div}(\mathbf{u}\otimes(\rho(\varphi)\mathbf{u} - \vartheta m(\varphi)\nabla\mu)) - \operatorname{div}(2\nu(\varphi)\epsilon(\mathbf{u})) + \nabla p &= \mu\nabla\varphi + u, \\ \operatorname{div}\mathbf{u} &= 0, \\ \partial_t\varphi + \mathbf{u}\nabla\varphi - \operatorname{div}(m(\varphi)\nabla\mu) &= 0, \\ -\Delta\varphi + \partial\Psi(\varphi) - \varphi &\ni \mu. \end{aligned} \tag{CHNS}$$

Here, φ denotes the relative concentration and is acting as an order parameter taking the values ± 1 for the pure phases, respectively. The mass density ρ is supposed to depend on the concentration φ in an affine way, i.e. it holds that

$$\rho(\varphi) = \frac{\rho_1 + \rho_2}{2} + \frac{\rho_2 - \rho_1}{2}\varphi$$

with ρ_1 and ρ_2 denoting the densities of the pure phases. The variables $\mathbf{u}, \psi, \mu$ denote the fluid velocity, the pressure and the chemical potential, respectively.

The effect of the applied voltage and of gravity is assembled by the control u. Moreover, m and ν denote the mobility and viscosity coefficients, respectively, which are fluid dependent via the order parameter φ, and $\epsilon(\mathbf{u}) := \frac{1}{2}(D\mathbf{u} + D\mathbf{u}^t)$. The double-obstacle potential ψ is given by $\psi(r) := 0$ if $r \in [-1, 1]$ and $\psi(r) = +\infty$ otherwise, the functional $\Psi : \varphi \mapsto \mathbb{R} \cup \{+\infty\}$ is defined as $\int_\Omega \psi \circ \varphi$, and ∂ denotes the convex subdifferential. It is complemented by suitable boundary and initial conditions. The spatial domain is $\Omega \subset \mathbb{R}^n$, $n = 1, 2, 3$, and the time horizon is $[0, T]$, with $T > 0$. Anticipating the design, analysis and implementation of a solution algorithm for this system, in [3] we propose the following time discretized version of (CHNS)

$$
\begin{aligned}
&\frac{1}{\tau}(\rho(\varphi_i)\mathbf{u}_{i+1} - \rho(\varphi_{i-1})\mathbf{u}_i) - \operatorname{div}(2\nu(\varphi_i)\epsilon(\mathbf{u}_{i+1})) + \nabla p_{i+1} \\
&\qquad +\operatorname{div}(\mathbf{u}_{i+1} \otimes (\rho(\varphi_{i-1})\mathbf{u}_i - \vartheta m(\varphi_{i-1})\nabla\mu_i)) \;=\; \mu_{i+1}\nabla\varphi_i + u_{i+1}, \\
&\qquad\qquad \operatorname{div}\mathbf{u}_{i+1} \;=\; 0, \\
&\frac{1}{\tau}(\varphi_{i+1} - \varphi_i) + \mathbf{u}_{i+1}\nabla\varphi_i - \operatorname{div}(m(\varphi_i)\nabla\mu_{i+1}) \;=\; 0, \\
&\qquad\qquad -\Delta\varphi_{i+1} + \partial\Psi(\varphi_{i+1}) - \varphi_i \;\ni\; \mu_{i+1}.
\end{aligned}
\tag{CHNS1}
$$

together with boundary and initial conditions. Here, $\tau > 0$ is the time step size and the index $i \in \{1, \ldots, M\}$ refers to the time instance $t_i = i\tau$. The characteristic feature of the above time discretization is that it allows the derivation of crucial energy estimates, which decoupled discretizations do not allow. Associated to (CHNS1) we consider the following optimal control problem

$$
\min_V \mathcal{J}(\varphi, \mu, \mathbf{u}, V), \quad \text{s.t. (CHNS1)}, \tag{1}
$$

for a general class of objectives $\mathcal{J}$, including in particular the prototypical tracking functional

$$
\mathcal{J}(\varphi, \mu, \mathbf{u}, V) := 1/2(||\varphi_M - \tilde{\varphi}||^2_{L^2(\Omega)} + \sum_{i=1}^{M} ||V_i||^2_{L^2(\Omega)})
$$

with a desired fluid profile $\tilde{\varphi}$ at final time. In contrast to the method of instantaneous control at every single time point $t_i = i\tau$ of the time discretization, problem (1) constitutes a single optimization problem incorporating the solutions $(\varphi, \mu, \mathbf{u})$ for all points t_i of the time discretization. The occurrence of the subdifferential of Ψ renders (1) a non-convex, non-smooth optimization problems with state systems involving variational inequalities. Therefore, standard methods for deriving first-order necessary optimality conditions cannot be applied directly. Nevertheless, in [3], the existence of minimizers was shown and a C-stationarity system in function space was established by using a Moreau-Yosida type regularization technique resulting in a family of smooth approximations of problem (1) and passing to the limit in the corresponding first-order conditions. As a further step towards the design of an efficient solver for the optimal control problem for time-discretized Cahn–Hilliard/Navier–Stokes, a goal-oriented dual-weighted error estimator for the adaptive finite element approach was derived for solving the stationarity system. In addition to the primal residuals the estimator includes primal

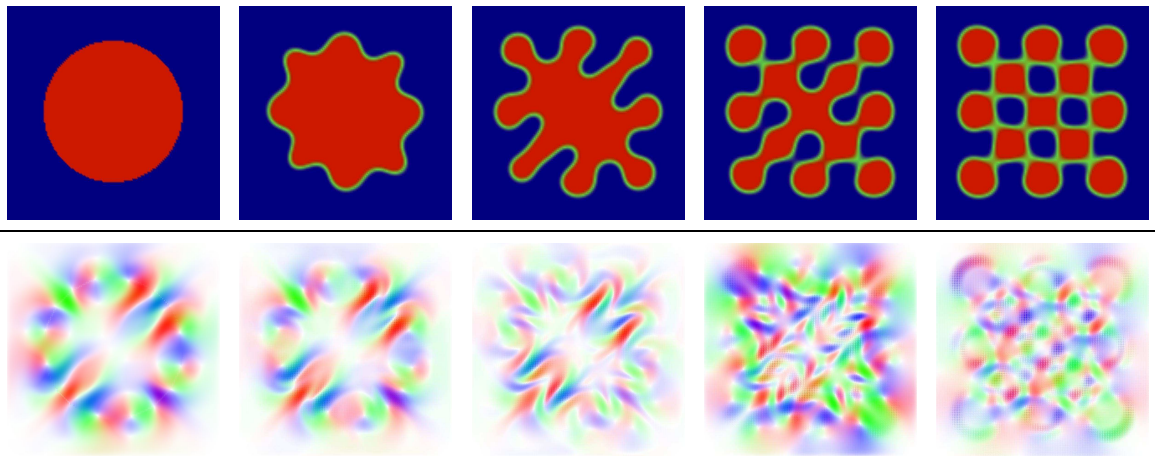

FIGURE 1. Optimal distributed control of CH/NS with constant density: Evolution of the concentration from the initial state to an approximation of a target state (upper row) and the applied control (lower row).

weighted dual residuals and an error term covering the mismatch in complementarity which contributes to the location of the coincidence sets coming from the variational inequality constraint. At the moment, an optimization solver based on this error estimator and the gradient descent method is being implemented. For the simpler case of single densities, a numerical implementation was realized using a gradient descent scheme [4]; see Figure 1.

2. Instantaneous control of a EWOD model with pinning

In order to describe the evolution of droplets between two narrow plates and under the influence of an applied electric field, in [7] and [5] a model based on a Hele-Shaw type equation in two dimensions with an additional inertial term and contact line pinning was proposed:

$$\text{(HS)} \qquad \begin{aligned} \alpha\partial_t \mathbf{u} + \beta\mathbf{u} &= -\nabla p, \quad \operatorname{div}\mathbf{u} = 0 && \Omega_1(t), \\ p &= \kappa + E(V) + \lambda + D_{\text{visc}}\mathbf{u}\cdot\vec{\mathbf{n}}, \quad \lambda \in P_0 \operatorname{sign}(\mathbf{u}\cdot\vec{\mathbf{n}}) && \Gamma(t). \end{aligned}$$

Here, the droplet occupies the time-dependent subset Ω_1 of Ω and having liquid-gas interface Γ with κ denoting its curvature. The quantity $\operatorname{sign}(\mathbf{u}\cdot\vec{\mathbf{n}})$ describes the damping due to pinning, where the multi-valued operator "sign" has to be understood in the sense of $\partial|.|$. Moreover, the viscous damping is modeled by $D_{\text{visc}}\mathbf{u}\cdot\vec{\mathbf{n}}$, $E(V)$ is the impact of the applied voltage V on the boundary Γ, and α, β and P_0 are positive constants. This process is also known as electrowetting on dielectric (EWOD) with contact line pinning. In [6], the following time discretization of (HS) was considered and existence of a solution for a single time step in a

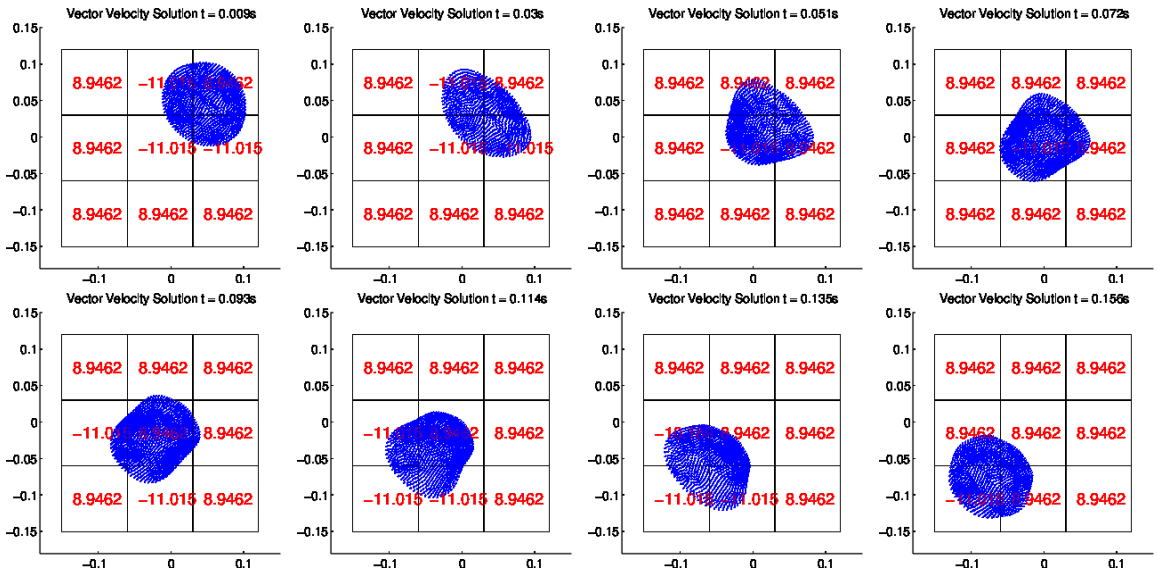

FIGURE 2. Evolution of a single droplets under a sequence of controls acting on a 3x3 grid of electrodes that can be controlled individually and using a barycenter matching.

regular situation was shown:
(HS1)

$$\frac{\alpha}{\tau}(\mathbf{u}_{i+1}-\mathbf{u}_i)+\beta\mathbf{u}_{i+1} \;=\; -\nabla p_{i+1}, \quad \mathrm{div}\mathbf{u}_{i+1} \;=\; 0 \qquad \Omega_{1i},$$

$$p_{i+1} \;=\; \tilde{\kappa}_{i+1}+E(V_i)+\lambda_{i+1}+D_{\mathrm{visc}}\mathbf{u}_{i+1}\cdot\vec{\mathbf{n}}_i, \quad \lambda_{i+1} \;\in\; P_0\,\mathrm{sign}(\mathbf{u}_{i+1}\cdot\vec{\mathbf{n}}_i) \qquad \Gamma_i.$$

Here, $\tilde{\kappa}_{i+1}$ denotes a suitable approximation on Γ_i of the curvature of Γ_{i+1}. For (HS1), we consider the optimal control problem for a single time step

$$\min_V \mathcal{J}(\mathbf{u},V), \qquad \text{s.t. (HS1).} \tag{2}$$

This optimization problem involves a control of the curvature driven evolution and a variational inequality with renders the problem non-smooth, non-convex and, thus, a mathematical program with equilibrium constraints (MPEC). In [2], the existence of minimizer was established for a general class of objectives $\mathcal{J}$. Again using a Moreau-Yosida-type regularization of the variational inequality, the problem was approximated by a family of smooth problems. For those first-order optimality conditions can be derived and by a consequent passage to the limit, a C-stationarity system in function space was derived for the limit problem, cf. [2]. Figure 2 presents a numerical example of the results of sequence of control actions on a single droplet. Each control is given by the solution of an optimization problem of type (2) with an objective which penalizes the difference of the current barycenter of the droplets with the desired position of the barycenter. After each step in time, a regularization is performed in order to regain a regular configuration.

References

[1] H. Abels, H. Garcke, and G. Grün. Thermodynamically consistent, frame indifferent diffuse interface models for incompressible two-phase flows with different densities. Math. Models Methods Appl. Sci., 22(3):1150013, 40, 2012.

[2] H. Antil, M. Hintermüller, R.H. Nochetto, T.M. Surowiec, and D. Wegner. Finite horizon model predictive control of Electowetting on dielectric. 2015.

[3] M. Hintermüller, T. Keil, and D. Wegner. Optimal control of a semidiscrete Cahn-Hilliard-Navier-Stokes system with non-matched fluid densities. 2015.

[4] M. Hintermüller and D. Wegner. Distributed and boundary control problems for the semidiscrete Cahn-Hilliard/Navier-Stokes system with nonsmooth Ginzburg-Landau energies. Newton Institute, Preprint NI14042, 2014.

[5] S. W. Walker. Electrowetting with contact line pinning: Computational modeling and comparisons with experiments. Physics of Fluids, 21(10):102103-102103-16, 2009.

[6] S.W. Walker, A. Bonito, and R.H. Nochetto. Mixed finite element method for elec-trowetting on dielectric with contact line pinning. Interfaces Free Bound., 12(1):85–119, 2010.

[7] S. W. Walker and B. Shapiro. Modeling the fluid dynamics of electrowetting on dielectric (EWOD). Journal of Microelectromechanical Systems, 15(4):986–1000, 2006.

Optimal boundary control problems for Cahn–Hilliard systems with dynamic boundary conditions

Jürgen Sprekels

(joint work with Pierluigi Colli, M. Hassan Farshbaf-Shaker, Gianni Gilardi)

Let $\Omega \subset \mathbb{R}^3$ denote a smooth domain with smooth boundary Γ, $T > 0$ be given, and $Q := \Omega \times (0,T)$, $\Sigma := \Gamma \times (0,T)$. Denoting by $\partial_n, \nabla_\Gamma, \Delta_\Gamma$ the outward normal derivative, the tangential gradient, and the Laplace–Beltrami operator on Γ, and assuming that nonnegative constants $b_Q, b_\Sigma, b_\Omega, b_\Gamma, b_0$ and square integrable target functions $z_Q, z_\Sigma, z_\Omega, z_\Gamma$ are given, we consider the following optimal control problem:

(CP) Minimize the cost functional

$$\begin{aligned}\mathcal{J}(y, y_\Gamma, u_\Gamma) \;:=\; & \frac{b_Q}{2} \|y - z_Q\|^2_{L^2(Q)} + \frac{b_\Sigma}{2} \|y_\Gamma - z_\Sigma\|^2_{L^2(\Sigma)} + \frac{b_\Omega}{2} \|y(T) - z_\Omega\|^2_{L^2(\Omega)} \\ & + \frac{b_\Gamma}{2} \|y_\Gamma(T) - z_\Gamma\|^2_{L^2(\Gamma)} + \frac{b_0}{2} \|u_\Gamma\|^2_{L^2(\Sigma)} \,,\end{aligned}$$

subject to the state system

$$\partial_t y - \Delta w = 0 \quad \text{in } Q \,, \tag{1}$$

$$w = \tau\, \partial_t y - \Delta y + f'(y) \quad \text{in } Q \,, \tag{2}$$

$$\partial_n w = 0 \quad \text{on } \Sigma \,, \tag{3}$$

$$y_\Gamma = y_{|\Gamma} \quad \text{and} \quad \partial_t y_\Gamma + \partial_n y - \Delta_\Gamma y_\Gamma + f'_\Gamma(y_\Gamma) = u_\Gamma \quad \text{on } \Sigma \,, \tag{4}$$

$$y(0) = y_0 \quad \text{in } \Omega \,, \tag{5}$$

and to the control constraint

$$u_\Gamma \in \mathcal{U}_{\rm ad} := \{v_\Gamma \in H^1(0,T;L^2(\Gamma)) \cap L^\infty(\Sigma) : \|\partial_t v_\Gamma\|_{L^2(\Sigma)} \le M_0\,, \\ u_{\Gamma,\min} \le u_\Gamma \le u_{\Gamma,\max} \ \text{ a.e. on } \Sigma\}\,,$$

where $u_{\Gamma,\min}$, $u_{\Gamma,\max} \in L^\infty(\Sigma)$ and $M_0 > 0$ are such that $\mathcal{U}_{\rm ad} \neq \emptyset$.

The state system (1)–(5) models a phase separation process in a body Ω, governed by the (viscous, if $\tau > 0$) Cahn–Hilliard system (1), (2), which through the dynamical boundary condition (4) for the trace y_Γ of the order parameter y (typically the density of one of the involved phases) is coupled to a nonconserving phase transition on the surface Γ. In this connection, w denotes the chemical potential, u_Γ is a boundary control, and f, f_Γ are double-well potentials acting in the bulk and on the surface, respectively. Typical cases are the logarithmic potential

$$f_{\log}(r) := \hat{c}_1\,((1+r)\,\ln(1+r) + (1-r)\,\ln(1-r)) - \hat{c}_2\,r^2, \quad \text{for } r \in (-1,1), \tag{6}$$

or the double obstacle potential

$$f_{\rm obs}(r) := I_{[-1,1]}(r) - \hat{c}_3\,r^2, \quad \text{for } r \in \mathbb{R}\,, \tag{7}$$

where $I_{[-1,1]}$ is the indicator function of the interval $[-1,1]$.

Viscous and nonviscous Cahn–Hilliard systems with dynamic boundary conditions have been investigated repeatedly in the past years. In this regard, we refer to [4], where general well-posedness results for both the viscous and the nonviscous case were established. In contrast to this, only very few contributions exist on the control theory of Cahn–Hilliard systems for dynamic boundary conditions involving the Laplace–Beltrami operator. In [7], the corresponding Allen–Cahn case was discussed for the logarithmic potential, which then was extended to the double obstacle potential in [3] using a "deep quench" approximation. In the present talk, results for the viscous case $\tau > 0$ from the papers [1], [2], and [6], are presented; the nonviscous case $\tau = 0$ was the subject of [5].

The results are as follows: we choose, for simplicity, the logarithmic potential $f_{\log}$ defined in (6) for both f and f_Γ and put $\tau = 1$. If we assume that

$$y_0 \in H^2(\Omega), \quad y_{0|\Gamma} \in H^2(\Gamma), \tag{8}$$

$$-1 < y_0(x) < 1 \quad \forall\, x \in \overline{\Omega}, \tag{9}$$

and use the abbreviating notation

$$V := H^1(\Omega)\,, \quad H := L^2(\Omega)\,, \quad H_\Gamma := L^2(\Gamma)\,, \quad V_\Gamma := H^1(\Gamma)\,,$$
$$\mathcal{H} := H \times H_\Gamma\,, \quad \mathcal{V} := \{(v, v_\Gamma) \in V \times V_\Gamma : v_\Gamma = v_{|\Gamma}\}\,,$$

then the state system (1)–(5) has a unique (weak) solution triple (y, y_Γ, w) having the properties (see Theorems 2.2–2.4 in [4])

$$y \in W^{1,\infty}(0,T;H) \cap H^1(0,T;V) \cap L^\infty(0,T;H^2(\Omega))\,, \tag{10}$$

$$y_\Gamma \in W^{1,\infty}(0,T;H_\Gamma) \cap H^1(0,T;V_\Gamma) \cap L^\infty(0,T;H^2(\Gamma))\,, \tag{11}$$

$$-1 < \inf_Q \operatorname{ess} y \le \sup_Q \operatorname{ess} y < 1, \tag{12}$$

$$w \in L^\infty(0,T;H^2(\Omega))\,. \tag{13}$$

The control-to-state operator $\mathcal{S} : u_\Gamma \mapsto (y, y_\Gamma)$ is thus well-defined, and it follows from Theorem 4.2 in [6] that $\mathcal{S}$ is Fréchet differentiable on every bounded open subset $\mathcal{U}$ of $H^1(0,T;L^2(\Gamma)) \cap L^\infty(\Sigma)$ which contains $\mathcal{U}_{\rm ad}$, if we view $\mathcal{S}$ as a mapping from $\mathcal{U}$ into the Banach space $\mathcal{Y} := H^1(0,T;\mathcal{H}) \cap L^\infty(0,T;\mathcal{V})$. Moreover, it can be shown (see Proposition 6.1 in [6]) that the control problem **(CP)** admits a solution, and the first-order necessary conditions of optimality are established in terms of the standard variational inequality and the (unique) solution to the associated adjoint system. The corresponding results have been stated in the Theorems 2.5 and 2.6 in [6].

While in [2] and [6] the viscous case with differentiable nonlinearities was treated, an analysis for the nondifferentiable case of the double obstacle potential was performed in [1].

References

[1] P. Colli, M. H. Farshbaf-Shaker, G. Gilardi, J. Sprekels, *Optimal boundary control of a viscous Cahn–Hilliard system with dynamic boundary condition and double obstacle potentials*, SIAM J. Control Optim. **53** (2015), 2696–2721.

[2] P. Colli, M. H. Farshbaf-Shaker, G. Gilardi, J. Sprekels, *Second-order analysis of a boundary control problem for the viscous Cahn–Hilliard equation with dynamic boundary condition*, Ann. Acad. Rom. Sci. Ser. Mat. Appl. **7** (2015), 41–66.

[3] P. Colli, M. H. Farshbaf-Shaker, J. Sprekels, *A deep quench approach to the optimal control of an Allen–Cahn equation with dynamic boundary condition and double obstacle potentials*, Appl. Math. Optim. **71** (2015), 1–24.

[4] P. Colli, G. Gilardi, J. Sprekels, *On the Cahn–Hilliard equation with dynamic boundary conditions and dominating boundary potential*, J. Math. Anal. Appl. **419** (2014), 972–994.

[5] P. Colli, G. Gilardi, J. Sprekels, *A boundary control problem for the pure Cahn–Hilliard equation with dynamic boundary conditions*, Adv. Nonlinear Anal. **4** (2015), 311–325.

[6] P. Colli, G. Gilardi, J. Sprekels, *A boundary control problem for the viscous Cahn–Hilliard equation with dynamic boundary conditions*, Appl. Math. Optim., published online 28 April 2015.

[7] P. Colli, J. Sprekels, *Optimal control of an Allen–Cahn equation with singular potentials and dynamic boundary condition*, SIAM J. Control Optim. **53** (2015), 213–234.

A general finite element analysis for partial differential equations in evolving domains

Thomas Ranner
(joint work with Charles M. Elliott)

We give some ideas of a unified theory for finite element discretisations of partial differential equations posed in evolving domains. We consider equations posed on evolving surface and bulk domains, as well as coupled bulk-surface systems. This is achieved using an abstract variational setting with time-dependent function spaces and time-dependent finite element spaces.

Given a time-dependent Hilbert space triple

$$\mathcal{V}(t) \subset \mathcal{H}(t) \subset \mathcal{V}^*(t),$$

the abstract strong formulation is to find $u \in \mathcal{V}(t)$ such that

$$\begin{aligned} \partial^\bullet u + \mathcal{G}(t)u + \mathcal{L}(t)u = 0 \qquad & \text{in } V^*(t) \\ u(0) = u_0. & \end{aligned}$$

A key property of the time-dependent Hilbert spaces is compatibility with a linear homomorphism. We say a pair $(\mathcal{X}(t), \phi_t)_{t\in[0,T]}$, consisting of a time-dependent family of Hilbert spaces, $\mathcal{X}(t)$, and a time-dependent family of linear homomorphisms ,$\phi_t \colon \mathcal{X}(0) \to \mathcal{X}(t)$, is a compatible pair if the linear homomorphisms a uniformly continuous with uniformly continuous inverse. This allows us to define Bochner-type spaces $L^2_{\mathcal{X}}$, material derivatives and trasport laws which depend on the choice of ϕ_t.

Similar to the case of time independent function spaces the strong form may be written in variational form as

Problem (Continuous problem)**.** *Given $u_0 \in \mathcal{V}_0$, find $u \in L^2_{\mathcal{V}}$ with $\partial^\bullet u \in L^2_{\mathcal{H}}$ such that for almost every $t \in [0,T]$,*

$$m(t; \partial^\bullet u, \varphi) + g(t; u, \varphi) + a(t; u, \varphi) = 0 \qquad \text{for all } \varphi \in \mathcal{V}(t), \tag{1}$$

subject to the initial condition $u(\cdot, 0) = u_0$.

Here $L^2_{\mathcal{V}}$ and $L^2_{\mathcal{H}}$ are generalisations of the Bochner spaces $L^2(0,T;V)$ and $L^2(0,T;H)$ in the case of time independent spaces [1]. The bilinear form $a(t;\cdot,\cdot)$ is associated with the elliptic operator $\mathcal{L}$, $g(t;\cdot,\cdot)$ is a weighted $\mathcal{H}(t)$-inner product associated with the operator $\mathcal{G}$ and $m(t;\cdot,\cdot)$ with a $\mathcal{H}(t)$-inner product.

To fix ideas, let us give an example of the setting we are considering. Let $T > 0$. For $t \in [0,T]$ let $\Omega(t)$ denote an $(n+1)$-dimensional bounded, open, connected domain in $\mathbb{R}^{n+1}$, for $n = 2, 3$. We denote by $\Gamma(t)$ the boundary of $\Omega(t)$ and assume that $\Gamma(t)$ is a compact, smooth hypersurface. We write $\Omega_0 = \Omega(0)$, $\Gamma_0 = \Gamma(t)$ and $\nu(\cdot,t)$ the normal to $\Gamma(t)$. We assume that $\Omega(t)$ is given by a parametrisation $G \colon \bar{\Omega}_0 \times [0,T] \to \mathbb{R}^{n+1}$ such that $\Omega(t) = G(\Omega_0, t)$ and $\Gamma(t) = G(\Gamma_0, t)$. We write $\boldsymbol{w}$ for the velocity defined by $\boldsymbol{w}(G(\cdot),t) = \frac{d}{dt}G(\cdot,t)$. We will write G in terms of a flow $\mathcal{P}hi_t \colon \bar{\Omega}_0 \to \bar{\Omega}(t)$, with inverse $\mathcal{P}hi_{-t} \colon \bar{\Omega}(t) \to \bar{\Omega}_0$, given by $\mathcal{P}hi_t(\cdot) = G(\cdot,t)$.

Remark. *Note that velocity field $\boldsymbol{w}$ is the velocity of the parametrisation. Different choices of parametrisation can lead to the same shaped domain evolution and it maybe useful in practical situations to use a non-physical parametrisation. For example, we may use such a velocity in order to achieve a mesh with good properties as in the Arbitrary Lagrangian–Eulerian approach* [3, 5]. *This means that the precise definition of coefficients in the applications we consider may depend on the particular choice of velocity field.*

As an example of the equations we are studying, we consider a parabolic equation in an evolving domain coupled to a parabolic equation on the boundary. We seek a time-dependent pair (u, v) with u a scalar volumetric field and v a scalar surface field such that

$$\partial^\bullet u + u\nabla\cdot\boldsymbol{w} - \mathcal{L}_\Omega u = 0 \qquad \text{on } \Omega(t) \tag{2a}$$

$$(\mathscr{A}_\Omega\nabla u + \mathscr{B}_\Omega u)\cdot\nu + (\alpha u - \beta v) = 0 \qquad \text{on } \Gamma(t) \tag{2b}$$

$$\partial^\bullet v + v\nabla_\Gamma\cdot\boldsymbol{w} - \mathcal{L}_\Gamma v - (\mathscr{A}_\Omega\nabla u + \mathscr{B}_\Omega u)\cdot\nu = 0 \qquad \text{on } \Gamma(t) \tag{2c}$$

$$u(\cdot,0) = u_0 \qquad \text{on } \Omega_0 := \Omega(0) \tag{2d}$$

$$v(\cdot,0) = v_0 \qquad \text{on } \Gamma_0 := \Gamma(0), \tag{2e}$$

where $\mathcal{L}_\Omega, \mathcal{L}_\Gamma$ are operators given by:

$$\mathcal{L}_\Omega u := \nabla\cdot(\mathscr{A}_\Omega\nabla u) + \nabla\cdot(\mathscr{B}_\Omega u) + \mathscr{C}_\Omega u,$$
$$\mathcal{L}_\Gamma v := \nabla_\Gamma\cdot(\mathscr{A}_\Gamma\nabla_\Gamma v) + \nabla_\Gamma\cdot(\mathscr{B}_\Gamma v) + \mathscr{C}_\Gamma v.$$

The well-posedness of this problem was considered by [2].

We formulate and analyse an abstract finite element discretisation based on a Galerkin ansatz with perturbations of the bilinear forms. This work is a generalisation of the analysis presented in [4].

For $h \in (0, h_0)$, let $\{\mathcal{V}_h(t)\}_{t\in[0,T]}$ be a time-dependent family of discrete spaces which form a uniformly compatible pair $(\mathcal{V}_h(t), \phi_t^h)_{t\in[0,T]}$ with respect to two different norms $\|\cdot\|_{\mathcal{V}_h(t)}$ and $\|\cdot\|_{\mathcal{H}_h(t)}$. We denote by a_h and m_h bilinear forms which approximate the continuous bilinear forms a and m.

Problem (Discrete problem)**.** *Given $U_0 \in \mathcal{V}_{h,0}$, find $U_h \in C^1_{\mathcal{V}_h}$ such that*

$$\frac{d}{dt}m_h(t; U_h, \phi_h) + a_h(t; U_h, \phi_h) = m_h(t; U_h, \partial_h^\bullet\phi_h) \qquad \text{for all } \phi_h \in C^1_{\mathcal{V}_h}. \tag{3}$$

Theorem (Existence and stability of discrete problem)**.** *Under various assumptions on the discrete spaces and bilinear forms,* (3) *has a unique solution $U_h \in C^0_{\mathcal{V}_h}$ with $\partial_h^\bullet U_h \in C^0_{\mathcal{V}_h}$. There exists a constant $C > 0$ independent of $h \in (0, h_0)$ such that*

$$\sup_{t\in(0,T)} \|U_h\|^2_{\mathcal{H}_h(t)} + \int_0^T \|U_h\|^2_{\mathcal{V}_h(t)}\, dt \le C\,\|U_{h,0}\|^2_{\mathcal{H}_h(t)}\,.$$

Under assumptions on the approximation of function spaces by abstract finite element spaces and the continuous bilinear forms m and a by discrete bilinear

forms m_h and a_h, optimal order error bounds are proved. The key idea is to transform the discrete scheme to a conforming subspace with variational crimes.

For each $t \in [0,T]$, we assume that there exists map $\Lambda_h(\cdot,t)\colon \mathcal{V}_h(t) \to \mathcal{V}(t)$. We denote by $V_h^\ell := \Lambda_h(V_h,t) \in \mathcal{V}_h^\ell(t) := \Lambda_h(\mathcal{V}_h(t),t)$ the lift of a element $V_h \in \mathcal{V}_h(t)$. Under assumptions on the base finite element space and lifting operator we can show that the pair $\{\mathcal{V}_h^\ell(t), \phi_t^\ell\}_{t\in[0,T]}$ is compatible (uniformly in h) in the $\mathcal{H}(t)$ and $\mathcal{V}(t)$-norms. In particular, we have $L^2_{\mathcal{V}_h^\ell}$ is a subset of $L^2_{\mathcal{V}}$.

Using the lift operator, we can show an error bond of the following form. It is based on a standard splitting argument using a Ritz projection operator.

Theorem (Error estimate)**.** *Let various approximation assumptions hold. Denote by u the solution of* (1) *and by $U_h \in C^1_{\mathcal{V}_h}$ the solution of* (3) *with lift $u_h \in C^1_{\mathcal{V}_h^\ell}$. Then, there exists constant $c > 0$ such that for $h \in (0,h_0)$ we have the error estimate*

$$\sup_{t\in[0,T]} \|u-u_h\|^2_{\mathcal{H}(t)} + h^2 \int_0^T \|u-u_h\|^2_{\mathcal{V}(t)}\, dt \leq \|u-u_{h,0}\|^2_{\mathcal{H}(t)} + C_u h^{2k+2}, \tag{4}$$

where C_u depends on the regularity of the smooth solution.

This approach can be applied to three model problems: a linear parabolic problem on an evolving compact n-dimensional surface, a linear parabolic problem in an evolving, bounded bulk domain in $\mathbb{R}^{n+1}$ and a linear parabolic problem coupling problems in an evolving, bounded bulk domain in $\mathbb{R}^{n+1}$ to a problem on its boundary.

Evolving finite element spaces for bulk and surfaces are constructed. These are based on evolving Lagrange isoparametric finite elements. The key ideas in introducing these spaces is to reformulate the global properties required of the spaces $\mathcal{H}(t)$ and $\mathcal{V}(t)$ into element-wise smooth properties which are combined on an initial domain and transformed forwards in time.

Numerical results to demonstrate the results are work in progress.

References

[1] Amal Alphonse, Charles M. Elliott, and Björn Stinner. An abstract framework for parabolic PDEs on evolving spaces. *Port. Math.*, (accepted), 2015.

[2] Amal Alphonse, Charles M. Elliott, and Björn Stinner. On some linear parabolic PDEs on moving hypersurfaces. *Interfaces Free Bound.*, (accepted), 2015.

[3] Andrea Bonito, Irene Kyza, and Ricardo H. Nochetto. Time-discrete higher-order ale formulations: Stability. *SIAM Journal on Numerical Analysis*, 51(1):577–604, 2013.

[4] Gerhard Dziuk and Charles M. Elliott. L^2-estimates for the evolving surface finite element method. *Mathematics of computation*, 82:1–24, 2013.

[5] Charles M. Elliott and Vanessa Styles. An ALE ESFEM for Solving PDEs on Evolving Surfaces. *Milan Journal of Mathematics*, pages 1–33, 2012.

Coupling Navier–Stokes to Willmore: Numerical approximation of dynamic biomembranes

Robert Nürnberg
(joint work with John W. Barrett, Harald Garcke)

We present a finite element scheme for the approximation of the dynamics of two and three dimensional fluidic biomembranes in Navier–Stokes flow. The model was introduced by Arroyo and DeSimone ([1]) and is given by a coupling of the incompressible Navier–Stokes equations in the bulk, an incompressible surface Navier–Stokes equation on the membrane, and the forces stemming from a curvature elasticity energy.

In order to present the model, we assume that the closed, time dependent membrane $(\Gamma(t))_{t\geq 0}$ lies inside a spatial domain $\Omega \subset \mathbb{R}^d$, $d = 2, 3$. For all times the membrane separates Ω into an inner domain $\Omega_-(t)$ and an outer domain $\Omega_+(t)$. Denoting by $\vec{u}$ the fluid velocity and by p the pressure, the bulk stress tensor is given by $\underline{\underline{\sigma}} = 2\,\mu\,\underline{\underline{D}}(\vec{u}) - p\,\underline{\underline{\mathrm{Id}}}$, with $\underline{\underline{D}}(\vec{u}) = \frac{1}{2}\,(\nabla\,\vec{u} + (\nabla\,\vec{u})^T)$ being the bulk rate-of-strain tensor. We assume that the Navier–Stokes system

$$\rho\,(\vec{u}_t + (\vec{u}\,.\,\nabla)\,\vec{u}) - \nabla\,.\,\underline{\underline{\sigma}} = 0\,, \quad \nabla\,.\,\vec{u} = 0$$

holds in $\Omega_-(t)$ and $\Omega_+(t)$. Here ρ and μ are the density and dynamic viscosity of the fluid, which can take different (constant) values $\rho_\pm$, $\mu_\pm$ in $\Omega_\pm(t)$. In the model the fluid velocity is assumed to be continuous across the membrane, the membrane is moved in the normal direction with the normal velocity of the bulk fluid and, in addition, the surface Navier–Stokes equations

$$\rho_\Gamma\,\partial_t^\bullet\,\vec{u} - \nabla_s\,.\,\underline{\underline{\sigma}}_\Gamma = [\underline{\underline{\sigma}}]_-^+\,\vec{\nu} + \alpha\,\vec{f}_\Gamma\,, \quad \nabla_s\,.\,\vec{u} = 0$$

have to hold on $\Gamma(t)$. Here ρ_Γ is the surface material density, $\partial_t^\bullet$ is the material derivative and $\nabla_s, \nabla_s\,.$ are the gradient and divergence operators on the surface. The surface stress tensor is given by

$$\underline{\underline{\sigma}}_\Gamma = 2\,\mu_\Gamma\,\underline{\underline{D}}_s(\vec{u}) - p_\Gamma\,\underline{\underline{\mathcal{P}}}_\Gamma\,,$$

where p_Γ is the surface pressure, μ_Γ is the surface shear viscosity, $\underline{\underline{\mathcal{P}}}_\Gamma$ is the projection onto the tangent space and

$$\underline{\underline{\mathcal{D}}}_s(\vec{u}) = \tfrac{1}{2}\,\underline{\underline{\mathcal{P}}}_\Gamma\,(\nabla_s\,\vec{u} + (\nabla_s\,\vec{u})^T)\,\underline{\underline{\mathcal{P}}}_\Gamma$$

is the surface rate-of-strain tensor. Furthermore, the term $[\underline{\underline{\sigma}}]_-^+\,\vec{\nu} = \underline{\underline{\sigma}}_+\,\vec{\nu} - \underline{\underline{\sigma}}_-\,\vec{\nu}$ is the force exerted by the bulk on the membrane, where $\vec{\nu}$ denotes the exterior unit normal to $\Omega_-(t)$. The remaining term $\alpha\,\vec{f}_\Gamma$ denotes the forces stemming from the elastic bending energy. These forces are given by the first variation of the bending energy $\alpha\,E(\Gamma(t))$, where

$$E(\Gamma) = \frac{1}{2}\int_\Gamma \varkappa^2\,\mathrm{d}s$$

is the well-known Willmore energy, with $\varkappa$ denoting the mean curvature (the sum of the principal curvatures) of Γ. It turns out that $\vec{f}_\Gamma$ points in the normal

direction, i.e. $\vec{f}_\Gamma = f_\Gamma\,\vec{\nu}$, where

$$f_\Gamma = -\Delta_s\,\varkappa - \varkappa\,|\nabla_s\,\vec{\nu}|^2 + \tfrac{1}{2}\,\varkappa^3\,.$$

Here Δ_s is the surface Laplace operator, and $\nabla_s\,\vec{\nu}$ is the Weingarten map. Assuming e.g. no-slip boundary conditions on $\partial\Omega$, the boundary of Ω, it is possible to show that the total energy can only decrease, i.e.

$$\begin{aligned}&\frac{\mathrm{d}}{\mathrm{d}t}\left(\int_\Omega \frac{\rho}{2}\,|\vec{u}|^2\,\mathrm{d}x + \frac{\rho_\Gamma}{2}\int_\Gamma |\vec{u}|^2\,\mathrm{d}s + \alpha\,E(\Gamma)\right)\\ &\qquad = -2\left(\int_\Omega \mu\,|\underline{\underline{D}}(\vec{u})|^2\,\mathrm{d}x + \mu_\Gamma\int_\Gamma |\underline{\underline{D}}_s(\vec{u})|^2\,\mathrm{d}s\right) \leq 0\,.\end{aligned} \tag{1}$$

Using a stable discretization of Willmore flow due to Dziuk ([7]), which is based on the identity

$$\begin{aligned}\tfrac{1}{2}\,\frac{\mathrm{d}}{\mathrm{d}t}\,\langle\vec{\varkappa},\vec{\varkappa}\rangle_{\Gamma(t)} &= -\left\langle\nabla_s\,\vec{\varkappa},\nabla_s\,\vec{\mathcal{V}}\right\rangle_{\Gamma(t)} - \left\langle\nabla_s\,.\,\vec{\varkappa},\nabla_s\,.\,\vec{\mathcal{V}}\right\rangle_{\Gamma(t)}\\ &\quad - \tfrac{1}{2}\left\langle|\vec{\varkappa}|^2\,\nabla_s\,\vec{\mathrm{id}},\nabla_s\,\vec{\mathcal{V}}\right\rangle_{\Gamma(t)} + 2\left\langle(\nabla_s\,\vec{\varkappa})^T,\underline{\underline{D}}_s(\vec{\mathcal{V}})\,(\nabla_s\,\vec{\mathrm{id}})^T\right\rangle_{\Gamma(t)},\end{aligned} \tag{2}$$

where $\langle\cdot,\cdot\rangle_{\Gamma(t)}$ denotes the L^2–inner product on $\Gamma(t)$, we develop a stable parametric finite element method for the coupled bulk Navier–Stokes, surface Navier–Stokes, Willmore system. In particular, a semidiscrete continuous-in-time discretization satisfies a discrete analogue of (1). In our approach, the bulk and surface degrees of freedom are discretized independently, which leads to an unfitted finite element approximation of the underlying free boundary problem, similarly to our previous work in [6] on two-phase flow. Using a pseudo-XFEM finite element extension for the pressure space in the bulk leads to volume conservation on the discrete level. Moreover, the natural weak approximation of the surface incompressibility condition with piecewise linear surface finite elements gives surface area conservation and, in addition, good mesh properties. For further details we refer to [5]. The numerical simulation of four vesicles flowing through a constriction can be seen in Figure 1.

Finally, we note that on using ideas from formal calculus of PDE constrained optimization, it is possible to extend the stable approximation (2) to more general curvature energies of the form

$$E(\Gamma) = \frac{1}{2}\int_\Gamma(\varkappa-\overline{\varkappa})^2\,\mathrm{d}s + \frac{\beta}{2}\left(\int_\Gamma \varkappa\,\mathrm{d}s - M_0\right)^2, \tag{3}$$

see [2]. Here $\overline{\varkappa}\in\mathbb{R}$ is a so-called spontaneous curvature, and for $\beta>0$ the second term in (3) models an area difference elasticity (ADE) which accounts for an asymmetry in the surface area between the two lipid layers of the membrane. As before, the stable approximation of the first variation of (3) can be coupled to approximations of the fluid flow in the bulk and the fluid flow on the membrane to yield a stable numerical approximation of the evolution of fluidic biomembranes taking spontaneous curvature and ADE affects into account. We refer to [4, 3] for more details.

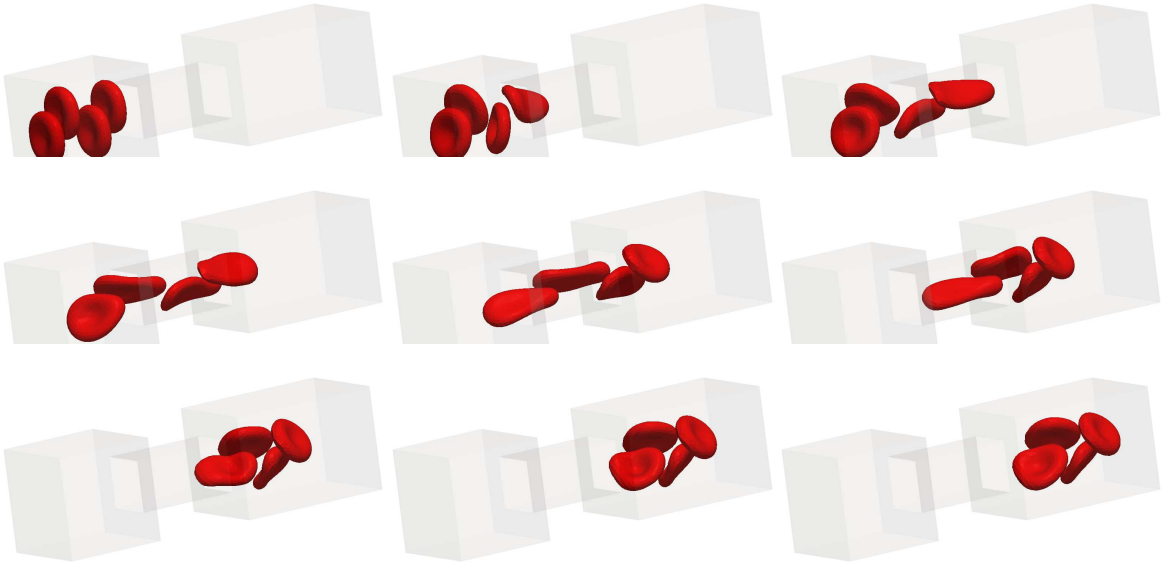

FIGURE 1. Flow through a constriction.

REFERENCES

[1] M. Arroyo and A. DeSimone, *Relaxation dynamics of fluid membranes*, Phys. Rev. E **79** (2009), 031915.

[2] J. W. Barrett, H. Garcke and R. Nürnberg, *Computational parametric Willmore flow with spontaneous curvature and area difference elasticity effects*, 2015, preprint No. 14/2015, University Regensburg, Germany.

[3] J. W. Barrett, H. Garcke and R. Nürnberg, *Finite element approximation for the dynamics of asymmetric fluidic biomembranes*, 2015, preprint No. 03/2015, University Regensburg, Germany.

[4] J. W. Barrett, H. Garcke and R. Nürnberg, *Numerical computations of the dynamics of fluidic membranes and vesicles*, Phys. Rev. E **92** (2015), 052704.

[5] J. W. Barrett, H. Garcke and R. Nürnberg, *A stable numerical method for the dynamics of fluidic biomembranes*, Numer. Math. (accepted for publication, DOI:10.1007/s00211-015-0787-5).

[6] J. W. Barrett, H. Garcke and R. Nürnberg, *A stable parametric finite element discretization of two-phase Navier–Stokes flow*, J. Sci. Comp. **63** (2015), 78–117.

[7] G. Dziuk, *Computational parametric Willmore flow*, Numer. Math. **111** (2008), 55–80.

A spatially one-dimensional hyperbolic-parabolic model for the polymerization of the filaments in the cellular cytoskeleton

ANGELA STEVENS

(joint work with Jan Fuhrmann)

The main motivation of the presented talk was to introduce a minimal model for the polymerization and depolymerization of the filaments of the actin cytoskeleton of cells. A free boundary value problem was formulated and analyzed w.r.t. the possible existence of polymerization shocks, which would indicate cell polarization and/or cell movement.

The filaments of the cellular cytoskeleton have a so-called barbed end and a pointed end, since the actin monomers out of which these filaments are build, are asymmetric. When just modeling the dynamics of these end densities we obtain for the barbed ends of the right oriented filaments that

$$\partial_t B_r + \partial_x \left(v_B(a) B_r\right) = 0 \ ,$$

where the barbed end velocity is given by

$$v_B(a) = -v_R + \kappa_B(a - a_B) \ .$$

Here the first term is the so-called retrograde flow, an experimentally observed pulling back of the filaments, and the second term describes growth by polymerization/negative growth by depolymerization, where a denotes the actin monomer concentration. Similarly for the other filament ends, the barbed ends of the left oriented filamens, the pointed ends of the right oriented filaments, and the pointed ends of the left oriented filaments, one has

$$\partial_t B_l = \partial_x \left(v_B(a) B_l\right) \ , \ \partial_t P_r = -\partial_x \left(v_P(a) P_r\right) \ , \ \partial_t P_l = \partial_x \left(v_P(a) P_l\right) \ .$$

where the pointed end velocity fulfills $v_P(a) = -v_R - \kappa_P(a - a_P)$. For the monomer concentration we assume

$$\partial_t a = D\partial_{xx} a + R(a, B_r, B_l, P_r, P_l)$$

with reaction term $R = \kappa_B(a_B - a)(B_r + B_l) + \kappa_P(a_P - a)(P_r + P_l)$.
Our free boundary value problem for $(u^1, u^2, u^3, u^4)^T = (B_l, P_r, P_l, B_r)^T$ and $\Lambda = diag(\lambda^1, \ldots, \lambda^4) := diag(-\nu_B, \nu_P, -\nu_P, \nu_B)$ now reads

$$\partial_t u + \partial_x(\Lambda u) = 0$$

$$\partial_t a - D\partial_{xx} a = R(a, u) = -c \cdot ua + \tilde{c} \cdot u \ ,$$

where $c = (\kappa_B, \kappa_P, \kappa_P, \kappa_B)$, $\tilde{c} = (\kappa_B\, a_B, \kappa_P\, a_P, \kappa_P\, a_P, \kappa_B\, a_B)$. We assume that the cell membrane is infinitely soft, i.e. the outermost filament tips move at their free velocity λ^j, $j = 1, ..., 4$.

The hyperbolic part of the system is diagonal, so one can directly read off the characteristic velocities. Define $l(t) = \min_{j=1,\ldots,4} l^j(t)$, $r(t) = \max_{j=1,\ldots,4} r^j(t)$. The boundary curves of the j^{th} characteristic familiy are given by

$$(l^j)'(t) = \lambda^j(a(t, l^j(t)) \ , \ (r^j)'(t) = \lambda^j(a(t, r^j(t))) \ .$$

For the leading end densities, which support the membrane, we have a characteristic boundary.

On $Q_T = \{(t, x) \ | \ 0 < t < T, \ l(t) < x < r(t)\}$ we impose no-flux boundary conditions for $a(t)$, $0 < t < T$, i.e.

$$D\partial_x a(t, l(t)) + a(t, l(t))l'(t) = 0 = D\partial_x a(t, r(t)) + a(t, r(t))r'(t) \ .$$

The barbed ends of the right oriented filaments are positioned further to the right than the corresponding pointed ends, i.e. initially we assume that
$\int_0^x u_0^2(y)dy > \int_0^x u_0^4(y)dy$, $x \in (0, L)$. After decomposition of Q_T we obtain for the hyperbolic part

- one Cauchy problem and
- two characteristic boundary value problems on 'fan shaped' domains.

Short time well-posedness could be proved under the assumption of strict hyperbolicity at the boundary.

Explicit solutions could be constructed, where Dirac peaks occured for the end densities with a continuous monomer distribution. Further, a formula for the distance between the end densities could be derived in case the mass of pointed and barbed ends, which was concentrated in the Dirac peaks, was equal.

Also, moving profiles of end densities could be contructed, where its constant velocity could be calculated in terms of the ratio of the barbed and pointed end densities.

Shocks could be constructed for the hyperbolic limiting system of our model, i.e. for $D = 0$. Further, moving shocks could be constructed and an asymptotic shock speed could be calculated.

An open question is, if these phenomena can also result dynamically from a suitable class of smooth initial data. Answers to this question are so far only given by numerical results.

References

[1] J. Fuhrmann, J. Käs, A. Stevens, *Initiation of cytoskeletal asymmetry for cell polarization and movement*, J. Theor. Biol. *249* (2007), 278–288.
[2] J. Fuhrmann, *On a Minimal Model for the Initiation of Cell Movement*, (2012) Ph.D.-Thesis, University of Heidelberg.
[3] H. Freistühler, J. Fuhrmann, A. Stevens, *Travelling waves emerging in a diffusive moving filament system*, in Managing Complexity, Reducing Perplexity. Modeling Biological Systems. Eds. G. Ajmone-Marsan, M. Delitala, (2014), Springer Verlag.
[4] J. Fuhrmann, A. Stevens, *free boundary problem for cell motion*, Differential Integral Equations *28* (2015), no. 7/8, 695–732

Finite element analysis for a parabolic equation on a solution-driven evolving surface

Christian Lubich

(joint work with Balázs Kovács, Buyang Li, Christian Power Guerra)

Starting from a paper by Dziuk & Elliott in 2007, much insight into the stability and convergence properties of finite elements on evolving surfaces (ESFEM) has been obtained by studying a linear parabolic equation on a given moving closed surface $\Gamma(t)$. The strong formulation of this model problem is to find a solution $u(x,t)$ (for $x \in \Gamma(t)$ and $0 \le t \le T$) with given initial data $u(x,0) = u_0(x)$ to the linear partial differential equation

$$\partial^\bullet u(x,t) + u(x,t)\nabla_{\Gamma(t)} \cdot v(x,t) - \Delta_{\Gamma(t)} u(x,t) = 0, \qquad x \in \Gamma(t),\ 0 < t \le T,$$

where $\partial^\bullet$ denotes the material time derivative, $\Delta_{\Gamma(t)}$ is the Laplace–Beltrami operator on the surface, and $\nabla_{\Gamma(t)} \cdot v$ is the tangential divergence of the *given* velocity v of the surface.

Beyond the above model problem, there is considerable interest in cases where the velocity of the evolving surface is not given explicitly, but depends on the solution u of the parabolic equation. Contrary to the situation for surfaces with prescribed motion, there exists so far no numerical analysis for solution-driven surfaces, to the best of our knowledge. For the case of evolving curves, there is a recent arXiv preprint by Pozzi & Stinner, who couple the curve-shortening flow with diffusion on the curve and study the convergence of a finite element semi-discretization. The analogous problem for two- or higher-dimensional surfaces would be to couple mean curvature flow with diffusion on the surface. Studying the convergence of finite elements for this coupled problem, however, remains illusive as long as the convergence of ESFEM for mean curvature flow of closed surfaces is not understood. This has remained an open problem since Dziuk's formulation of such a method for mean curvature flow in his 1990 paper.

In our current work in progress, we consider different velocity laws for coupling the surface motion with the solution of the diffusion equation on the surface. Conceivably the most simple velocity law would be to prescribe the normal velocity at any point as a function of the solution value and possibly its tangential gradient at this point: $v(x,t) = g(u(x,t), \nabla_{\Gamma(t)} u(x,t))\, \nu_{\Gamma(t)}(x)$ for $x \in \Gamma(t)$, where $\nu_{\Gamma(t)}(x)$ denotes the outer normal vector and g is a given smooth scalar-valued function. This does, however, not appear to lead to a well-posed problem (and definitely not to smooth surfaces). Here we study instead a *regularized velocity law*:

$$v(x,t) - \alpha \Delta_{\Gamma(t)} v(x,t) = g\big(u(x,t), \nabla_{\Gamma(t)} u(x,t)\big)\, \nu_{\Gamma(t)}(x), \qquad x \in \Gamma(t),$$

with a fixed regularization parameter $\alpha > 0$. This elliptic regularization permits us to give a complete stability and convergence analysis of the ESFEM semi-discretization, for finite elements of degree at least two. The case of linear finite elements is currently left open. Our approach can be extended to full discretizations with linearly implicit backward difference time-stepping, as we plan to show in subsequent work.

Our approach also applies to the ESFEM discretization of a *regularized* coupling of mean curvature flow and diffusion:

$$v - \alpha \Delta_{\Gamma(t)} v = \Big(-H + g\big(u, \nabla_{\Gamma(t)} u\big) \Big) \nu_{\Gamma(t)},$$

where H denotes mean curvature.

The error analysis is further extended to a *dynamic velocity law*

$$\partial^\bullet v + v \nabla_{\Gamma(t)} \cdot v - \alpha \Delta_{\Gamma(t)} v = g\big(u, \nabla_{\Gamma(t)} u\big)\, \nu_{\Gamma(t)}.$$

A physically more relevant dynamic velocity law would be based on momentum and mass balance, such as incompressible Navier–Stokes motion of the surface

coupled to diffusion on the surface:

$$\begin{aligned}
&\rho\,\partial^\bullet v - \alpha\Delta_{\Gamma(t)} v = -\nabla_{\Gamma(t)} p + g(u, \nabla_{\Gamma(t)} u)\,\nu_{\Gamma(t)}\\
&\partial^\bullet \rho = 0\\
&\nabla_{\Gamma(t)} \cdot v = 0.
\end{aligned}$$

We expect that our analysis can be extended also to such a system.

Coupled bulk-surface free boundary problems from a model for receptor-ligand dynamics

Chandrasekhar Venkataraman
(joint work with Charles M. Elliott, Thomas Ranner)

Let Γ be a smooth, compact closed n-dimensional hypersurface contained in a domain $D \subset \mathbb{R}^{n+1}$, $n = 1, 2$. The surface Γ separates a domain D into an interior domain I and an exterior domain Ω. We will denote by $\partial_0\Omega$ the outer boundary of Ω, i.e., the boundary ∂D. We will assume that this boundary is Lipschitz. We consider the following problem: Find $u\colon \bar{\Omega} \times [0,T] \to \mathbb{R}^+$ and $w\colon \Gamma \times [0,T] \to \mathbb{R}^+$ such that

$$\delta_\Omega \partial_t u - \Delta u = 0 \qquad \text{in } \Omega \tag{1a}$$

$$\nabla u \cdot \vec{\nu} = -\frac{1}{\delta_k} uw \qquad \text{on } \Gamma \tag{1b}$$

$$u = u_D \text{ or } \nabla u \cdot \vec{\nu}_\Omega = 0 \qquad \text{on } \partial_0\Omega \tag{1c}$$

$$\partial_t w - \delta_\Gamma \Delta_\Gamma w = \nabla u \cdot \vec{\nu} \qquad \text{on } \Gamma \tag{1d}$$

$$u(\cdot, 0) = u^0(\cdot) \qquad \text{in } \Omega \tag{1e}$$

$$w(\cdot, 0) = w^0(\cdot) \qquad \text{on } \Gamma, \tag{1f}$$

where $\delta_\Omega, \delta_\Gamma, \delta_k > 0$ are given model parameters and the initial data are bounded, non-negative functions, i.e., $u^0 \in L^\infty(\Omega)$, $w^0 \in L^\infty(\Gamma)$ and $u^0, w^0 \geq 0$. In the above Δ_Γ denotes the Laplace-Beltrami operator on the surface Γ and Δ the usual Cartesian Laplacian in $\mathbb{R}^{n+1}$.

Problem (1) may be regarded as a basic model for receptor-ligand dynamics in cell biology, modelling the dynamics of mobile cell surface receptors, w reacting with a mobile bulk ligand, u. The model arises, after nondimensionalisation, as a large binding affinity reduction of a model including receptor-ligand complexes, in which we neglect the complexes. Taking biologically realistic parameter values (c.f., [1]) for the characteristic scales used to nondimsionalise the model, motivates the consideration of the following three biologically relevant asymptotic limits

$$(1)\ \delta_k \to 0, \quad (2)\ \delta_\Gamma = \delta_k \to 0, \quad \text{and } (3)\ \delta_\Omega = \delta_\Gamma = \delta_k \to 0.$$

We prove the existence and uniqueness of a (weak) solution pair (u, w) to (1) together with rigorous convergence of (u, v), with $v = -w$ to weak solutions of three limiting bulk-surface free boundary problems in the biologically relevant limits above.

The limiting problems correspond to interesting free boundary problems due to the complementarity nature of the fast reaction limit ($\delta_k \to 0$), i.e., in the limit one has

$$u \geq 0, \qquad w \geq 0, \qquad uw = 0 \qquad \text{on } \Gamma.$$

The three limiting problems are given by
Coupled parabolic-parabolic limit problem ($\delta_k \to 0$): Find $\bar{u}\colon \Omega \times (0,T) \to \mathbb{R}^+$, $\bar{v}\colon \Gamma \times (0,T) \to \mathbb{R}^-$ such that

$$\delta_\Omega \partial_t \bar{u} - \Delta \bar{u} = 0 \qquad \text{in } \Omega \times (0,T) \tag{2a}$$

$$\nabla \bar{u} \cdot \vec{\nu} + \partial_t \bar{v} - \delta_\Gamma \Delta_\Gamma \bar{v} = 0 \quad \text{and} \quad \bar{v} \in \beta(\bar{u}) \qquad \text{on } \Gamma \times (0,T) \tag{2b}$$

$$\bar{u} = u_D \quad \text{or} \quad \nabla \bar{u} \cdot \vec{\nu}_\Omega = 0 \qquad \text{on } \partial_0\Omega \times (0,T) \tag{2c}$$

$$\bar{u}(\cdot,0) = u^0(\cdot) \geq 0 \qquad \text{in } \Omega \tag{2d}$$

$$\bar{v}(\cdot,0) = v^0(\cdot) \leq 0 \qquad \text{on } \Gamma. \tag{2e}$$

Parabolic limit problem with dynamic boundary conditions ($\delta_k = \delta_\Gamma \to 0$): Find $\tilde{u}\colon \Omega \times (0,T) \to \mathbb{R}^+$ and $\tilde{v}\colon \Gamma \times (0,T) \to \mathbb{R}^-$ such that

$$\delta_\Omega \partial_t \tilde{u} - \Delta \tilde{u} = 0 \qquad \text{in } \Omega \times (0,T) \tag{3a}$$

$$\nabla \tilde{u} \cdot \vec{\nu} + \partial_t \tilde{v} = 0 \qquad \text{on } \Gamma \times (0,T) \tag{3b}$$

$$\tilde{v} \in \beta(\tilde{u}) \qquad \text{on } \Gamma \times (0,T) \tag{3c}$$

$$\tilde{u} = u_D \quad \text{or} \quad \nabla \tilde{u} \cdot \vec{\nu} = 0 \qquad \text{on } \partial_0\Omega \times (0,T) \tag{3d}$$

$$\tilde{u}(\cdot,0) = u_0(\cdot) \geq 0 \qquad \text{on } \Omega \tag{3e}$$

$$\tilde{v}(\cdot,0) = v_0(\cdot) \leq 0 \qquad \text{on } \Gamma. \tag{3f}$$

Elliptic limit problem with dynamic boundary conditions ($\delta_\Omega = \delta_k = \delta_\Gamma \to 0$):

$$-\Delta \hat{u} = 0 \qquad \text{in } \Omega \times (0,T) \tag{4a}$$

$$\nabla \hat{u} \cdot \vec{\nu} + \partial_t \hat{v} = 0 \qquad \text{on } \Gamma \times (0,T) \tag{4b}$$

$$\hat{v} \in \beta(\hat{u}) \qquad \text{on } \Gamma \times (0,T) \tag{4c}$$

$$\hat{u} = u_D \qquad \text{on } \partial_0\Omega \times (0,T) \tag{4d}$$

$$\hat{u}(\cdot,0) = u^0(\cdot) \geq 0 \qquad \text{on } \Omega \tag{4e}$$

$$\hat{v}(\cdot,0) = v^0(\cdot) \leq 0 \qquad \text{on } \Gamma. \tag{4f}$$

For problems (2), (3) and (4) the complementarity is encoded in the constraint $v \in \beta(u)$ with β defined by

$$\beta(r) = \begin{cases} \emptyset & \text{if } r < 0 \\ [-\infty, 0] & \text{if } r = 0 \\ \{0\} & \text{if } r > 0. \end{cases}$$

For the latter two problems, i.e., (3) and (4), we are further able to prove that the solution is unique.

We may write the problems as abstract degenerate parabolic equations holding on the surface Γ which reveals their structure. Introducing a parabolic and an elliptic Dirichlet to Neumann (DtN) map $\mathcal{A}^{\delta_\Omega}$ and $\mathcal{A}^0$ respectively (see [2] for details), we may write problems (2), (3) and (4) as follows.
Fast reaction problem ($\delta_k = 0$)

$$\partial_t \bar{v} + \delta_\Gamma L\bar{v} + \mathcal{A}^{\delta_\Omega}\bar{u} + \nabla(U_D^{\delta_\Omega} + U_I^{\delta_\Omega}) \cdot \nu = 0 \qquad \text{in } L^2(0,T;H^{-1}(\Gamma)), \tag{5}$$

Parabolic problem with dynamic boundary condition ($\delta_k = \delta_\Gamma = 0$)

$$\partial_t \tilde{v} + \mathcal{A}^{\delta_\Omega}\tilde{u} + \nabla(U_D^{\delta_\Omega} + U_I^{\delta_\Omega}) \cdot \nu = 0 \qquad \text{in } L^2(0,T;H^{-1/2}(\Gamma)), \tag{6}$$

Elliptic problem with dynamic boundary condition ($\delta_k = \delta_\Gamma = \delta_\Omega = 0$)

$$\partial_t \hat{v} + \mathcal{A}^0\hat{u} + \nabla U_D \cdot \nu = 0 \qquad \text{in } L^2(0,T;H^{-1/2}(\Gamma)), \tag{7}$$

with $v \in \beta(u)$ for each problem, $v^0 = -w^0$, $L := -\Delta_\Gamma$ and with U_D and U_I extensions associated with the boundary and initial data for u. Written in this way, one sees that problems (6) and (7) may be thought of as analogues of the Hele-Shaw or steady one phase Stefan problems on the surface Γ with the operators $\mathcal{A}^{\delta_\Omega}$ and $\mathcal{A}^0$ in place of the usual Laplacian (Laplace-Beltrami). Interpreting the operator $\mathcal{A}^0$, which is the DtN map of the harmonic extension of the function off Γ, as $(-\Delta_\Gamma)^{1/2}$ we may think of (7) as a surface Hele Shaw problem with the half-Laplacian in place of the usual Laplacian.

Following techniques employed for the resolution of the one-phase Stefan and Hele Shaw problems [3, 4, 5] we may integrate in time and reformulate problems (6) and (7), respectively, as parabolic and elliptic variational inequalities of obstacle type. The obstacle problem lies on the surface Γ and is a consequence of the complementarity which is maintained after an integration with respect to time, noting that this integration commutes with the operators $\mathcal{A}^{\delta_\Omega}$ and $\mathcal{A}^0$. In the latter case, i.e., the elliptic variational inequality, time simply enters as a parameter and hence the problem may be solved at any given time independent of the values at other times leading to significant speed up in terms of computations.

References

[1] García-Peñarrubia P, Gálvez JJ and Gálvez J, *Mathematical modelling and computational study of two-dimensional and three-dimensional dynamics of receptor–ligand interactions in signalling response mechanisms*, Journal of Mathematical Biology **69**, 3, (2014), 553–582.

[2] C. M. Elliott, T. Ranner, and C. Venkataraman, *Coupled bulk-surface free boundary problems arising from a mathematical model of receptor-ligand dynamics*, ArXiv e-prints (2015).

[3] G. Duvaut, *Résolution d'un probleme de Stefan (fusion d'un bloc de glacea zéro degré)*, Comptes rendus de l'Acadmie des Sciences. Série A **276**, (1973).

[4] C. M. Elliott, *On a variational inequality formulation of an electrochemical machining moving boundary problem and its approximation by the finite element method*, IMA Journal of Applied Mathematics **25**, 2, (1980), 121–131.

[5] C. M. Elliott and V. Janovskỳ, *A variational inequality approach to Hele-Shaw flow with a moving boundary*, Proceedings of the Royal Society of Edinburgh: Section A Mathematics **88**, 1-2, (1981), 93–107.

Geometric errors in finite volume schemes for hyperbolic conservation laws on manifolds

Jan Giesselmann

We study the approximation of nonlinear (scalar) hyperbolic conservation laws posed on Riemannian manifolds by finite volume schemes. The analysis of these methods was initiated in [1] and has been the focus of many papers in recent years, also allowing for Riemannian metrics changing in time. The latter can be seen as a framework which, in particular, enables the study of problems posed on moving hypersurfaces of Euclidean space. Most of the existing literature considers a geometric setting in which all geometric quantities are known exactly and also readily available in defining and applying the finite volume method. In particular, the finite volume methods studied in [1] and the ensuing literature require an exact knowledge of cell areas, face areas and conormals. In most applications, however, the evaluation of exact geometric quantities or their approximation with high order accuracy is by orders of magnitude exceeding the computational costs of the finite volume method itself. This issue arises in particular when moving surfaces are considered which do not have "standard" shapes, i.e., are not spheres or tori.

Thus, we have initiated in [3] the study of finite volume schemes posed on polyhedra approximating moving hypersurfaces in Euclidean space. The polyhedra readily supply approximations of geometric quantities on the surface. These approximations obviously introduce certain "geometry approximation" errors into the scheme whose influence on the overall accuracy needs to be tracked.

Based on the fact that there are a priori error estimates available for the schemes assuming full knowledge of all geometric quantities [4, 5], it only remains to compute the difference between solutions u^h of these schemes and solutions $\bar{u}^h$ of schemes using only approximate geometric quantities coming from the polyhedral approximation of the surface. Our analysis in [3] shows that the L_1-difference between the solutions of both types of schemes is at most of the order of the mesh width h. As the L_1-difference between u^h and the (exact) entropy solution u is bounded by terms of order $h^{1/4}$, the same is true for the difference between $\bar{u}^h$ and u. Hence, with regard to the convergence rate of (first order) finite volume schemes to discontinuous entropy solutions, the geometric errors introduced by the polyhedral approximation of the surface are of negligible.

However, if the construction of higher order methods is considered, the situation changes. We numerically investigate an example in [3] in which a trivial conservation law is solved on a stationary sphere. In this example the geometric errors add up in such a way that the L_1-difference between u^h and $\bar{u}^h$ is indeed of order h. This observation is not altered when we use Muscl type reconstructions for the computation of the numerical fluxes which in the Euclidean case lead to second order methods (as long as the exact solution is sufficiently smooth). This example shows that polyhedral approximations of surfaces pose an obstacle to second order convergence of numerical methods for hyperbolic conservation laws on these surfaces. Note that this is different from the situation for parabolic problems [8, 7].

Concerning the refinement and extension of the analysis described above, there remain the following open questions:

- Can the analysis be extended to cases where the problem is not posed on hypersurfaces of Euclidean space but on Riemannian or Lorentzian manifolds or more general space times without ambient space and what is the appropriate way to discretize the geometry in these cases? For examples of problems posed on manifolds without ambient space, see [6, e.g.] and references therein.
- Can a fully practical numerical scheme be defined in an intrinsic way, i.e., without reference to (and dependence on) local charts?
- In case higher order methods, e.g., discontinuous Galerkin finite element methods, are used for the approximation of hyperbolic conservation laws on surfaces: What is the appropriate order of approximation of the geometry and how can it be achieved at a reasonable numerical cost? This is similar to the question answered for the elliptic case in [2].

A more fundamental open question, which by far exceeds the scope of the analysis discussed above, is how error estimates for nonlinear systems of hyperbolic conservation laws on manifolds can be obtained.

References

[1] P. Amorim, M. Ben-Artzi and P. G. LeFloch, *Hyperbolic conservation laws on manifolds: total variation estimates and the finite volume method,* Methods Appl. Anal. **12** (2005), 291–323.

[2] A. Demlow, *Higher-order finite element methods and pointwise error estimates for elliptic problems on surfaces,* SIAM J. Numer. Anal., **247** (2009), 805–827.

[3] J. Giesselmann and T. Müller, *Geometric Error of Finite Volume Schemes for Conservation Laws on Evolving Surfaces,* Numer. Math., **128** (2014), 489–516.

[4] J. Giesselmann, *A convergence result for finite volume schemes on Riemannian manifolds*, M2AN Math. Model. Numer. Anal., **43** (2009), 929–955.

[5] P. G. LeFloch, B. Okutmustur and W. Neves, *Hyperbolic conservation laws on manifolds. An error estimate for finite volume schemes*, Acta Math. Sin. (Engl. Ser.), **25** (2009), 1041–1066.

[6] P. G. LeFloch and H. Makhlof, *A geometry-preserving finite volume method for compressible fluids on Schwarzschild spacetime*, Commun. Comput. Phys. **15** (2014), 827–852.

[7] M. Lenz, S. F. Nemadjieu and M. Rumpf, *A convergent finite volume scheme for diffusion on evolving surfaces*, SIAM J. Numer. Anal., **29** (2011), 15–37.

[8] G. Dziuk and C. M. Elliott, *Surface finite elements for parabolic equations*, J. Comput. Math., **25** (2007), 385–407.

Optimal control of PDEs on surfaces

Michael Hinze

(joint work with Morten Vierling)

We consider optimal control problems of elliptic and parabolic PDEs on (moving) hypersurfaces Γ in $\mathbb{R}^n$ for $n = 2, 3$. The leading part of the PDE is given by the Laplace-Beltrami operator, which is discretized by finite elements on a polyhedral

approximation of Γ. The discrete optimal control problem is formulated on the approximating surface and is solved numerically with a semi-smooth Newton algorithm. We derive optimal a priori error estimates for problems including control constraints and provide numerical examples confirming our analytical findings. The basic ingredients for our method in the Elliptic case is Dziuk's finite element concept for the Laplace Beltrami operator [2] for the discretization of the state equation, and in the parabolic case the ESFEM method developed by Dziuk and Elliott [3] for the discretization of the parabolic PDE on the evolving surface. This in both cases is combined with variational discretization developed by the author [4] for the discretization of the control problem, and a semismooth Newton method developed by Hintermller et al. [5] and Michael Ulbrich [7] to solve the resulting nonlinear systems.

More specifically we in the elliptic case consider

$$(P) \quad \begin{cases} \min\limits_{u\in L^2(\Gamma),\, y\in H^1(\Gamma)} J(u,y) = \dfrac{1}{2}\|y-z\|^2_{L^2(\Gamma)} + \dfrac{\alpha}{2}\|u\|^2_{L^2(\Gamma)} \\ \text{subject to} \quad u \in U_{ad} \text{ and} \\ \underbrace{\displaystyle\int_\Gamma \nabla_\Gamma y \nabla_\Gamma \varphi + \mathbf{c} y\varphi \,\mathrm{d}\Gamma = \int_\Gamma u\varphi \,\mathrm{d}\Gamma \,, \forall \varphi \in H^1(\Gamma),}_{:\Leftrightarrow y = Su} \end{cases}$$

where $U_{ad} = \left\{ v \in L^2(\Gamma) \mid a \le v \le b \right\}$, $a < b \in \mathbb{R}$. It follows by standard arguments that problem (P) admits a unique solution $u \in U_{ad}$ with unique associated state $y =: Su \in H^2(\Gamma)$, and

$$u = \mathrm{P}_{U_{ad}} \left(-\frac{1}{\alpha} p(u) \right), \quad p(u) := S^*(Su - z).$$

Here, $\mathrm{P}_{U_{ad}}(\cdot)$ denotes the orthogonal projection in $L^2(\Gamma)$ onto U_{ad}. Problem (P) is approximated by the following sequence of optimal control problems

$$(P_h) \quad \begin{cases} \min\limits_{u\in L^2(\Gamma^h),\, y\in V_h} J(u,y) = \dfrac{1}{2}\|y-z_l\|^2_{L^2(\Gamma^h)} + \dfrac{\alpha}{2}\|u\|^2_{L^2(\Gamma^h)} \\ \text{subject to} \quad u \in U^h_{ad} \text{ and} \\ y_h = S_h u, \end{cases}$$

with $U^h_{ad} = \left\{ v \in L^2(\Gamma^h) \mid a \le v \le b \right\}$. For some $v \in L^2(\Gamma^h)$ let $S_h v := y_h \in V_h$ solve

$$\int_{\Gamma^h} \nabla_{\Gamma^h} y_h \nabla_{\Gamma^h} \varphi + \mathbf{c} y_h \varphi \,\mathrm{d}\Gamma^h = \int_{\Gamma^h} v\varphi \,\mathrm{d}\Gamma^h \quad \forall \varphi \in V_h,$$

where

$$V_h = \left\{ \varphi \in C^0\left(\Gamma^h\right) \;\middle|\; \forall i \in I_h : \varphi|_{T^i_h} \in \mathcal{P}^1(T^i_h) \right\} \subset H^1(\Gamma^h).$$

It follows by standard arguments that problem (P_h) admits a unique solution $u_h \in U^h_{ad}$ with unique associated state $y_h \in V_h$, and

$$u_h = \mathrm{P}_{U^h_{ad}} \left(-\frac{1}{\alpha} p_h(u_h) \right), \quad p_h(u_h) := S^*_h(S_h u_h - z_l).$$

Here, similar as above $\mathrm{P}_{U_{ad}^h}(\cdot)$ denotes the orthogonal projection in $L^2(\Gamma_h)$ onto U_{ad}^h. With the help of

$$\left(\mathrm{P}_{U_{ad}^h}(v_l)\right)^l = \mathrm{P}_{U_{ad}}(v) \text{ for all } v \in L^2(\Gamma)$$

and the error estimates of [2]

$$\|(\cdot)^l S_h(\cdot)_l - S\|_{\mathcal{L}(L^2(\Gamma),L^2(\Gamma))} \leq Ch^2.$$

we in [6] prove

$$\begin{aligned}(1)\quad &\alpha\left\|u_h^l - u\right\|_{L^2(\Gamma)}^2 + \left\|y_h^l - y\right\|_{L^2(\Gamma)}^2 \leq \\ &C\left(\frac{1}{\alpha}\left\|\left((\cdot)^l S_h^*(\cdot)_l - S^*\right)(y-z)\right\|_{L^2(\Gamma)}^2 + \left\|\left((\cdot)^l S_h(\cdot)_l - S\right)u\right\|_{L^2(\Gamma)}^2\right) \leq Ch^4.\end{aligned}$$

Here u_h^l and u_l denote appropriate lift operations from the discrete to the continuous surface, and vice versa.

This result is confirmed by the following numerical example from [6]. Let Γ denote the unit sphere in $\mathbb{R}^3$ and $\alpha = 1.5 \cdot 10^{-6}$. We consider

$$\min_{u\in L^2(\Gamma),\, y\in H^1(\Gamma)} J(u,y) \text{ subject to } -\Delta_\Gamma y + y = u - r, \quad -1 \leq u \leq 1,$$

and choose $z = 52\alpha x_3(x_1^2 - x_2^2)$ to obtain the solution

$$\bar{u} = r = \min\left(1, \max\left(-1, 4x_3(x_1^2 - x_2^2)\right)\right).$$

The numerical findings are reported in Table 1, where the number of iterations of the semi-smooth Newton method applied to the numerical solution of problem (P_h) is displayed together with the experimental order of convergence (EOC) for several refinement steps. The result of error estimate (1) is clearly confirmed. Moreover, mesh–independence of the semi–smooth Newton solver is clearly confirmed. Figure 1 illustrates these results graphically.

reg. refs.	0	1	2	3	4	5
$L2$-error	5.8925e-01	1.4299e-01	3.5120e-02	8.7123e-03	2.2057e-03	5.4855e-04
EOC	-	2.0430	2.0255	2.0112	1.9818	2.0075
# Steps	6	6	6	6	6	6

TABLE 1. L^2-error, Experimental Order of Convergence and number of semismooth Newton iterations.

Control of parabolic PDEs on evolving surfaces is investigated by Vierling in [8]. In this work he among other things introduces a concept of time–dependent function spaces to handle functions defined on evolving spaces, and introduces a weak solution concept for parabolic equations on moving surfaces which represents an elegant extension of the weak solution concept of parabolic equations in the plane. With his concept Vierling lays the foundation for the new abstract functional analytic framework to treat PDEs on evolving surfaces proposed in [1]. Moreover, he presents a complete theory for control constrained optimal control

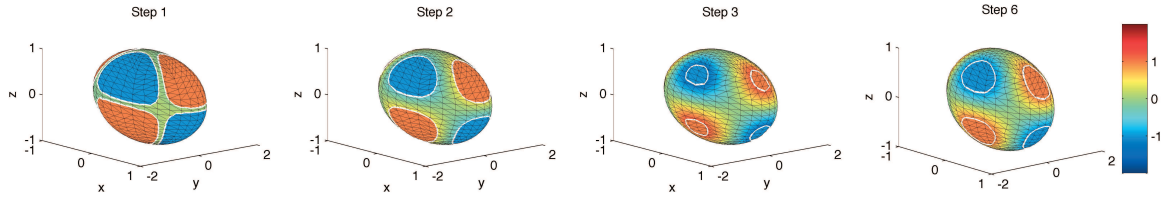

FIGURE 1. Selected steps of semismooth Newton method for the numerical solution of (P_h).

of parabolic PDEs on evolving surfaces, including error analysis with numerical confirmation.

REFERENCES

[1] A. Alphonse, C. Elliott, and B. Stinner, *An Abstract Framework for Parabolic PDEs on Evolving Spaces*, Portugal Math. **72** (2015), 1–46.
[2] G. Dziuk, *Finite elements for the Beltrami operator on arbitrary surfaces*, Partial differential equations and calculus of variations, Lect. Notes Math. **1357**, Springer (1988), 142–155.
[3] G. Dziuk and C. Elliott, *Finite elements on evolving surfaces*, IMA J. Numer. Anal. **27** (2007), 262–292.
[4] M. Hinze, *A variational discretization concept in control constrained optimization: The linear-quadratic case*, Comput. Optim. Appl. **30** (2005), 45–61.
[5] M. Hintermüller, K. Ito, and K. Kunisch, *The primal-dual active set strategy as a semismooth Newton method*, SIAM J. Optim. **13** (2003), 865–888.
[6] M. Hinze and M. Vierling, *Optimal control of the Laplace-Beltrami operator on compact surfaces - concept and numerical treatment*, J. Comput. Math. **30** (2012), 392–403.
[7] M. Ulbrich, *Semismooth Newton methods for operator equations in function spaces*, SIAM J. Optim. **13** (2003), 805–841.
[8] M. Vierling, *Parabolic optimal control problems on evolving surfaces subject to point-wise box constraints on the control – theory and numerical realization*, IFB **16** (2014), 137–173.

Discretization of Parabolic Problems on Moving Domains with Moving Interfaces

THOMAS RICHTER
(joint work with Stefan Frei)

We discuss the accurate discretization of parabolic problems with moving interfaces and moving domains. Let

$$Q := \{(t, \Omega(t)),\ t \in I := [0,T]\} \subset \mathbb{R}^{d+1},$$

be a space-time domain, that is split into two sub-domains $Q = Q_1 \cup G \cup Q_2$ by an interface $G \subset \mathbb{R}^d$, where $\Omega(t) = \Omega_1(t) \cup \Gamma(t) \cup \Omega_2(t)$:

$$Q_i := \{(t, \Omega_i(t)),\ t \in I := [0,T]\} \subset \mathbb{R}^{d+1}, \quad G := \{(t, \Gamma(t)),\ t \in I := [0,T]\}.$$

Then, given a right hand side f we find $u : Q \to \mathbb{R}$ such that

$$
\begin{aligned}
\partial_t u_i - \operatorname{div}(\kappa_i \nabla u_i) &= f_i && \text{in } Q_i,\ i = 1, 2, \\
u_1 = u_2, \quad \vec{n} \cdot \kappa_1 \nabla u_1 &= \vec{n} \cdot \kappa_2 \nabla u_2 && \text{on } \Gamma(t), \\
u(\cdot, 0) = u^0 \text{ on } \omega(0), \quad u(\cdot, t) &= 0 && \text{on } \partial\Omega(t),
\end{aligned} \tag{1}
$$

where the coefficient $\kappa_i \in \mathbb{R}_+$ is defined piece-wise constant on Q_1 and Q_2. Standard finite element formulations for the approximation of such problems suffer from various problems

- Given sufficient regularity of the domain and the data, it holds $u \in L^2(I; H^1(\Omega))$ and $\partial_t u \in L^2(I; H^{-1}(\Omega))$. Higher regularity of the data carries over to higher smoothness within the two domains Q_1 and Q_2, the solution however will lack better regularity across the interface, both in spatial and in temporal direction.
- If a fixed mesh Ω_h is used, which is good for reasons of efficiency, spatial convergence will be limited to $O(\sqrt{h})$ in the energy norm and $O(h)$ in the L^2-norm. This result is not improved with higher order finite elements.
- Considering time-stepping schemes, a fixed spatial point $x \in \mathbb{R}^d$ can change its affiliation $x \in \Omega_1(t_1)$ to $x \in \Omega_2(t_2)$. Difference approximations $(u(x, t_1) - u(x, t_2))/(t_2 - t_1)$ will not converge.
- If the outer domain is moving in time, a point $x \in \Omega_1(t)$ can even be outside of both domains at a time $t' > t$.

The problem of spatial discretization is well discussed in literature. Among the most prominent approaches to achieve high accuracy is the enrichment of the finite element space to capture the interface, the *extended finite element method XFEM*. We present a locally modified finite element scheme [2], that is based on an isoparametric implicit discretization, that adjusts to the interface by local transformations, see Figure 1. The benefit of this approach lies in the very simple structure using static meshes and finite element spaces, with a fixed number of unknowns and a system matrix, whose connectivity does not depend on the interface location. In [2], we show for elliptic interface problems

$$
h\|\nabla(u - u_h)\|_\Omega + \|u - u_h\|_\Omega \le ch^2\|f\|_\Omega, \quad \operatorname{cond}_2(\mathbf{A}_h) \le ch^{-2},
$$

where the constant $c > 0$ does not depend on the interface location.

In [3] we tackle the problem of deriving an accurate second order time-stepping scheme. The main problem is described by the standard difference approximation

$$
k^{-1}(u^m - u^{m-1}, \phi)_\Omega.
$$

Several questions arise: if the domains are changing $\Omega_m \neq \Omega_{m-1}$, the function spaces also change, $u^m \in V_h^m$ vs. $u^{m-1} \in V_h^{m-1}$. Most likely, $u^m - u^{m-1}$ is not defined. Which domain is used to define the scalar product, what is the correct space for the test-function ϕ?

To address all these issues, we derive in a first step a space-time Galerkin formulation of the moving interface problem, where trial- and test-spaces are aligned

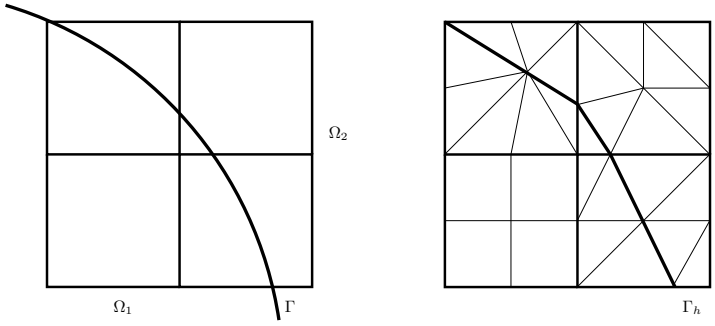

FIGURE 1. Spatial resolution of the interface by using a locally modified isoparametric finite element space. At the interface, each element is mapped using a piece-wise affine partitioning into eight triangles.

with the moving interface, see Figure 2. The space-time formulation can be written as

$$B(u,\phi) := (\partial_t u, \phi)_Q + (\kappa \nabla u, \nabla \phi)_Q + (u(0), \phi(0)) = F(\phi), \tag{2}$$

with suitable function spaces for u and ϕ. The disadvantage of temporal Galerkin formulations is the high computational effort connected to the required higher order approximation of the temporal integrals. Hence, we aim at deriving an approximative scheme that takes the form of an efficient time-stepping method.

In a second step, we introduce an ALE-like formulation for each time-step of (2) by mapping the space-time slice to a reference domain

$$T^m : \hat{Q}^m \to Q^m, \quad \hat{Q}^m := (t_{m-1}, t_m] \times \{\Omega_1(t_m) \cup \Gamma(t_m) \cup \Omega_2(t_m)\}.$$

The resulting formulation can be expressed on a space-time domain $\hat{Q}^m$ without moving boundaries or interfaces. Finally, in a third step, this time-step ALE formulation is approximated by evaluating the domain map T^m by the trapezoidal rule

$$\bar{T}^m(\hat{x}) := \frac{T^m(\hat{x}, t_{m-1}) + T^m(\hat{x}, t_m)}{2}.$$

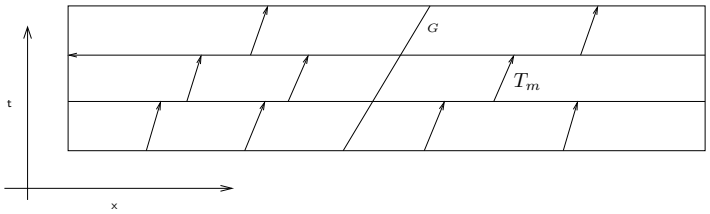

FIGURE 2. Space-time Galerkin formulation for a parabolic interface problem. The continuous, piece-wise linear trial-functions and the discontinuous piece-wise constant test-functions are aligned with the moving interface.

For the resulting time-stepping method we show in [3] the following result:

Theorem: *Let u be the solution to 1 and u_k be the discrete solution to the approximated temporal Galerkin scheme. Given sufficient regularity of the initial solution u^0, the right hand side f and the domain- and interface-parametrization, it holds*

$$\|u(T) - u_k(T)\| \leq ck^2 \exp(T) \left(\|u^0\|_{H^6(\Omega_1(0)\cup\Omega_2(0))} + \sum_{k=0}^{2} \|f\|_{W^{k,2(m-k)}(Q)} \right)$$

The required regularity of this error estimate can be lessened to $u^0 \in H^4$ in a longer proof, that is based on the introduction of adjoint solutions. In numerical examples, we validate this result and observe the expected order of convergence.

Aim of this discretization scheme is gaining second order convergence while making an efficient realizatioan possible. The focus of our applications is in the interaction of incompressible fluids with elastic structures. When large deformation and structural motion appear, an Eulerian formulation based on fixed meshes is a promising model [1]. This is a prototypical example for interface problems with moving interfaces and moving domains.

References

[1] T. Richter, *A Fully Eulerian Formulation for Fluid-Structure-Interaction Problems*, JCP **233** (2013), 227-240

[2] S. Frei and T. Richter, *A locally modified parametric finite element method for interface problems*, SIAM J. Numer. Math. **52** (2015), 2315-2334

[3] S. Frei and T. Richter, *Second order time-stepping for parabolic interface problems with moving interfaces*, submitted to SIAM J. Numer. Math. (2015)

A higher order finite element method for partial differential equations on surfaces

Arnold Reusken

(joint work with Jörg Grande)

In the past decade the study of numerical methods for PDEs on surfaces has been a rapidly growing research area [2]. Different classes of finite element discretization techniques can be distinguished. The most popular technique, developed mainly by Dziuk and Elliott, uses a finite element space on a triangulation of the discrete surface. This approach has been extensively analyzed and extended in several directions. Another approach applies to cases in which the surface is given implicitly by some level set function and the key idea is to extend and solve the partial differential equation on a narrow band around the surface. Unfitted finite element spaces on this narrow band are used for discretization. Another surface finite element aproach, called the trace finite element method, is based on an outer (bulk) mesh. The main idea of this method is to use finite element spaces that are induced by triangulations of an outer domain to discretize the partial differential

equation on the surface by considering traces of the bulk finite element space on the surface, instead of extending the PDE off the surface.

Most of the methods mentioned above have been studied both for stationary and evolving surfaces.

In almost all the papers we know of, the discretization that is studied is based on piecewise *linear* finite elements. The paper [1] is the only one in which rigorous a priori error bounds for *higher order* finite element methods for partial differential equations on (stationary) surfaces are derived. In that paper the Laplace-Beltrami equation on a stationary smooth closed manifold Γ is considered. It is assumed that Γ is represented as the zero level of a smooth signed distance function d. The exact surface is approximated by a quasi-uniform shape-regular polyhedral surface $\hat{\Gamma}_h$ having triangular faces, and with vertices on Γ. Based on the distance function d a parametric mapping, consisting of piecewise polynomial mappings of degree k, is defined on $\hat{\Gamma}_h$, which results in a corresponding discrete surface $\hat{\Gamma}_h^k$. Using the same mapping a standard higher order finite element space on $\hat{\Gamma}_h$ is lifted to $\hat{\Gamma}_h^k$. This lifted space on $\hat{\Gamma}_h^k$ is used for the discretization of the surface PDE. An extensive error analysis of this method is presented in [1], resulting in optimal error bounds. For example, for the $H^1(\Gamma)$ error (where the discrete solution is lifted to Γ) a bound of the form $c(h^m + h^{k+1})$ is proved. Here k is the degree of the polynomials used in the parametrization of $\hat{\Gamma}_h^k$ and m the degree of the polynomials in the finite element space on $\hat{\Gamma}_h$. We emphasize that in this method explicit knowledge of the exact signed distance function to Γ is an essential requirement.

In many applications the exact signed distance function to the surface Γ is not known. One often encounters situations in which Γ is the zero level of a smooth level set function ϕ (not necessarily a signed distance function) and one only has a finite element approximation of ϕ available.

In this presentation, we address the question: (how) can one develop a higher order finite element method in such a setting? We present a constructive affirmative answer to this question. The results that we present are given in the paper [3].

We restrict ourselves to the model problem of the Laplace-Beltrami equation on a stationary smooth surface Γ. Our approach is fundamentally different from the one in [1], in the sense that we do not need the exact distance function d. Instead, we only(!) need a finite element approximation ϕ_h^k of a level set function ϕ, which has Γ as its zero level. The discrete level set function ϕ_h^k comes from a standard finite element space on a quasi-uniform triangulation of a bulk domain that contains Γ. In the error analysis we assume that ϕ_h^k satisfies an error bound of the form

$$\|\phi_h^k - \phi\|_{L^\infty(U)} + h\|\phi_h^k - \phi\|_{H^1_\infty(U)} \leq ch^{k+1}, \tag{1}$$

where U is a (small) neighborhood of Γ in $\mathbb{R}^3$. The zero level of ϕ_h^k is denoted by Γ_h^k. Note that for $k > 1$, Γ_h^k cannot be easily constructed. From (1) it follows

that $\mathrm{dist}(\Gamma, \Gamma_h^k) \leq ch^{k+1}$ holds. The method that we introduce is new and is built upon the following key ingredients:

- For $k = 1$ the function $\hat{\phi}_h := \phi_h^1$ is piecewise linear, hence its zero level is piecewise planar, consisting of quadrilaterals and triangles, and can easily be determined. The quadrilaterals are subdivided into triangles. The resulting triangulation is denoted by $\hat{\Gamma}_h$. This triangulation is in general *very* shape-*ir*regular. Nevertheless, the trace of an outer finite element space or a standard finite element space directly on $\hat{\Gamma}_h$ turns out to have optimal approximation properties. Such a finite element space on $\hat{\Gamma}_h$ is denoted by $\hat{S}_h$.
- We take $k > 1$. For the parametrization of Γ_h^k we use a *quasi-normal field*. Given ϕ_h^k we apply a gradient recovery method which results in a Lipschitz continuous vector field n_h that is close to the normal field n that corresponds to ϕ. Using this quasi-normal field, there is a unique decomposition $x = p_h(x) + d_h(x)n_h(p_h(x))$ for all x in a neighborhood of Γ_h^k, with $p_h(x) \in \Gamma_h^k$ and $d_h \in \mathbb{R}$ an *approximate* signed distance function. It can be shown that $p_h : \hat{\Gamma}_h \to \Gamma_h^k$ is a *bijection*. This p_h is used for the parametrization of Γ_h^k. For given $x \in \hat{\Gamma}_h$ its image $p_h(x) \in \Gamma_h^k$ can be determined (with high accuracy) using the known field n_h and only few evaluations of ϕ_h^k.
- Using the parametrization p_h the finite element space $\hat{S}_h$ on $\hat{\Gamma}_h$ is lifted to Γ_h^k and used for a Galerkin type discretization, i.e., we replace Γ by Γ_h^k, and $H^1(\Gamma)$ is replaced by the lifted finite element space, f is suitably extended, and instead of ∇_Γ we use the tangential gradient along Γ_h^k.
- Only evaluations of p_h and Dp_h can be computed. Hence, *quadrature* is needed. The finite element space is pulled back to $\hat{\Gamma}_h$, integrals over Γ_h^k are transformed to integrals over $\hat{\Gamma}_h$ and quadrature is applied on triangles in $\hat{\Gamma}_h$. We then (only) need evaluations of p_h, Dp_h, and of exact normals on $\hat{\Gamma}_h$ and on Γ_h^k. The latter are easily determined using ϕ_h^k.

In the presentation this method and its implementation are discussed. A further topic is an error analysis of this method. A key point related to this is the following. On each triangle T of the "base" triangulation $\hat{\Gamma}_h$ the parametrization p_h is *only Lipschitz*. This low regularity is due to the construction of the quasi-normal field n_h. Hence, the bilinear form pulled back to $\hat{\Gamma}_h$ consists of a sum of integrals of the form $\int_T G \nabla_{\hat{\Gamma}_h} \hat{u}_h \cdot \nabla_{\hat{\Gamma}_h} \hat{v}_h \, d\hat{s}_h$ with a function G that has very low smoothness (not even continuous). Due to this the analysis of the quadrature error is not straightforward. The structure of the error analysis is outlined. As a main result, we present an $H^1(\Gamma)$ error bound (where the discrete solution is lifted to Γ) of the form $c(h^m + h^{k+1})$. Here m is the degree of the polynomials used in the finite element space $\hat{S}_h$.

References

[1] A. Demlow *Higher-order finite element methods and pointwise error estimates for elliptic problems on surfaces*, SIAM J. Numer. Anal. **47** (2009), 805–827.

[2] G. Dziuk, C. Elliott, *Finite element methods for surface PDEs*, Acta Numerica **2013**, 289–396.

[3] J. Grande, A. Reusken *A higher order finite element method for partial differential equations on surfaces*, IGPM report **403** (2014), Accepted for publication in SIAM J. Numer. Anal.

Reporter: Tobias Kies

Participants

Prof. Dr. Helmut Abels
Fakultät für Mathematik
Universität Regensburg
93040 Regensburg
GERMANY

Dr. Amal C. Alphonse
Mathematics Institute
University of Warwick
Coventry CV4 7AL
UNITED KINGDOM

Prof. Dr. Sören Bartels
Abtlg. f. Angewandte Mathematik
Universität Freiburg
Hermann-Herder-Strasse 10
79104 Freiburg i. Br.
GERMANY

Prof. Dr. David L. Chopp
Technological Institute
Northwestern University
2145 Sheridan Road
Evanston, IL 60208-3125
UNITED STATES

Prof. Dr. Klaus Deckelnick
Institut für Analysis u. Numerik
Otto-von-Guericke-Universität
Magdeburg
Universitätsplatz 2
39106 Magdeburg
GERMANY

Luca Dede
Section de Mathématiques
École Polytechnique Fédérale de
Lausanne
SB-MATHICSE-CMCS
Station 8
1015 Lausanne
SWITZERLAND

Ana Djurdjevac
Institut für Mathematik
Freie Universität Berlin
Arnimallee 6
14195 Berlin
GERMANY

Prof. Dr. Charles M. Elliott
Mathematics Institute
University of Warwick
Gibbet Hill Road
Coventry CV4 7AL
UNITED KINGDOM

Dr. Hans Fritz
Mathematics Institute
University of Warwick
Coventry CV4 7AL
UNITED KINGDOM

Prof. Dr. Harald Garcke
Fakultät für Mathematik
Universität Regensburg
93040 Regensburg
GERMANY

Prof. Dr. Maria L. Garzón Martin
Faculty of Sciences
University of Oviedo
Calvo Sotelo s/n.
33007 Oviedo
SPAIN

Dr. Jan Giesselmann
Institut für Angewandte Analysis
und Numerische Simulation
Universität Stuttgart
70569 Stuttgart
GERMANY

Dr. Carsten Gräser
Fachbereich Mathematik & Informatik
Freie Universität Berlin
Arnimallee 6
14195 Berlin
GERMANY

Hanne Hardering
Institut für Numerische Mathematik
Fachrichtung Mathematik
Technische Universität Dresden
Willersbau C311
01062 Dresden
GERMANY

Prof. Dr. Michael Hintermüller
Institut für Mathematik
Humboldt-Universität zu Berlin
10099 Berlin
GERMANY

Prof. Dr. Michael Hinze
Fachbereich Mathematik
Universität Hamburg
Bundesstrasse 55
20146 Hamburg
GERMANY

Graham Hobbs
MASDOC DTC
University of Warwick
Zeeman Building
Coventry CV4 7AL
UNITED KINGDOM

Tobias Kies
Institut für Mathematik
Freie Universität Berlin
Arnimallee 6
14195 Berlin
GERMANY

Prof. Dr. Rupert Klein
Fachbereich Mathematik & Informatik
Freie Universität Berlin
Arnimallee 6
14195 Berlin
GERMANY

Prof. Dr. Ralf Kornhuber
Institut für Mathematik
Freie Universität Berlin
Arnimallee 6
14195 Berlin
GERMANY

Balázs Kovács
Mathematisches Institut
Universität Tübingen
Auf der Morgenstelle 10
72076 Tübingen
GERMANY

Prof. Dr. Dietmar Kröner
Abteilung für Angewandte Mathematik
Universität Freiburg
Hermann-Herder-Strasse 10
79104 Freiburg i. Br.
GERMANY

Prof. Dr. Philippe G. LeFloch
Laboratoire Jacques-Louis Lions
Université Paris 6
4, Place Jussieu
75252 Paris Cedex 05
FRANCE

Buyang Li
Mathematisches Institut
Universität Tübingen
Auf der Morgenstelle 10
72076 Tübingen
GERMANY

Prof. Dr. Reinhard Lipowsky
Max-Planck-Institut für Kolloid & Grenzflächenforschung
Potsdam-Golm Science Park
Am Mühlenberg 1, OT Golm
14476 Potsdam
GERMANY

Prof. Dr. Christian Lubich
Mathematisches Institut
Universität Tübingen
Auf der Morgenstelle 10
72076 Tübingen
GERMANY

Prof. Dr. Stephan Luckhaus
Mathematisches Institut
Universität Leipzig
Postfach 10 09 20
04109 Leipzig
GERMANY

Prof. Dr. John A. Mackenzie
Department of Mathematics & Statistics
University of Strathclyde
Livingstone Tower
26, Richmond Street
Glasgow G1 1XH
UNITED KINGDOM

Prof. Dr. Anotida Madzvamuse
Department of Mathematics
University of Sussex
Mantell Building
Falmer, Brighton BN1 9RF
UNITED KINGDOM

Dr. Annibale Magni
Mathematisches Institut
Universität Münster
48149 Münster
GERMANY

Dr. Robert Nürnberg
Department of Mathematics
Imperial College London
Huxley Building
London SW7 2AZ
UNITED KINGDOM

Prof. Dr. Maxim A. Olshanskii
Department of Mathematics
University of Houston
Houston, TX 77204-3476
UNITED STATES

Christian Power
Mathematisches Institut
Universität Tübingen
Auf der Morgenstelle 10
72076 Tübingen
GERMANY

Prof. Paola Pozzi
Fachbereich Mathematik
Universität Duisburg-Essen
Thea-Leymann-Straße 9
45127 Essen
GERMANY

Dr. Tom Ranner
School of Computing
University of Leeds
Leeds LS2 9JT
UNITED KINGDOM

Prof. Dr. Arnold Reusken
Institut f. Geometrie & Prakt. Mathematik
RWTH Aachen
Templergraben 55
52061 Aachen
GERMANY

Prof. Dr. Thomas Richter
Department Mathematik, AM3
Universität Erlangen-Nürnberg
Cauerstraße 11
91058 Erlangen
GERMANY

Prof. Dr. Matthias Röger
Fachbereich Mathematik
Technische Universität Dortmund
Vogelpothsweg 87
44227 Dortmund
GERMANY

Prof. Dr. Martin Rumpf
Institut für Numerische Simulation
Endenicher Allee 60
53115 Bonn
GERMANY

Prof. Dr. Oliver Sander
Institut für Numerische Mathematik
Technische Universität Dresden
Zellescher Weg 12-15
01069 Dresden
GERMANY

Prof. Dr. Christian Schmeiser
Fakultät für Mathematik
Universität Wien
Oskar-Morgenstern-Platz 1
1090 Wien
AUSTRIA

Prof. Dr. James A. Sethian
Department of Mathematics
University of California
Berkeley CA 94720-3840
UNITED STATES

Dr. Andriy Sokolov
Fakultät für Mathematik
Lehrstuhl III
Technische Universität Dortmund
Vogelpothsweg 87
44227 Dortmund
GERMANY

Prof. Dr. Jürgen Sprekels
Weierstraß-Institut für
Angewandte Analysis und Stochastik
Mohrenstrasse 39
10117 Berlin
GERMANY

Prof. Dr. Angela Stevens
Institut für Numerische und
Angewandte Mathematik
Universität Münster
Einsteinstrasse 62
48149 Münster
GERMANY

Dr. Björn Stinner
Mathematics Institute
University of Warwick
Coventry CV4 7AL
UNITED KINGDOM

Dr. Robert Strehl
Department of Mathematics
Ryerson University
350 Victoria Street
Toronto, Ontario M5B 2K3
CANADA

Dr. Laura Stricker
Max Planck Institute for Dynamics and
Self-Organization (MPIDS)
Am Faßberg 17
37077 Göttingen
GERMANY

Prof. Dr. Lutz Tobiska
Institut für Analysis und Numerik
Otto-von-Guericke-Universität
Magdeburg
Postfach 4120
39016 Magdeburg
GERMANY

Ethan van Andel
Department of Mathematics
University of California, Berkeley
970 Evans Hall
Berkeley CA 94720-3840
UNITED STATES

Dr. Chandrasekhar Venkataraman
Mathematics Institute
University of St. Andrews
North Haugh
St. Andrews KY16 9SS
UNITED KINGDOM

Maren-Wanda Wolf
Institut für Mathematik
Freie Universität Berlin
Arnimallee 6
14195 Berlin
GERMANY

Prof. Dr. Harry Yserentant
Institut für Mathematik
Technische Universität Berlin
Straße des 17. Juni 136
10623 Berlin
GERMANY